

Effective Equilibrium, Power Functional, and Interface Structure for Phase-Separating Active Brownian Particles

Von der Universität Bayreuth
zur Erlangung des Grades eines
Doktors der Naturwissenschaften (Dr. rer. nat.)
genehmigte Abhandlung

von

Philip Krinninger

aus Altötting

1. Gutachter: Prof. Dr. Matthias Schmidt
2. Gutachter: Prof. Dr. Martin Oettel

Tag der Einreichung: 26.09.2018

Tag des Kolloquiums: 30.01.2019

Abstract

In this thesis we approach the physics of active Brownian particles (ABP) and particularly the emergence of motility induced-phase separation (MIPS) by (i) an effective equilibrium description for small activities [1], (ii) a formally exact power functional theory [2, 3], and (iii) a computer simulation study of the free interface between coexisting phases [4]. Active Brownian particles are modeled as spherical particles that obey Brownian motion described by an overdamped Langevin equation of motion. Activity is thereby induced by a self-propulsion force. This force acts along the built-in orientation of each individual particle, and the time dependence of the orientation is given by an additional Langevin equation that describes free rotational diffusion. This intrinsic out-of-equilibrium system shows a wide variety of phenomena, where phase separation in absence of explicit interparticle attraction between the particles is one of the most spectacular open problems.

In the effective equilibrium approach the active system is mapped onto a system of passive Brownian particles that interact via a modified effective interparticle interaction [1]. This is achieved by integrating out the orientations. The resulting Langevin equation contains colored noise. From this equation of motion an approximated Fokker-Planck equation is constructed. In this Fokker-Planck equation an activity-dependent effective interaction force between the particles is identified. In the case of pairwise interaction, the effective interaction can be represented as an activity-dependent effective pair interaction potential. For purely repulsive interaction potentials, an attractive tail develops above an activity threshold. The strength of this attraction increases even further with increasing activity, eventually leading to bulk phase separation. Furthermore, passively attractive interactions are considered, namely the Lennard-Jones potential. In this case, the attractive minimum of the potential weakens at first when activity is increased and suppression of phase separation is observed. Increasing the activity further, the attractive minimum deepens again and a reentrance of phase separation emerges. As the activity determines only the form of the effective interaction and the many-body dynamics resemble the passive dynamics, common methods of liquid state theory can be applied to active systems. We use them for instance to calculate spinodals and the pair correlation function for the active system. An important part of the work is the validation via computer simulations, where the orientations are not integrated out, i.e., the full many-body problem of ABP is considered. The result is that in all situations presented we find a good match between theory and the simulation. Despite the success of the effective equilibrium description in many situations, possible applications are rather limited to low activity cases due to the approximations made in the construction of the Fokker-Planck equation. In order to overcome these limitations we develop a power functional theory (PFT) for active particles [2, 3]. Therein, the orientations are considered as

additional degrees of freedom and enter the many-body dynamics as such. Starting from the many-body description, i.e., the Smoluchowski equation, power functional theory offers an exact formalism to determine the correct physical time evolution of the one-body density, the translation, and rotational current distributions from a microscopically defined power functional. We apply this framework to steady states, where the coupling between the translational and rotational dynamics is realized by the self-propulsion force that determines the magnitude of the activity, and we give a simple approximation for the dissipative parts of the power functional that applies to bulk states. Furthermore, we show that in steady state the value of the power functional is determined by the negative value of half of the external power and is thus trivially related to the swimming of the particles. For soft repulsive spheres we perform Brownian dynamics computer simulations in bulk and develop sampling strategies for the power functional. Comparing our theory with the numerics shows a good agreement.

Going beyond the bulk properties of ABP that undergo MIPS a detailed study of the interface between the phases is required [4]. The reason is that the dissipation functional presented for the bulk studies [2, 3] denotes only the friction (drag) induced by particle interactions in bulk. For inhomogeneous situations further superadiabatic contributions have to be considered and thus the dissipation functional has to be generalized in order to cover these contributions. As the corresponding manuscript is in preparation [4], results from computer simulations are presented in Sec. 4. In agreement with the literature we find that the interface is polarized and hence the orientations of the particles are not evenly distributed there (as it would be in bulk). By analyzing the results for the one-body distribution of the density and the current we give an interpretation of the particles' behavior at the interface. Further insights are provided by the explicit analysis of the orientation dependence of the one-body distributions including an angular Fourier decomposition which is used to describe the anisotropies that emerge at the interface. Our findings serve as a reference point for an extended power functional theory that can describe the physics of the active particles in bulk and at the interface.

Kurzfassung

Diese Dissertation behandelt die statistische Physik aktiver Brownscher Teilchen, im speziellen das Auftreten von Phasenseparation aufgrund der Aktivität der Teilchen. Dazu werden verschiedene Herangehensweisen verwendet: (i) eine Methode, die das aktive System auf ein effektives Gleichgewichtssystem abbildet [1], (ii) eine formal exakte Powerfunktionaltheorie [2, 3] sowie (iii) die explizite Betrachtung der Grenzfläche, die sich im Falle von Phasenseparation ausbildet, mit Hilfe von Computersimulationen [4]. Die aktiven Schwimmer werden als sphärische Teilchen beschrieben, die Brownscher Bewegung unterliegen, und durch eine überdämpfte Langevin-Bewegungsgleichung modelliert. Die Aktivität wird dabei durch eine Antriebskraft induziert, die in Richtung der Orientierung eines jeden einzelnen Teilchens wirkt. Die Zeitentwicklung der Orientierungen ist durch eine zusätzliche Langevingleichung gegeben und beschreibt freie Rotationsdiffusion. Durch die Aktivität ist das System weg vom thermodynamischen Gleichgewicht getrieben. Aktive Brownsche Teilchen zeigen eine Vielzahl von Phänomenen, von denen die Phasenseparation in Abwesenheit von expliziter Attraktion zwischen den Teilchen im passiven Zustand wohl das spektakulärste offene Problem ist.

Eine Beschreibung des aktiven System als effektives Gleichgewichtssystem wird durch Ausintegration der Orientierung der Teilchen erreicht [1]. Als Ergebnis erhält man eine einzige Langevingleichung, die einen Markov-Prozess beschreibt. Aus dieser wird eine approximierete Fokker-Planck hergeleitet, in der sich eine effektive Wechselwirkung zwischen den Teilchen identifizieren lässt. Diese hängt in Form und Stärke von der Aktivität ab. Handelt es sich eingangs um eine Paarwechselwirkung zwischen den Teilchen, so ist die resultierende effektive Wechselwirkung ebenfalls eine Paarwechselwirkung. Zunächst werden Wechselwirkungen betrachtet, die im passiven Fall rein repulsiv sind. Wird die Aktivität über einen bestimmten Schwellwert erhöht, bildet sich im effektiven Potential ein attraktiver Anteil aus. Erhöht man die Aktivität weiter, wird diese Anziehung größer. Dieses Ausbilden von Anziehung zwischen den Teilchen ist der Grund für die Phasenseparation, die im aktiven System auftritt. Für das Lennard-Jones Potential, also eine Wechselwirkung, die auch im passiven Fall Attraktion beinhaltet, zeigt sich, dass bei kleiner Aktivität die Anziehung zwischen den Teilchen abnimmt und die Phasenseparation damit unterdrückt wird. Bei weiterer Erhöhung der Aktivität steigt die Anziehung wieder an und die Phasenseparation setzt wieder ein. Dadurch, dass die Aktivität der Teilchen lediglich die Form des Wechselwirkungspotentials bestimmt, können Methoden angewandt werden, die sonst nur für Systeme im Gleichgewicht anzuwenden sind. So werden beispielsweise die Spinodalen für die Phasenseparation und die Paarkorrelationsfunktion berechnet. Ein wichtiger Teil der Arbeit ist auch der Vergleich der Ergebnisse der Theorie mit numerischen Simulationen, um die Ergebnisse des Modells zu verifizieren. Dies ist möglich, da für die Simulationen die Orientierungen nicht

ausintegriert werden und beide Langevingleichungen iterativ gelöst werden, sprich die gesamte Vielteilchendynamik von ihr abgebildet wird. Dabei ist die Übereinstimmung in allen getesteten Fällen sehr gut.

Obwohl die effektive Gleichgewichtsbeschreibung in vielen Situationen sehr gute Ergebnisse liefert, sind ihre möglichen Anwendungsfälle auf Systeme mit niedriger Aktivität beschränkt, da zur Herleitung der Fokker-Planck Gleichung einige vereinfachende Annahmen getroffen werden müssen. Um diese Einschränkungen zu überwinden, haben wir eine Powerfunktionaltheorie für aktive Teilchen entwickelt [2, 3]. Dabei werden die Orientierungen der Teilchen als zusätzliche Freiheitsgrade betrachtet, die als solche auch zur Vielteilchendynamik beitragen. Ausgehend von dieser, beschrieben durch die entsprechende Smoluchowski-Gleichung, liefert die Powerfunktionaltheorie einen formal exakten Formalismus, um die korrekte physikalisch realisierte Dynamik der Einteilchendichte- und Einteilchenströmeverteilungen zu erhalten. Wir wenden diese Powerfunktionaltheorie auf stationäre Zustände an, wobei die Kopplung von Translations- und Rotationsdynamik durch eine externe Kraft, die die Aktivität bestimmt, beschrieben wird und geben eine einfache Approximation für den dissipativen Anteil des Powerfunktional für Zustände im Bulk an. In diesem Fall ist der Wert des Powerfunktional durch die Hälfte des negativen Wertes des externen Funktional gegeben und ist damit trivial mit der Aktivität der Teilchen verknüpft. Zum Vergleich werden Computersimulationen für weiche Teilchen mit repulsiven Wechselwirkungen im Bulk durchgeführt. Dazu werden auch neue Samplingmethoden entwickelt. Es zeigt sich eine gute Übereinstimmung von Simulationsdaten mit der Theorie, sogar in inhomogenen, also phasenseparierten, Systemen.

Dennoch reicht eine Betrachtung des Bulks nicht aus, um die Phasenseparation abschließend zu erklären. Dazu ist eine genaue Betrachtung der Grenzfläche zwischen den Phasen nötig, da das Dissipationsfunktional lediglich die durch Wechselwirkung zwischen den Teilchen induzierte Reibung modelliert [4]. Dabei zeigt sich, dass das Dissipationsfunktional zu einem superadiabatischen Funktional verallgemeinert werden muss, um superadiabatische Effekte, die über die Reibung hinausgehen, mit einzubeziehen. Im Rahmen dieser Studie werden Resultate von Computersimulationen in Kapitel 4 vorgestellt. In Übereinstimmung zur Literatur zeigt sich eine Polarisierung der Grenzfläche, d.h. die Orientierungen sind hier nicht gleichverteilt, wie es im Bulk der Fall ist. Wir analysieren die Einteilchendichte und -ströme und geben darauf basierend eine Interpretation des Verhaltens der Teilchen an der Grenzfläche. Besonders die explizite Betrachtung der Abhängigkeiten der Einteilchenverteilungen der Dichte sowie der Ströme von der Orientierung bieten weitreichende Möglichkeiten zur Beschreibung der Grenzfläche. Dazu wird die Einteilchendichte in ihrem Orientierungsfreiheitsgrad in Fourierkomponenten entwickelt, die über die Anisotropie der Dichteverteilung an der Grenzfläche Aufschluß gibt. Die Ergebnisse fügen sich gut in den Kontext aktueller Literatur ein und bieten einen Referenzpunkt für die Entwicklung einer erweiterten Powerfunktionaltheorie, die sowohl Bulkeigenschaften als auch die Grenzflächenphysik beinhaltet.

Contents

Abstract	3
Kurzfassung	5
1 Introduction	11
1.1 Active Brownian particles	11
1.2 One-body descriptions of classical fluids	13
2 Aim of this thesis and author's contribution to publications	21
2.1 Brownian dynamics simulations of active Brownian particles	21
2.2 Power sampling	24
3 Overview of the publications	33
3.1 Effective interactions in active Brownian suspensions	33
3.2 Power functional theory for active Brownian particles	36
4 Structure of the fluid-fluid interface in phase-separated active Brownian suspensions	39
4.1 Brownian dynamics simulations	40
4.2 Results	41
4.2.1 One-body density, current, and velocity	41
4.2.2 Density, current, and velocity profiles with respect to the Gibbs dividing surface	46
4.2.3 Polarization profile	48
4.2.4 Angular Fourier decomposition of the density distribution	49
5 Conclusion and outlook	51
References	53
6 Publications	57
[1] Effective interactions in active Brownian suspensions	59
[2] Nonequilibrium Phase Behavior from Minimization of Free Power Dissipation . .	69
[3] Power functional theory for active Brownian particles: general formulation and power sum rules.	75
[4] Interfaces in phase-separated active Brownian particles.	88
Acknowledgements	89

1 Introduction

1.1 Active Brownian particles

Brownian particles are nano- to micron-sized particles that display Brownian motion, which is the agitation of particles due to the thermal motion of their surrounding. The size of Brownian particles is big enough such that the system can be described by classical physics. A perfect example for Brownian particles are colloids. Colloidal particles are suspended in a solvent, which is usually a liquid such as water. Colloidal suspensions are interesting from fundamental and applied points of view, since they are present in our daily life. Milk [5], ice cream [6], human blood [7] and paint [8] serve as examples. From a physical point of view, special interest lies in the thermodynamic properties of colloids, such as phase transitions and mechanisms of self assembly.

Active systems are composed of individual units that can transform energy from their surrounding into self-propelled movement. With the interest in living systems, such as bacteria, the research effort in active matter has gradually increased over the last decade. Realizations of active systems can be found in nature on almost every length- and time-scale. The individuals are often living biological units. Examples are flocks of birds, schools of fish, and microorganisms. Figure 1.1 illustrates how collective motion of individual units occurs on a wide range of length scales in nature. The first row represents examples of animal colonies. Figure 1.1(a) shows a flock of birds [9], while in Fig. 1.1(b) a collective of ducks is shown [10]. Examples from biological microsystems are displayed in the second row. Figure 1.1(c) shows a snapshot from a system of active vortexes of microtubes [11] and Fig. 1.1(d) shows a bacteria colony [12]. The arrows indicate the direction of swimming of the particles and the color shows which group of individual units moves collectively. All of these examples show at some point the crossover from individual and undirected motion to collective and directed motion. Hence, studying the physics of active matter allows insight to fundamental questions. For example, how do migrant birds form a flock and how does the collective find their way? Or what drives bacterial swarming in biological samples?

Beyond biological systems, a variety of artificial realizations of active matter have been created in recent years. Among these are active colloidal particles. Colloidal Janus particles are spheres where the two hemispheres are made of different materials, or one hemisphere is coated with a certain material. For example silica particles that are coated with platinum on one side are activated by light [13]. The self-propulsion force for such particles is perpendicular to the equator where the two hemispheres meet. A snapshot of a cluster of light-activated particles is shown in Fig. 1.2, where the red arrows indicate the swimming direction. Hence Janus particles allow

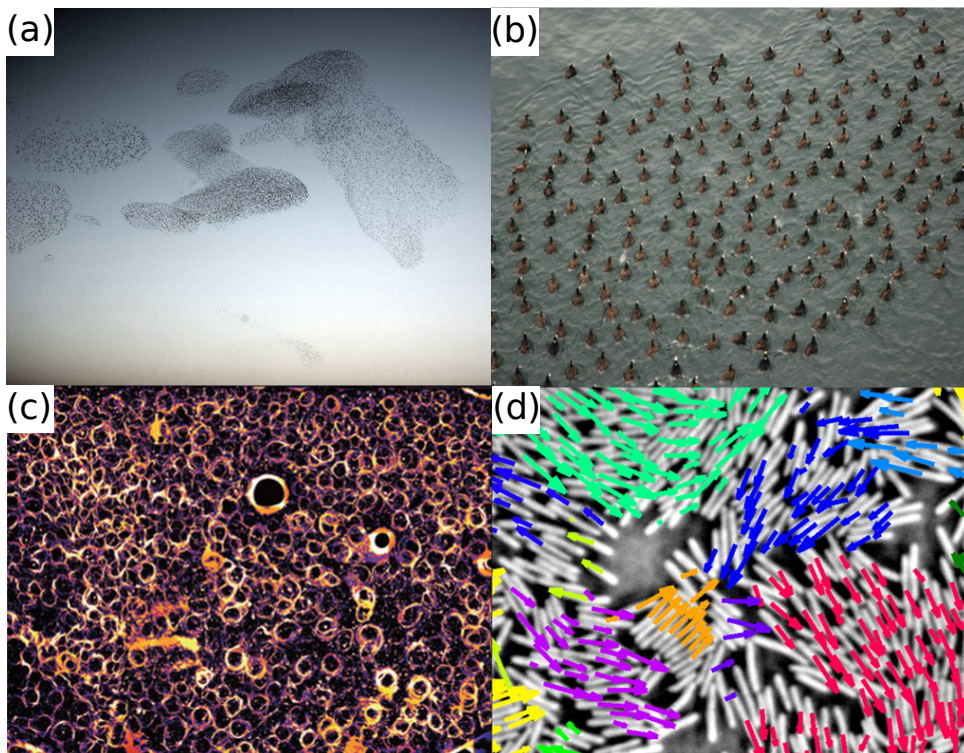


Figure 1.1: Examples of collective motion in nature on macroscopic (top) and microscopic length scales (bottom). (a) Various flocks of birds consisting of several hundreds to thousands of birds. Adapted from [9], copyright (2008) National Academy of Sciences. (b) A group of ducks where the individuals tend to move in line with other individuals in front of them. Adapted from [10], copyright (2010) National Academy of Sciences. (c) Self-organization of microtubes with average size of $15 \mu\text{m}$ into vortices of diameter around $400 \mu\text{m}$. Adapted from [11], Reprinted with permission from Permissions Springer Customer Service Centre GmbH, copyright (2012) Nature. (d) Clusters of collectively moving *Bacillus subtilis* bacteria. The arrows indicate the direction of motion of the individual bacteria and the colors show which bacteria move collectively. Adapted from [12], copyright (2010) National Academy of Sciences.

to perform experiments in a controlled way with small effort, compared to biological samples. Active colloids serve as an ideal model to study the phenomena in active matter regarding their dependence on activity and other physical properties. This model system is often referred to as active Brownian particles (ABP) and it is the basis of the present thesis.

In common theoretical ABP models the dynamics of each particle is described by two coupled overdamped Langevin equations; one for the trajectory of the particles itself (translational motion), and one for the direction of the self-propulsion of the particles (rotational motion). The orientation of the particles enters the translational Langevin equation via a self-propulsion force, of which the magnitude is given by the free swimming speed of the particles multiplied by the friction coefficient, where the orientation is described by a unit vector. Additional forces that enter the Langevin equation are external forces, and interparticle forces. The interparticle forces are commonly pair interaction forces that only depend on the distance between the particles. The rotational equation of motion describes free rotational diffusion. Hence the interaction of

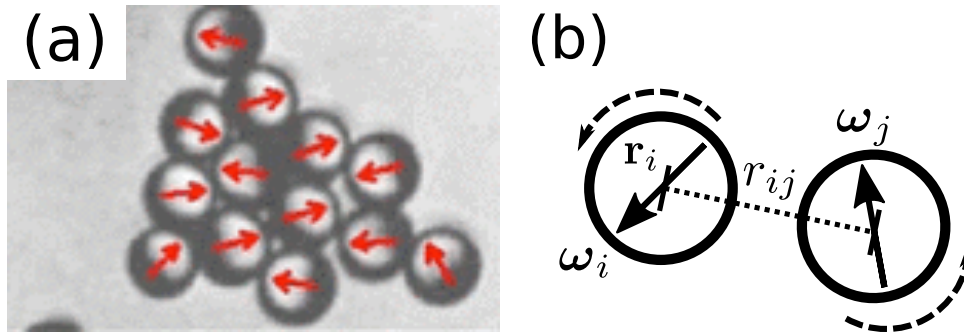


Figure 1.2: Active Brownian particle systems. (a) Experimental realization with Janus particles. The red arrows indicate the direction of swimming. At the rear end of each arrow the platinum coating on the silica colloids is visible in gray. Adapted from [13], copyright (2013) American Physical Society. (b) Illustration of active Brownian particles as disks with positions \mathbf{r}_i and \mathbf{r}_j , and orientations ω_i and ω_j .

the particles is isotropic, as the particles are often modeled as spheres, or disks in two space dimensions. However, isotropy breaks down in many situations, e.g. at interfaces [14] or when sedimentation is considered [15]. Figure. 1.2(b) shows an illustration of an ABP model. The particles i and j are spheres with positions \mathbf{r}_i and \mathbf{r}_j , and orientations ω_i and ω_j . The length of the dotted line indicates the distance between the centers of mass of the particles $r_{ij} = |\mathbf{r}_i - \mathbf{r}_j|$ that determines the force between the particles. The dashed line indicates the rotational diffusion of the orientation.

The ABP model is a popular starting point for carrying out theoretical studies of active system. As the model is rather simple, the same questions can be studied as for passive colloidal system, e.g. phase behavior, clustering, and self-organization, etc. Particular interest lies in phase separation that is caused by the motility of the particles. Motility induced phase separation (MIPS) does not require an attractive force between the particles and occurs in systems with purely repulsive interactions between the particles. The basic idea of MIPS is that particles swim into each other and block their ways. This leads to a local clustering as it is shown in Fig. 1.2(a). At sufficiently high activity and particle density, the growth of local clusters is observed, leading eventually to a macroscopic phase separation in the system. For an overview of the literature that deals with MIPS we refer to the introduction of Ref. [3] and to the review article [16]. What makes ABP fundamentally different from passive Brownian particles is the driving of the particles due to activity. This drives ABPs far from equilibrium, and hence many techniques established in equilibrium colloidal science are not appropriate for ABP, including proper definitions of thermodynamic variables, such as thermodynamic potentials and the derivatives of them, and the use of Monte Carlo computer simulations.

1.2 One-body descriptions of classical fluids

As colloidal suspensions typically consist of large numbers of particles, a statistical description is a natural choice for such systems. Many of the physical effects originate in the interparticle

interactions between the colloids. Given the large number of degrees of freedom the many-body problem is a challenge. It is convenient to describe the system with one-body theories, where coarse-grained fields, such as the density distribution, are the central objects of the model. Many-body computer simulations are often used to validate theoretical models. In this section, the discussion is focused on one-body theories based on variational principles: density functional theory, dynamical density functional theory, and power functional theory. The equations in these theories can be derived from first principles, i.e. the microscopic many-body description of the system, which set them apart from other coarse-grained theories, such as hydrodynamics. A good overview of current research and important breakthroughs in density functional theory is given by Evans *et al.* in Ref. [17]. The use of numerical simulations and especially Brownian dynamics simulations for active matter is discussed in Sec. 2.1.

Density Functional Theory

Density functional theory (DFT) for classical fluids in thermodynamic equilibrium is based on the theorem that the grand potential is a unique functional of the one-body density [18]. DFT allows the study of equilibrium thermodynamics of fluids and is especially useful for spatially inhomogeneous situations. In the following discussion classical fluids consisting of N interacting particles with positions $\{\mathbf{r}_1 \dots \mathbf{r}_N\} \equiv \mathbf{r}^N$ and interaction potential $U(\mathbf{r}^N)$ in an external potential $V^{\text{ext}}(\mathbf{r})$ are considered. The equilibrium one-body density distribution for such systems is [19]

$$\bar{\rho}(\mathbf{r}) = \langle \hat{\rho}(\mathbf{r}) \rangle_{\text{eq}}, \quad (1.1)$$

where

$$\hat{\rho}(\mathbf{r}) = \sum_{i=1}^N \delta(\mathbf{r} - \mathbf{r}_i) \quad (1.2)$$

is the density operator, with $\delta(\cdot)$ being the Dirac distribution, and \mathbf{r}_i the position of particle $i = 1 \dots N$. The average in (1.1) is an equilibrium ensemble average according to $\langle f \rangle_{\text{eq}} = \int d\mathbf{r}^N f \Phi(\mathbf{r}^N)$, where f is a test function and $\Phi(\mathbf{r}^N)$ is the normalized many-body equilibrium probability distribution in configuration space. The variational principle for the grand potential density functional Ω states that the functional is minimal at the equilibrium density profile. That is,

$$\left. \frac{\delta \Omega[\tilde{\rho}]}{\delta \tilde{\rho}(\mathbf{r})} \right|_{\tilde{\rho}=\bar{\rho}} = 0 \quad (\text{min}). \quad (1.3)$$

where $\tilde{\rho}(\mathbf{r})$ is a trial density field. The functional derivative vanishes at the equilibrium density profile and therefore $\bar{\rho}(\mathbf{r})$ minimizes the functional $\Omega[\rho]$. Furthermore, the thermodynamic grand potential, Ω_0 , is given by the minimal value of the grand potential density functional, $\Omega[\bar{\rho}] = \Omega_0$.

As the Helmholtz free energy $F[\rho]$ is a unique functional of the one-body density [18] and

$$\Omega[\rho] = F[\rho] + \int d\mathbf{r} \rho(\mathbf{r}) V^{\text{ext}}(\mathbf{r}) - \mu \int d\mathbf{r} \rho(\mathbf{r}), \quad (1.4)$$

where μ is the chemical potential, the discussion is based on the free energy functional $F[\rho]$ in the following. Using (1.4) the minimization principle (1.3) becomes

$$\left. \frac{\delta F[\tilde{\rho}]}{\delta \tilde{\rho}(\mathbf{r})} \right|_{\tilde{\rho}=\bar{\rho}} = \mu - V^{\text{ext}}(\mathbf{r}). \quad (1.5)$$

The free energy can be split into an ideal part and an excess (over ideal) part, $F[\rho] = F_{\text{id}}[\rho] + F_{\text{exc}}[\rho]$, with the ideal part being exactly

$$F_{\text{id}}[\rho] = k_{\text{B}} T \int d\mathbf{r} \rho(\mathbf{r}) \left(\ln \left(\lambda^d \rho(\mathbf{r}) \right) - 1 \right), \quad (1.6)$$

where k_{B} is the Boltzmann constant, T is the absolute temperature, λ is the thermal de Broglie wavelength, and d is the spatial dimensionality of the system.

The excess part accounts for the interactions between the particles given by the interparticle interaction potential $U(\mathbf{r}^N)$. The interactions between the particles can be very complex as U depends on the complete configuration of the particles. Hence, F_{exc} contains the full complexity of the many-body problem and is not known exactly in most cases. One exception is the system of one-dimensional hard rods, for which the free energy functional was obtained by Percus [20]. Commonly used approximations for other systems are for example the mean-field approximation (see Ref. [21] and references therein) and Rosenfeld's fundamental measure theory for hard systems [22, 23]. The latter has also been successfully applied to two-dimensional systems of hard disks [24, 25].

Equation (1.5) is the fundamental equation for DFT and forms a basis in the theory of non-uniform liquids, as it allows the calculation of equilibrium densities and thermodynamics.

Dynamical Density Functional Theory

As systems at equilibrium make up only the minority of the physical systems in nature, a treatment of out-of-equilibrium systems is needed. The fundamental equation for a system of N interacting overdamped Brownian particles is the Smoluchowski equation [26]. The Smoluchowski equation is a partial differential equation for the time-dependent probability distribution $\Phi(\mathbf{r}^N, t)$:

$$\frac{\partial \Phi(\mathbf{r}^N, t)}{\partial t} = - \sum_{i=1}^N \nabla_i \cdot \hat{\mathbf{v}}_i \Phi(\mathbf{r}^N, t), \quad (1.7)$$

where ∇_i is the derivative with respect to \mathbf{r}_i , and $\hat{\mathbf{v}}_i$ is the velocity operator. The latter is in general given by

$$\gamma \hat{\mathbf{v}}_i = -(\nabla_i U(\mathbf{r}^N)) - (\nabla_i V^{\text{ext}}(\mathbf{r}_i, t)) + \mathbf{X}(\mathbf{r}_i, t) - k_B T \nabla_i, \quad (1.8)$$

where γ is the friction coefficient and $\mathbf{X}(\mathbf{r}_i, t)$ is a non-conservative external force. In the following we derive a partial differential equation for the one-body density from (1.7). This involves an exact sum rule derived from DFT. Therefore the approach presented here is referred to as an extension to DFT to nonequilibrium called dynamical density functional theory (DDFT) [18, 27]. In the following, the interparticle interaction is considered to be a pairwise interparticle interaction, i.e. $U(\mathbf{r}^N) = \frac{1}{2} \sum_{i \neq j} \phi(\mathbf{r}_i, \mathbf{r}_j)$, where $\sum_{i \neq j}$ is the double sum over all $i = 1..N$, $j = 1..N$, excluding the term $i = j$. Following the approach of Archer and Evans [28], the next step is integrating (1.7) over all particle coordinates but one. This yields an equation for the one-body density

$$\begin{aligned} \gamma \frac{\partial \rho(\mathbf{r}_1, t)}{\partial t} = & k_B T \nabla_1^2 \rho(\mathbf{r}_1, t) + \nabla_1 \cdot \rho(\mathbf{r}_1, t) \nabla_1 V^{\text{ext}}(\mathbf{r}_1, t) \\ & - \nabla_1 \cdot \rho(\mathbf{r}_1, t) \mathbf{X}(\mathbf{r}_1, t) + \nabla_1 \cdot \int d\mathbf{r}_2 \rho^{(2)}(\mathbf{r}_1, \mathbf{r}_2, t) \nabla_1 \phi(\mathbf{r}_1, \mathbf{r}_2), \end{aligned} \quad (1.9)$$

where the one-body density is given by integrating the time-dependent probability function,

$$\rho(\mathbf{r}_1, t) = N \int d\mathbf{r}_2 \dots d\mathbf{r}_N \Phi(\mathbf{r}^N, t). \quad (1.10)$$

Similarly, the two-body density is

$$\rho^{(2)}(\mathbf{r}_1, \mathbf{r}_2, t) = N(N-1) \int d\mathbf{r}_3 \dots d\mathbf{r}_N \Phi(\mathbf{r}^N, t). \quad (1.11)$$

In equilibrium there exist an exact sum rule for the integral term in (1.9) [18],

$$\int d\mathbf{r}_2 \frac{\rho^{(2)}(\mathbf{r}_1, \mathbf{r}_2)}{\rho(\mathbf{r}_1)} \nabla_1 \phi(\mathbf{r}_1, \mathbf{r}_2) = \nabla_1 \left. \frac{\delta F_{\text{exc}}[\tilde{\rho}(\mathbf{r}_1)]}{\delta \tilde{\rho}(\mathbf{r}_1)} \right|_{\tilde{\rho}=\rho(\mathbf{r}_1)}, \quad (1.12)$$

where $\tilde{\rho}(\mathbf{r})$ is a trial density field. Inserting (1.12) in (1.9) yields

$$\gamma \frac{\partial \rho(\mathbf{r}, t)}{\partial t} = \nabla \cdot \rho(\mathbf{r}, t) \left(k_B T \nabla \ln \rho(\mathbf{r}, t) + \nabla V^{\text{ext}}(\mathbf{r}, t) - \mathbf{X}(\mathbf{r}, t) + \nabla \left. \frac{\delta F_{\text{exc}}[\tilde{\rho}(\mathbf{r})]}{\delta \tilde{\rho}(\mathbf{r})} \right|_{\tilde{\rho}=\rho(\mathbf{r}, t)} \right), \quad (1.13)$$

where the first term in the brackets accounts for the first term on the right hand side of (1.9), as $\nabla \cdot \rho \nabla \ln \rho = \nabla \cdot \rho^{\frac{1}{2}} \nabla \rho = \nabla^2 \rho$. Approximating the expression involving the two-body density by an equilibrium sum rule, which is formally exact only in equilibrium, is known as the adiabatic approximation. The underlying idea is that the one-body density evolves adiabatically through a series of states that are approximated by equilibrium states and genuine nonequilibrium effects

are absent.

Equation (1.13) is the fundamental equation of DDFT. Alternatively the DDFT equation (1.13) can be given in the form of the continuity equation,

$$\frac{\partial \rho(\mathbf{r}, t)}{\partial t} = -\nabla \cdot \mathbf{J}^{\text{DDFT}}(\mathbf{r}, t), \quad (1.14)$$

where the one-body DDFT current is

$$\mathbf{J}^{\text{DDFT}}(\mathbf{r}, t) = -\gamma^{-1} \rho(\mathbf{r}, t) \left(k_{\text{B}} T \nabla \ln \rho(\mathbf{r}, t) + \nabla V^{\text{ext}}(\mathbf{r}, t) - \mathbf{X}(\mathbf{r}, t) + \nabla \frac{\delta F_{\text{exc}}[\tilde{\rho}(\mathbf{r})]}{\delta \tilde{\rho}(\mathbf{r})} \Big|_{\tilde{\rho}=\rho(\mathbf{r}, t)} \right). \quad (1.15)$$

Although DDFT only gives approximate results, it has been used for a variety of nonequilibrium systems, especially for systems close to equilibrium and relaxation processes. A typical problem studied with DDFT is a system in equilibrium with the density profile $\bar{\rho}(\mathbf{r})$ that is driven out of equilibrium at a certain time t_0 by e.g. an external driving force. The time dependent one-body density is then given by

$$\rho(\mathbf{r}, t) = \bar{\rho}(\mathbf{r}) - \int_{t_0}^t d\tilde{t} \nabla \cdot \mathbf{J}^{\text{DDFT}}(\mathbf{r}, \tilde{t}). \quad (1.16)$$

The adiabatic assumption in this context is that at each time t' the system is treated as an equilibrium system with the equilibrium density $\bar{\rho}' = \rho(\mathbf{r}, t')$. This density is then used to calculate the functional derivative of the excess free energy. With this the “new” density at time $t'' = t' + dt$, $\rho(\mathbf{r}, t'')$, is calculated by using (1.13). Next, it is used again as equilibrium density, $\bar{\rho}'' = \rho(\mathbf{r}, t'')$ which enters in the functional derivative. This iteration process eventually yields the whole time evolution of the one-body density.

Power Functional Theory

A general approach for nonequilibrium Brownian system that goes beyond DDFT is power functional theory (PFT) [29, 30]. PFT is the exact nonequilibrium generalization of equilibrium DFT. First developed for overdamped classical systems [29], PFT can be used to describe classical Newtonian [31] and quantum many-body systems [32]. The central object in PFT is the time-dependent power functional $R_t[\rho, \mathbf{J}]$, which is a unique functional of both the one-body density distribution

$$\rho(\mathbf{r}, t) = \langle \hat{\rho}(\mathbf{r}^N) \rangle, \quad (1.17)$$

and the one-body current distribution

$$\mathbf{J}(\mathbf{r}, t) = \left\langle \sum_{i=1}^N \delta(\mathbf{r} - \mathbf{r}_i) \hat{\mathbf{v}}_i(\mathbf{r}^N, t) \right\rangle, \quad (1.18)$$

where $\hat{\rho}(\mathbf{r}^N)$ is the density operator according to (1.2), and $\hat{\mathbf{v}}_i(\mathbf{r}^N, t)$ is the velocity operator according to (1.8). The average is an ensemble average in configuration space:

$$\langle f(\mathbf{r}^N, t) \rangle = \int d\mathbf{r}^N f(\mathbf{r}^N, t) \Phi(\mathbf{r}^N, t), \quad (1.19)$$

where the operator $f(\mathbf{r}^N, t)$ acts on $\Phi(\mathbf{r}^N, t)$, the time-dependent probability distribution determined by the Smoluchowski equation, (1.7) and (1.8). The physical time evolution of the system is such that R_t is minimal at any time with respect to the variation in the one-body current. Hence there exist a variational principle similar to DFT, but with respect to the current while keeping the density fixed,

$$\left. \frac{\delta R_t[\rho, \mathbf{J}]}{\delta \mathbf{J}(\mathbf{r}, t)} \right|_{\rho=\rho^0, \mathbf{J}=\mathbf{J}^0} = 0 \quad (\text{min}), \quad (1.20)$$

where the superscript in ρ^0 and \mathbf{J}^0 labels quantities at the minimum of R_t . Equation (1.20) gives the force balance equation on the one-body level; and thus the current \mathbf{J}^0 . This is equivalent to the eigenvalue of the velocity operator of a particle being the physically correct velocity, $\hat{\mathbf{v}}_i \Phi = \mathbf{v}_i \Phi$. Consequently the current at the minimum yields $\mathbf{J}^0 = \langle \sum_i \delta(\mathbf{r} - \mathbf{r}_i) \mathbf{v}_i \rangle$, and the velocity is

$$\gamma \mathbf{v}_i = -(\nabla_i U) - (\nabla_i V^{\text{ext}}) + \mathbf{X} - k_B T (\nabla_i \ln \Phi), \quad (1.21)$$

where the brackets in the last term indicate a gradient field and not a differential operation. Hence the one-body variational principle can be easily translated on the many-body level. The density follows then straightforwardly from integrating the continuity equation,

$$\frac{\partial \rho^0(\mathbf{r}, t)}{\partial t} = -\nabla \cdot \mathbf{J}^0(\mathbf{r}, t). \quad (1.22)$$

An Euler-Lagrange equation for the density while keeping the current fixed can be formulated as well,

$$\left. \frac{\delta R_t[\rho, \mathbf{J}]}{\delta \rho(\mathbf{r}, t)} \right|_{\rho=\rho^0, \mathbf{J}=\mathbf{J}^0} = \alpha(\mathbf{r}, t), \quad (1.23)$$

where α is a Lagrange multiplier imposed by the continuity equation (1.22). The power functional itself can be split into an external part and four internal parts: an ideal and an excess part for reversible processes, called *adiabatic* parts, and an ideal and an excess part for irreversible processes, called *superadiabatic* contributions. The external part is

$$X_t[\rho, \mathbf{J}] = \int d\mathbf{r} (-\nabla V^{\text{ext}}(\mathbf{r}, t) + \mathbf{X}(\mathbf{r}, t)) \cdot \mathbf{J}(\mathbf{r}, t), \quad (1.24)$$

which is the power due to external forces. The reversible internal parts are the time derivative (indicated by a dot) of the free energy $\dot{F}[\rho] = \dot{F}_{\text{id}}[\rho] + \dot{F}_{\text{exc}}[\rho]$. With (1.6) and (1.22) it yields

after integrating by parts

$$\dot{F}_{\text{id}}[\rho] = k_{\text{B}}T \int d\mathbf{r} \mathbf{J} \cdot \nabla \ln \rho(\mathbf{r}, t), \quad (1.25)$$

whereas the excess part is given by

$$\dot{F}_{\text{exc}}[\rho] = \int d\mathbf{r} \mathbf{J} \cdot \nabla \left. \frac{\delta F_{\text{exc}}[\tilde{\rho}]}{\delta \tilde{\rho}(\mathbf{r})} \right|_{\tilde{\rho}=\rho(\mathbf{r},t)}, \quad (1.26)$$

where we applied the adiabatic approximation for the functional derivative of F_{exc} . The irreversible parts of the internal power are split into an ideal and an excess part as well, where

$$P_t^{\text{id}}[\rho, \mathbf{J}] = \int d\mathbf{r} \frac{\gamma \mathbf{J}^2(\mathbf{r}, t)}{2\rho(\mathbf{r}, t)} \quad (1.27)$$

is the ideal part and the excess part, $P_t^{\text{exc}}[\rho, \mathbf{J}]$ is unknown as an explicit expression in general. As $P_t^{\text{exc}}[\rho, \mathbf{J}]$ is determined by the interparticle interactions, it has to be approximated, similar to $F_{\text{exc}}[\rho]$ in equilibrium DFT. The power functional can then be brought in the form

$$R_t[\rho, \mathbf{J}] = \dot{F}_{\text{id}}[\rho] + \dot{F}_{\text{exc}}[\rho] + P_t^{\text{id}}[\rho, \mathbf{J}] + P_t^{\text{exc}}[\rho, \mathbf{J}] - X_t[\rho, \mathbf{J}]. \quad (1.28)$$

Applying the variational principle (1.20) to (1.28) yields the force balance equation

$$\frac{\gamma \mathbf{J}^0(\mathbf{r}, t)}{\rho^0(\mathbf{r}, t)} = -k_{\text{B}}T \nabla \ln \rho^0(\mathbf{r}, t) - \nabla \left. \frac{\delta F_{\text{exc}}[\rho]}{\delta \rho(\mathbf{r})} \right|_{\rho=\rho^0} - \left. \frac{\delta P_t^{\text{exc}}[\rho, \mathbf{J}]}{\delta \mathbf{J}(\mathbf{r}, t)} \right|_{\rho=\rho^0, \mathbf{J}=\mathbf{J}^0} - \nabla V^{\text{ext}}(\mathbf{r}, t) + \mathbf{X}(\mathbf{r}, t). \quad (1.29)$$

PFT goes beyond DDFT accounting for dissipative and irreversible processes. No adiabatic approximation is necessary to obtain the force balance equation (1.29), contrary to DDFT. However, by setting the excess dissipation to zero, $P_t^{\text{exc}} = 0$, one obtains the DDFT current (1.15) from (1.29). The price to pay for the full nonequilibrium dynamics is that new approximations have to be found for the (excess dissipation) functional, $P_t^{\text{exc}}[\rho, \mathbf{J}]$ [33]. Thereby the nonequilibrium effects described by P_t^{exc} are generally beyond dissipation and cover for example structure formation [34]. Recent work by Fortini *et al.* demonstrated that the forces generated by the functional derivative of P_t^{exc} with respect to the current might not be a small correction to DDFT, and hence have to be taken into account in out-of-equilibrium situations [35]. In summary, PFT is an important extension to DDFT and allows a more detailed study and understanding of nonequilibrium systems. The theory connects the advantages of having a variational principle with the possibility of describing the full dynamics on the one-body level. The fundamental one-body fields $\rho(\mathbf{r}, t)$ and $\mathbf{J}(\mathbf{r}, t)$ are thereby determined by the continuity equation and a force balance equation, respectively.

PFT may be used in the same situations as DDFT, where for example a systems is driven out of equilibrium. This is necessary because the variational principle only gives the physical current,

which is used to calculate the dynamics of the density. Hence this only yields reasonable results if the density imposed in the variational calculus is already the physically correct one. A possible initial value for the density is the equilibrium value, as it can be obtained by DFT.

2 Aim of this thesis and author's contribution to publications

This cumulative thesis aims to provide new insights into the physical behavior of active Brownian particles (ABP) by formulating an effective equilibrium approach and a power functional theory (PFT) for the problem. Both approaches reduce the complexity in the description of the system. The effective equilibrium approach reduces the degrees of freedom significantly, as orientations are integrated out. PFT is a one-body theory and hence allows an even more efficient description of ABP, as the dynamics is given by only the one-body density and the one-body current.

There are four publications (two published [1, 2], one submitted [3], one in preparation [4]) that contribute to the thesis, each dealing either with the direct formulation of PFT for active systems [2, 3], the formulation of an effective equilibrium description of active Brownian particles [1] or applications of these approaches to phase separation [1, 2] and interfaces [4]. All results are tested against Brownian dynamics simulations, and all concepts are suitable for systems of active Brownian particles.

An overview of the articles is also given in Sec. 6, where all contributing publications are included in chronological order. Regarding the manuscript on the fluid-fluid interface in phase-separated active particle systems that is in preparation [4]; we include an abstract in Sec. 6 and we give results from computer simulation, relevant comparisons, and an outlook about the theory in Sec. 4.

In all publications the author's contribution is the performance of Brownian dynamics (BD) computer simulations, which includes the extension of the BD simulation scheme to active systems, and the improvement and development of sampling strategies, especially to sample currents, velocities, and the power functional in steady state. The simulations play a very important role as they give validation of the theoretical models. I have also contributed substantially to the development of the theoretical methods and the preparation of the manuscripts.

2.1 Brownian dynamics simulations of active Brownian particles

Brownian dynamics simulations

In order to test theoretical predictions, computer simulations became a widely spread tool over the last decades. Simulations are cheap and easy to realize compared to experiments. In contrast to the theoretical approaches discussed above, computer simulations are used to investigate the many-body dynamics and stationary states of many-body problems. In colloidal science Monte Carlo simulations are often used to understand the equilibrium properties of the sys-

tem [36]. Alongside other techniques, such as molecular dynamics simulations, the dynamics of out-of-equilibrium systems is frequently investigated with Brownian dynamics (BD) simulations. Therein the collisions between the particles and the solvent molecules are not explicitly calculated. Instead, the Brownian motion of the particles is recovered by considering the over-damped Langevin equation of motion

$$\dot{\mathbf{r}}_i(t) = \gamma^{-1} \mathbf{F}_i^{\text{det}}(\mathbf{r}^N) + \boldsymbol{\xi}_i(t), \quad (2.1)$$

where $\mathbf{F}_i^{\text{det}}$ is the total (deterministic) force that acts on particle i with coordinates \mathbf{r}_i . This force can in general consist of interparticle interaction forces imposed by the complete configuration of the N particles, and external forces that may be both conservative and non-conservative. Furthermore the random displacements imposed by the solvent molecules are modeled by a Gaussian random variable $\boldsymbol{\xi}_i(t)$ with zero mean, $\langle \boldsymbol{\xi}_i(t) \rangle = 0$, and time correlation $\langle \boldsymbol{\xi}_i(t) \boldsymbol{\xi}_j(t') \rangle = 2D_{\text{trans}} \mathbf{1} \delta_{ij} \delta(t - t')$, where $D_{\text{trans}} = k_B T / \gamma$ is the (translational) diffusion coefficient, δ_{ij} is the Kronecker symbol, $\delta(\cdot)$ is the Dirac distribution, and $\mathbf{1}$ is the identity matrix. For computer simulations the equation of motion is discretized and integrated by a forward Euler algorithm,

$$\mathbf{r}(t + \Delta t) = \mathbf{r}(t) + \gamma^{-1} \mathbf{F}_i^{\text{det}} \Delta t + \delta \mathbf{x} \Delta t, \quad (2.2)$$

where Δt is the discrete time step. The noise is modeled by the random displacement $\delta \mathbf{x}$, which is sampled from a Gaussian distribution with zero mean and a standard deviation given by $\sigma = \sqrt{2D_{\text{trans}} \Delta t}$, in order to fit the auto-correlator of $\boldsymbol{\xi}_i$ above [37].

Application to ABP

In general for ABP two Langevin equations have to be considered, one translational Langevin equation, and one rotational Langevin equation.

Computer simulations in [1] are performed in three dimensions, where the orientation of particle i , $\boldsymbol{\omega}_i$, is a unit vector. The equations of motion are

$$\dot{\mathbf{r}}_i(t) = s \boldsymbol{\omega}_i(t) - \gamma^{-1} \nabla_i \sum_{i \neq j} \phi(r_{ij}) + \boldsymbol{\xi}_i(t), \quad (2.3)$$

$$\dot{\boldsymbol{\omega}}_i(t) = \boldsymbol{\eta}_i(t) \times \boldsymbol{\omega}_i(t), \quad (2.4)$$

where s is the free swim speed of an individual particle, and the stochastic vectors $\boldsymbol{\xi}_i$ and $\boldsymbol{\eta}_i$ are both Gaussian white noise with zero mean and auto-correlations given by

$$\langle \boldsymbol{\xi}_i(t) \boldsymbol{\xi}_j(t') \rangle = 2D_{\text{trans}} \mathbf{1} \delta_{ij} \delta(t - t'), \quad (2.5)$$

$$\langle \boldsymbol{\eta}_i(t) \boldsymbol{\eta}_j(t') \rangle = 2D_{\text{rot}} \mathbf{1} \delta_{ij} \delta(t - t'), \quad (2.6)$$

where $D_{\text{trans}} = k_B T / \gamma$ and $D_{\text{rot}} = k_B T / \gamma^\omega$ are the translational and the rotational diffusion coefficient, with the corresponding friction coefficients γ and γ^ω , respectively.

Computer simulations contributing to [2–4], and Sec. 4 are carried out in two dimensions. There

the orientation vector is defined as

$$\boldsymbol{\omega}_i(t) = (\cos \varphi_i(t), \sin \varphi_i(t))^t, \quad (2.7)$$

where the angle φ_i is measured against the x -axis. Hence the equations of motion for translational and rotational motion are

$$\dot{\mathbf{r}}_i(t) = s\boldsymbol{\omega}_i(t) - \gamma^{-1}\nabla_i \sum_{i \neq j} \phi(r_{ij}) + \boldsymbol{\xi}_i(t), \quad (2.8)$$

$$\dot{\varphi}_i(t) = \eta_i(t), \quad (2.9)$$

respectively. The stochastic vector $\boldsymbol{\xi}_i$ has the same properties as in three dimensions given by the correlator (2.5). The stochastic variable η_i is a scalar describing Gaussian white noise with zero mean and auto-correlation

$$\langle \eta_i(t)\eta_j(t') \rangle = 2D_{\text{rot}}\delta_{ij}\delta(t-t'). \quad (2.10)$$

The interparticle interaction in two and three dimensions is given by a pair interaction potential $\phi(r_{ij})$ that only depends on the distance between the interacting particles $r_{ij} = |\mathbf{r}_i - \mathbf{r}_j|$. In this thesis we use a variety of interaction potentials. In [1] we used a soft core potential of the form

$$\phi_{\text{SC}}(r_{ij}) = \epsilon \left(\frac{\sigma}{r_{ij}} \right)^{12}, \quad (2.11)$$

where σ is the assigned diameter of the particles and serves as the fundamental unit of length, and ϵ is the fundamental unit of energy in the system. Furthermore in [1] we used a Lennard-Jones potential

$$\phi_{\text{LJ}}(r_{ij}) = 4\epsilon \left[\left(\frac{\sigma}{r_{ij}} \right)^{12} - \left(\frac{\sigma}{r_{ij}} \right)^6 \right]. \quad (2.12)$$

In the other publications, [2–4], and Sec. 4, we used the Weeks-Chandler-Anderson (WCA) potential [38]. The WCA potential is a Lennard-Jones potential that is cut and shifted at the minimum. Therefore force artifacts are prevented. The potential is given by

$$\phi_{\text{WCA}}(r_{ij}) = \begin{cases} 4\epsilon \left[\left(\frac{\sigma}{r_{ij}} \right)^{12} - \left(\frac{\sigma}{r_{ij}} \right)^6 \right] + \epsilon, & \text{for } r_{ij} < 2^{1/6}\sigma, \\ 0, & \text{otherwise.} \end{cases} \quad (2.13)$$

As a common measure for activity, the Peclet number,

$$\text{Pe} = \frac{\gamma s \sigma}{k_{\text{B}}T}, \quad (2.14)$$

is used. The Peclet number describes the ratio between self-propulsion motion and thermal motion. For $\text{Pe} \gg 1$ the dynamics is dominated by swimming, while for $\text{Pe} \ll 1$ thermal motion

is dominant.

In practice we consider N active particles in a cubic box in three dimension with side lengths L and total volume $V = L^3$ [1], and in a rectangle box with side lengths L_x and L_y in two dimensions [2, 3], and Sec. 4. In general periodic boundary conditions are used in all spatial dimensions and the particles are initialized with random positions and orientations. For the work on the bulk properties in two dimensions, i.e. [2, 3], we use a square box with $L_x = L_y$. The simulations of interfacial properties are carried out in an elongated box where $L_x > L_y$. Furthermore, we fix the center of mass of all particles to the center of the box. With this a stable interface parallel to the short side of the box emerges and good sampling statistics are achieved. After the random initialization we let the system reach a steady state for n_{equi} steps in all simulation runs. After that the relevant quantities are sampled for n_{sample} steps. The averaged results for a given quantity \mathcal{O} are obtained by averaging over time and over particles according to

$$\mathcal{O} = \langle \mathcal{O}_i(j) \rangle = \frac{1}{N} \sum_{i=1}^N \frac{1}{n_{\text{sample}}} \sum_{j=1}^{n_{\text{sample}}} \mathcal{O}_i(j), \quad (2.15)$$

where $\mathcal{O}_i(j)$ denotes the quantity for particle i at the discrete time j . With a sufficiently large number of particles and sampling steps the average (2.15) approaches the ensemble average (1.19).

Further simulation details depend on the particular systems. All details are included in the publications.

2.2 Power sampling

Power functional theory gives a many-body expression for the power functional evaluated at the minimum, R_t^0 , i.e. at the physical time evolution [2, 3]:

$$R_t^0 = -\frac{\gamma}{2} \left\langle \sum_i \mathbf{v}_i(t)^2 \right\rangle, \quad (2.16)$$

where $\mathbf{v}_i(t)$ is the velocity of particle i at time t , given as a configuration space function by (1.21), and the average $\langle \cdot \rangle$ is an ensemble average as given by (1.19). We aim to relate the Smoluchowski many-body description given by (2.16) and to the Langevin many-body description, i.e., a trajectory based approach to the many-body problem.

In this section the equivalence of both pictures is examined. This is particularly useful as the trajectories can explicitly be calculated in Brownian dynamics (BD) computer simulations. Following previous work on current sampling in BD [35, 39], the velocity of particle i in BD is calculated via the central time derivative of the position vector,

$$\mathbf{v}_i^{\text{BD}}(t) = \frac{\mathbf{r}_i(t + \Delta t) - \mathbf{r}_i(t - \Delta t)}{2\Delta t}, \quad (2.17)$$

where Δt is the discrete time step in the simulation.

Using this definition we can sample the quantity Λ_t , which is defined as

$$\Lambda_t = -\frac{\gamma}{2} \left\langle \sum_i \mathbf{v}_i^{\text{BD}}(t)^2 \right\rangle, \quad (2.18)$$

where the average is calculated according to (2.15). In the following we explain the sampling of Λ_t by considering $\langle \mathbf{v}_i^{\text{BD}}(t)^2 \rangle$ in detail, as is necessary in order to carry out the average (2.18) efficiently.

We take into account that the discrete dynamics is integrated by the Euler algorithm, c.f. (2.2).

The velocity (2.17) can be expressed as

$$\mathbf{v}_i^{\text{BD}}(t) = \frac{\Delta \mathbf{r}_i(t) + \Delta \mathbf{r}_i(t_-)}{2\Delta t}, \quad (2.19)$$

where t_- is a shorthand notation, $t_- = t - \Delta t$. The vector $\Delta \mathbf{r}_i(t) = \mathbf{r}_i(t + \Delta t) - \mathbf{r}_i(t)$ is the total displacement of particle i between t and $t + \Delta t$, and $\Delta \mathbf{r}_i(t_-) = \mathbf{r}_i(t) - \mathbf{r}_i(t - \Delta t)$ is the total displacement of particle i between $t - \Delta t$ and t . These displacements can be further split into displacements due to the interparticle interaction force, $\Delta \mathbf{r}_i^{\text{int}}(t)$, the external force, $\Delta \mathbf{r}_i^{\text{ext}}(t)$, and the random displacement, $\Delta \mathbf{r}_i^{\text{ran}}(t)$, i.e.,

$$\Delta \mathbf{r}_i(t) = \Delta \mathbf{r}_i^{\text{int}}(t) + \Delta \mathbf{r}_i^{\text{ext}}(t) + \Delta \mathbf{r}_i^{\text{ran}}(t). \quad (2.20)$$

For the active Brownian particles considered here, the individual contributions are defined by

$$\Delta \mathbf{r}_i^{\text{int}}(t) = \gamma^{-1} \mathbf{F}_i^{\text{int}}(t) \Delta t, \quad (2.21)$$

$$\Delta \mathbf{r}_i^{\text{ext}}(t) = s \boldsymbol{\omega}_i(t) \Delta t, \quad (2.22)$$

$$\Delta \mathbf{r}_i^{\text{ran}}(t) = \boldsymbol{\xi}_i(t) \Delta t, \quad (2.23)$$

where the internal force, $\mathbf{F}_i^{\text{int}}$, is given by the negative gradient with respect to the position of particle i of the interaction potential, $\mathbf{F}_i^{\text{int}} = -\nabla_i U(\mathbf{r}^N, \boldsymbol{\omega}^N)$. Inserting (2.19) in (2.18) with (2.20), (2.21), (2.22) and (2.23), yields 36 different contributions to $\langle \mathbf{v}_i^{\text{BD}}(t)^2 \rangle$ in total. Table 2.1 gives all possible terms. Of all 36 combinations only three are non-trivial, namely $\langle \Delta \mathbf{r}_i^{\text{int}}(t) \cdot \Delta \mathbf{r}_i^{\text{int}}(t) \rangle$, $\langle \Delta \mathbf{r}_i^{\text{int}}(t) \cdot \Delta \mathbf{r}_i^{\text{ext}}(t) \rangle$, and $\langle \Delta \mathbf{r}_i^{\text{ran}}(t_-) \cdot \Delta \mathbf{r}_i^{\text{int}}(t) \rangle$, which we refer to as INT – INT, INT – EXT, and RAN – INT, respectively, in table 2.1. In the following we will first discuss the trivial terms that are either zero or finite and constant. Second, the non-trivial correlators are discussed in detail. Next, we give a proof of concept of the power sampling method that is provided by a nonequilibrium sum rule, and discuss the relationship between R_t^0 and Λ_t .

Trivial correlators. All trivial correlators that vanish involve a random displacement combined with either an internal or an external displacement. As the random displacement is a Gaussian distributed random number, the average of this number multiplied by any arbitrary number (in this case an internal or an external displacement) is zero. The only exception is the RAN – INT (i.e. $\langle \Delta \mathbf{r}_i^{\text{ran}}(t_-) \cdot \Delta \mathbf{r}_i^{\text{int}}(t) \rangle$) correlator, as it gives a finite value. This correlator is discussed in

	$\Delta\mathbf{r}_i^{\text{int}}(t_-)$	$\Delta\mathbf{r}_i^{\text{ext}}(t_-)$	$\Delta\mathbf{r}_i^{\text{ran}}(t_-)$	$\Delta\mathbf{r}_i^{\text{int}}(t)$	$\Delta\mathbf{r}_i^{\text{ext}}(t)$	$\Delta\mathbf{r}_i^{\text{ran}}(t)$
$\Delta\mathbf{r}_i^{\text{int}}(t_-)$	INT – INT	INT – EXT	0	INT – INT	INT – EXT	0
$\Delta\mathbf{r}_i^{\text{ext}}(t_-)$	INT – EXT	$(s\Delta t)^2$	0	INT – EXT	$(s\Delta t)^2$	0
$\Delta\mathbf{r}_i^{\text{ran}}(t_-)$	0	0	$4D_{\text{trans}}\Delta t$	RAN – INT	0	0
$\Delta\mathbf{r}_i^{\text{int}}(t)$	INT – INT	INT – EXT	RAN – INT	INT – INT	INT – EXT	0
$\Delta\mathbf{r}_i^{\text{ext}}(t)$	INT – EXT	$(s\Delta t)^2$	0	INT – EXT	$(s\Delta t)^2$	0
$\Delta\mathbf{r}_i^{\text{ran}}(t)$	0	0	0	0	0	$4D_{\text{trans}}\Delta t$

Table 2.1: All combinations of displacement that contribute to $\langle \mathbf{v}_i^{\text{BD}}(t)^2 \rangle$. The table indicates that each cell is given by the product of the corresponding displacement given by the top row and the first column, averaged over the ensemble. The trivial correlators are given by their exact value, while the non-trivial correlators are labeled as INT – INT for $\langle \Delta\mathbf{r}_i^{\text{int}}(t) \cdot \Delta\mathbf{r}_i^{\text{int}}(t) \rangle$, INT – EXT for $\langle \Delta\mathbf{r}_i^{\text{int}}(t) \cdot \Delta\mathbf{r}_i^{\text{ext}}(t) \rangle$, and RAN – INT for $\langle \Delta\mathbf{r}_i^{\text{ran}}(t_-) \cdot \Delta\mathbf{r}_i^{\text{ext}}(t) \rangle$. For example $\Delta\mathbf{r}_i^{\text{int}}(t)$ combined with $\Delta\mathbf{r}_i^{\text{ext}}(t)$ gives $\langle \Delta\mathbf{r}_i^{\text{int}}(t) \cdot \Delta\mathbf{r}_i^{\text{ext}}(t) \rangle = \text{INT} - \text{EXT}$.

detail together with the other non-trivial correlators below.

Combining two random displacements gives a constant because of the δ -correlated noise $\boldsymbol{\xi}_i(t)$, given by (2.5). The trivial correlators that are constant are thus $\langle \Delta\mathbf{r}_i^{\text{ran}}(t) \cdot \Delta\mathbf{r}_i^{\text{ran}}(t) \rangle$ and $\langle \Delta\mathbf{r}_i^{\text{ran}}(t_-) \cdot \Delta\mathbf{r}_i^{\text{ran}}(t_-) \rangle$. As the δ -distribution of the auto-correlator of the random force, (2.5), is discretized by a random displacement sampled from a Gaussian distribution with zero mean and standard deviation $\sqrt{2D_{\text{trans}}/\Delta t}$, c.f. (2.2), the auto-correlator has the value $\langle \Delta\mathbf{r}_i^{\text{ran}}(t) \cdot \Delta\mathbf{r}_i^{\text{ran}}(t) \rangle = \langle \Delta\mathbf{r}_i^{\text{ran}}(t_-) \cdot \Delta\mathbf{r}_i^{\text{ran}}(t_-) \rangle = \frac{4D_{\text{trans}}}{\Delta t} \Delta t^2$ in two dimensions. Dividing by $4\Delta t^2$ to obtain the contribution of the correlator to the squared velocity gives $D_{\text{trans}}/\Delta t$. Hence the discretization of $\delta(\cdot)$ enters the squared velocity directly and creates a constant numerical value of the order $\mathcal{O}(10^5)$, as Δt is typically of order $\mathcal{O}(10^{-5})$.

The correlators of $\Delta\mathbf{r}_i^{\text{ext}}$ with itself with arbitrary time arguments each are constant, too, and give all the same value:

$\langle \Delta\mathbf{r}_i^{\text{ext}}(t_-) \cdot \Delta\mathbf{r}_i^{\text{ext}}(t) \rangle \approx \langle \Delta\mathbf{r}_i^{\text{ext}}(t) \cdot \Delta\mathbf{r}_i^{\text{ext}}(t) \rangle = \langle \Delta\mathbf{r}_i^{\text{ext}}(t_-) \cdot \Delta\mathbf{r}_i^{\text{ext}}(t_-) \rangle = (s\Delta t)^2$. The reason is that the orientation $\boldsymbol{\omega}_i(t)$ is a unit vector, c.f. (2.22), and because the orientation changes only slightly between two time-steps the correlator with mixed time arguments gives the same values as the correlators with both the same time arguments within small uncertainties due to numerical discretization effects.

Non-trivial correlators. As indicated in table 2.1, the INT – INT and INT – EXT correlators are independent of the time arguments.

Hence, $\langle \Delta\mathbf{r}_i^{\text{int}}(t) \cdot \Delta\mathbf{r}_i^{\text{int}}(t) \rangle = \langle \Delta\mathbf{r}_i^{\text{int}}(t_-) \cdot \Delta\mathbf{r}_i^{\text{int}}(t_-) \rangle \approx \langle \Delta\mathbf{r}_i^{\text{int}}(t) \cdot \Delta\mathbf{r}_i^{\text{int}}(t_-) \rangle$ and $\langle \Delta\mathbf{r}_i^{\text{ext}}(t) \cdot \Delta\mathbf{r}_i^{\text{ext}}(t) \rangle = \langle \Delta\mathbf{r}_i^{\text{ext}}(t_-) \cdot \Delta\mathbf{r}_i^{\text{ext}}(t_-) \rangle \approx \langle \Delta\mathbf{r}_i^{\text{ext}}(t) \cdot \Delta\mathbf{r}_i^{\text{ext}}(t_-) \rangle$. In both cases the first identity follows from the sampling method described above by (2.15), where all times are con-

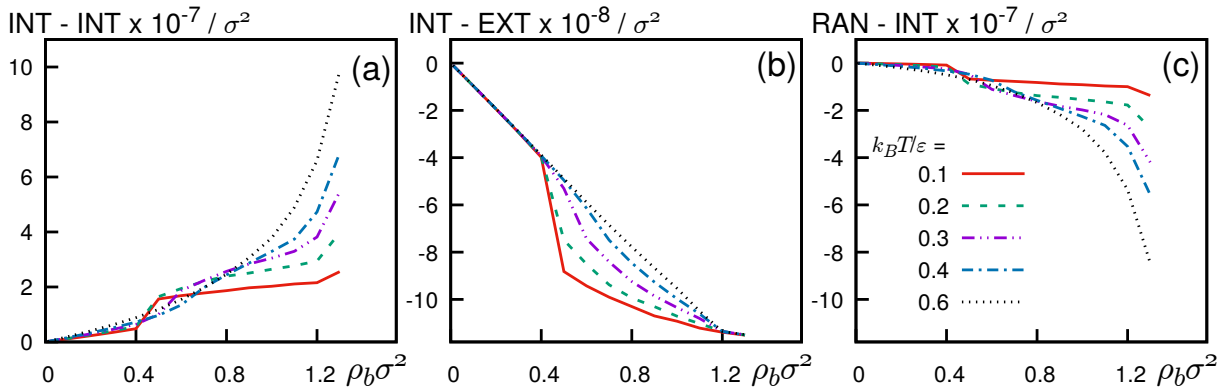


Figure 2.1: The three non-trivial correlators contributing to $\langle \mathbf{v}_i^{\text{BD}}(t)^2 \rangle$ sampled in BD simulations as a function of density for different temperatures. (a) The correlator $\langle \Delta \mathbf{r}_i^{\text{int}}(t) \cdot \Delta \mathbf{r}_i^{\text{int}}(t) \rangle$ is labeled with INT – INT. (b) The correlator $\langle \Delta \mathbf{r}_i^{\text{int}}(t) \cdot \Delta \mathbf{r}_i^{\text{ext}}(t) \rangle$ is labeled with INT – EXT. (c) The correlator $\langle \Delta \mathbf{r}_i^{\text{ran}}(t_-) \cdot \Delta \mathbf{r}_i^{\text{int}}(t) \rangle$ is labeled with RAN – INT. The simulation parameters are given in the text and in [3].

sidered. The correlators with mixed time arguments have in very good approximation the same value as the correlators with the same time arguments, as both the positions and orientations only change slightly during the small time step.

The non-trivial parts are shown in Fig. 2.1 as a function of bulk density for different temperatures, as indicated by color and linestyle. The values of the system parameters are identical to the ones given in Ref. [3]: $N = 5000$ particles are simulated in a two-dimensional square box with side length $L = \sqrt{N/\rho_b}$, interacting via the Weeks-Chandler-Anderson potential, c.f. (2.13). The fundamental units are σ, γ and ϵ . The activity parameters, i.e. the rotational diffusion coefficient and the self-propulsion speed, are given by $D_{\text{rot}}/D_{\text{trans}} = 3\sigma^{-2}$ and $s\sigma\gamma/\epsilon = 24$, respectively. The value of $\langle \Delta \mathbf{r}_i^{\text{int}}(t) \cdot \Delta \mathbf{r}_i^{\text{int}}(t) \rangle$, shown in Fig. 2.1(a), increases with bulk density, as the rate of collisions between the particles increases, and the magnitude of the internal forces increases. The displacements $\Delta \mathbf{r}_i^{\text{int}}(t)$ and $\Delta \mathbf{r}_i^{\text{ext}}$ are anticorrelated, as the negative value of $\langle \Delta \mathbf{r}_i^{\text{int}}(t) \cdot \Delta \mathbf{r}_i^{\text{ext}}(t) \rangle$ in Fig. 2.1(b) indicates. This means that the displacements caused by external forces are counteracted by internal interactions. In the low density limit, $\rho_b \rightarrow 0$, external displacements lead only in very rare events to a collision and no interparticle interaction takes place. As the bulk density increases the probability of collisions caused by external displacements increases as well. Therefore the absolute value of the correlator $\langle \Delta \mathbf{r}_i^{\text{int}}(t) \cdot \Delta \mathbf{r}_i^{\text{ext}}(t) \rangle$ increases.

It remains to specify the correlator $\langle \Delta \mathbf{r}_i^{\text{ran}}(t_-) \cdot \Delta \mathbf{r}_i^{\text{int}}(t) \rangle$ as the only non-zero correlator that involves only a single random displacement. This correlator is shown in Fig. 2.1(c) and is negative, i.e. the random displacement at time t_- anticorrelates with the displacement due to internal forces at time t . The reason is that a random displacement in a system with repulsive interactions and a finite bulk density typically pushes a tagged particle into the surrounding particles. Due to the repulsive interaction between the particles the tagged particle is repelled in the next time step. Hence the displacement at time t is in the opposite direction than the random displacement at the previous time t_- .

The squared velocity of one particle at time t is the sum of all correlators divided by $(2\Delta t)^2$, where we subtract $\langle \Delta \mathbf{r}_i^{\text{ran}}(t) \cdot \Delta \mathbf{r}_i^{\text{ran}}(t) \rangle$ and $\langle \Delta \mathbf{r}_i^{\text{ran}}(t_-) \cdot \Delta \mathbf{r}_i^{\text{ran}}(t_-) \rangle$. The reason is that the correlators $\langle \Delta \mathbf{r}_i^{\text{ran}}(t) \cdot \Delta \mathbf{r}_i^{\text{ran}}(t) \rangle$ and $\langle \Delta \mathbf{r}_i^{\text{ran}}(t_-) \cdot \Delta \mathbf{r}_i^{\text{ran}}(t_-) \rangle$ have a value of the order $\mathcal{O}(\Delta t^{-1})$, as discussed above. Thus we obtain

$$\tilde{\Lambda}_t = \Lambda_t - C, \quad (2.24)$$

where the constant

$$C = 2D_{\text{trans}}/\Delta t \quad (2.25)$$

contains the contributions to Λ_t that are given by $\langle \Delta \mathbf{r}_i^{\text{ran}}(t) \cdot \Delta \mathbf{r}_i^{\text{ran}}(t) \rangle$ and $\langle \Delta \mathbf{r}_i^{\text{ran}}(t_-) \cdot \Delta \mathbf{r}_i^{\text{ran}}(t_-) \rangle$.

Nonequilibrium sum rule. A proof of concept for power sampling is given by providing data for demonstrating a nonequilibrium sum rule that is presented in [3]. There R_t^0 is split into internal power, \mathcal{I}_t , and external power \mathcal{X}_t according to

$$R_t^0 = -\mathcal{I}_t/2 - \mathcal{X}_t/2, \quad (2.26)$$

where \mathcal{I}_t and \mathcal{X}_t are given by [3]

$$\begin{aligned} \mathcal{I}_t = \int d\mathbf{r}^N d\boldsymbol{\omega}^N \sum_i & [(-\nabla_i(U(\mathbf{r}^N, \boldsymbol{\omega}^N) - k_{\text{B}}T(\nabla_i \ln \Phi(\mathbf{r}^N, \boldsymbol{\omega}^N, t))) \cdot \hat{\mathbf{v}}_i \\ & + (-\nabla_i^\omega(U(\mathbf{r}^N, \boldsymbol{\omega}^N) - k_{\text{B}}T(\nabla_i^\omega \ln \Phi(\mathbf{r}^N, \boldsymbol{\omega}^N, t))) \cdot \hat{\mathbf{v}}_i^\omega] \cdot \Phi(\mathbf{r}^N, \boldsymbol{\omega}^N, t). \end{aligned} \quad (2.27)$$

and

$$\begin{aligned} \mathcal{X}_t = \int d\mathbf{r}^N d\boldsymbol{\omega}^N \sum_i & [(-\nabla_i V^{\text{ext}}(\mathbf{r}_i, \boldsymbol{\omega}_i, t) + \mathbf{X}(\mathbf{r}_i, \boldsymbol{\omega}_i, t) + \gamma s \boldsymbol{\omega}_i) \cdot \hat{\mathbf{v}}_i \\ & + (-\nabla_i^\omega V^{\text{ext}}(\mathbf{r}_i, \boldsymbol{\omega}_i, t) + \mathbf{X}^\omega(\mathbf{r}_i, \boldsymbol{\omega}_i, t)) \cdot \hat{\mathbf{v}}_i^\omega] \Phi(\mathbf{r}^N, \boldsymbol{\omega}^N, t). \end{aligned} \quad (2.28)$$

In the present situation, where $V^{\text{ext}} = \mathbf{X} = \mathbf{X}^\omega \equiv 0$, the external power reduces to

$$\mathcal{X}_t = \int d\mathbf{r}^N d\boldsymbol{\omega}^N \sum_i (\gamma s \boldsymbol{\omega}_i \cdot \hat{\mathbf{v}}_i) \Phi(\mathbf{r}^N, \boldsymbol{\omega}^N, t). \quad (2.29)$$

The sum rule [3] implies that

$$\mathcal{I}_t = 0, \quad (2.30)$$

and hence

$$R_t^0 = -\mathcal{X}_t/2, \quad (2.31)$$

in steady state.

In the Langevin picture we formulate an analogous identity:

$$\tilde{\Lambda}_t = -I_t/2 - X_t/2, \quad (2.32)$$

where I_t and X_t are given by

$$I_t = \left\langle \sum_i \mathbf{v}_i^{\text{BD}}(t) \cdot (\mathbf{F}_i^{\text{int}}(t) + \gamma \boldsymbol{\xi}_i(t)) \right\rangle - C, \quad (2.33)$$

and

$$X_t = \left\langle \sum_i \mathbf{v}_i^{\text{BD}}(t) \cdot (\gamma s \boldsymbol{\omega}_i(t)) \right\rangle, \quad (2.34)$$

respectively, where C is given by (2.25) [2]. Note that taking into account that the dynamics is evaluated at the minimum at the power functional and therefore $\hat{\mathbf{v}}_i \Phi = \mathbf{v}_i \Phi$ and assuming that \mathbf{v}_i^{BD} gives the correct velocity of particle i , the external power \mathcal{X}_t , given by (2.29), is equivalent to X_t . In simulations, X_t can be easily sampled with (2.19) and (2.22),

$$X_t = \left\langle \sum_i \frac{\Delta \mathbf{r}_i(t) + \Delta \mathbf{r}_i(t_-)}{2\Delta t} \cdot \frac{\gamma \Delta \mathbf{r}_i^{\text{ext}}(t)}{\Delta t} \right\rangle. \quad (2.35)$$

Splitting the displacements according to (2.16) and taking table 2.1 into account yields

$$X_t = \gamma s^2 + \frac{\gamma}{(\Delta t)^2} \sum_i \langle \Delta \mathbf{r}_i^{\text{int}}(t) \cdot \Delta \mathbf{r}_i^{\text{ext}}(t) \rangle. \quad (2.36)$$

In [2] we showed numerically that $I_t = 0$ by a direct comparison between $\tilde{\Lambda}_t$ and $-X_t/2$ that is shown in Fig. 1 therein, where the sampled R_t^0 therein corresponds to $\tilde{\Lambda}_t$ here. The agreement is very good which means that on the basis of the simulation data we conclude that

$$\tilde{\Lambda}_t = -X_t/2, \quad \text{and} \quad I_t = 0. \quad (2.37)$$

The identity $\tilde{\Lambda}_t = -X_t/2$ holds in general for nonequilibrium steady states and is proven below after the general relation of R_t^0 and Λ_t is discussed in detail. With the equivalence of X_t and \mathcal{X}_t follows that $\tilde{\Lambda}_0$ is equivalent to R_t^0 due to the exact sum rule. However, detailed studies suggest that these important results only hold in the special case of ABP in out-of-equilibrium steady states and are not true in general [40].

General relationship between R_t^0 and Λ_t . The general relationship between the Smoluchowski and the Langevin picture regarding power sampling is examined in the following. First, we write $\langle \sum_i (\mathbf{v}_i^{\text{BD}})^2 \rangle$ in steady state as

$$\left\langle \sum_i (\mathbf{v}_i^{\text{BD}})^2 \right\rangle = \gamma^{-2} \left\langle \sum_i \mathbf{F}_i^{\text{det}}(t_-)^2 \right\rangle + 2D_{\text{trans}} \delta(0) + \frac{1}{2\gamma} \left\langle \sum_i \boldsymbol{\xi}_i(t_-) \cdot \mathbf{F}_i^{\text{det}}(t) \right\rangle, \quad (2.38)$$

where $\mathbf{F}_i^{\text{det}} = \mathbf{F}_i^{\text{int}} + \mathbf{F}_i^{\text{ext}}$ is the total deterministic force as a sum of the internal force $\mathbf{F}_i^{\text{int}}$ and the external force $\mathbf{F}_i^{\text{ext}}$. Equation (2.38) follows from the definition of \mathbf{v}_i^{BD} as a central derivative (2.19) when the (general) equation of motion (2.1) is considered in two spatial dimensions. By Taylor expanding $\mathbf{F}_i^{\text{det}}(t)$ in the last term of (2.38) around the time t_- in linear order of Δt it can be shown that

$$\frac{1}{2} \left\langle \sum_i \boldsymbol{\xi}(t_-) \cdot \mathbf{F}_i^{\text{int}}(t) \right\rangle = D_{\text{trans}} \left\langle \sum_i \nabla_i \cdot \mathbf{F}_i^{\text{int}}(t) \right\rangle, \quad (2.39)$$

and hence (2.38) becomes

$$\left\langle \sum_i \mathbf{v}_i^{\text{BD}}(t)^2 \right\rangle = \gamma^{-2} \left\langle \sum_i \mathbf{F}_i^{\text{det}}(t_-)^2 \right\rangle + 2D_{\text{trans}}\delta(0) + \frac{D_{\text{trans}}}{\gamma} \left\langle \sum_i \nabla_i \cdot \mathbf{F}_i^{\text{det}}(t) \right\rangle. \quad (2.40)$$

Because of the fact that the random displacement $\boldsymbol{\xi}_i$ does not appear, (2.40) can be translated in the Smoluchowski description of the dynamics and written as an average in configuration space,

$$\left\langle \sum_i \mathbf{v}_i^{\text{BD}}(t)^2 \right\rangle = 2D_{\text{trans}}\delta(0) + \int d\mathbf{r}^N \sum_i \left(\gamma^{-2} (\mathbf{F}_i^{\text{det}})^2 + \frac{D_{\text{trans}}}{\gamma} \nabla_i \cdot \mathbf{F}_i^{\text{det}} \right) \Phi(\mathbf{r}^N, t). \quad (2.41)$$

Integrating by parts the last term in (2.41) and rearranging yields

$$\begin{aligned} \left\langle \sum_i (\mathbf{v}_i^{\text{BD}})^2 \right\rangle &= 2D_{\text{trans}}\delta(0) + \gamma^{-2} \int d\mathbf{r}^N \sum_i \mathbf{F}_i^{\text{det}} \cdot \left(\mathbf{F}_i^{\text{det}} - k_{\text{B}}T \nabla_i \ln \Phi \right) \Phi(\mathbf{r}^N, t) \\ &= 2D_{\text{trans}}\delta(0) + \gamma^{-2} \int d\mathbf{r}^N \sum_i \mathbf{F}_i^{\text{det}} \cdot \mathbf{F}_i^{\text{tot}} \Phi(\mathbf{r}^N, t), \end{aligned} \quad (2.42)$$

where $\mathbf{F}_i^{\text{tot}} = \mathbf{F}_i^{\text{det}} + \mathbf{F}_i^{\text{diff}}$ is the total force, i.e. the deterministic force $\mathbf{F}_i^{\text{det}}$ plus the diffusive force $\mathbf{F}_i^{\text{diff}} = -k_{\text{B}}T \nabla_i \ln \Phi$.

The result (2.42) is compared to $\langle \sum_i \mathbf{v}_i(t)^2 \rangle$ in the Smoluchowski picture, given by

$$\begin{aligned} \left\langle \sum_i \mathbf{v}_i(t)^2 \right\rangle &= \gamma^{-2} \int d\mathbf{r}^N \sum_i (\mathbf{F}_i^{\text{tot}})^2 \Phi(\mathbf{r}^N, t) \\ &= \gamma^{-2} \int d\mathbf{r}^N \left(\sum_i \mathbf{F}_i^{\text{det}} \cdot \mathbf{F}_i^{\text{tot}} + \sum_i \mathbf{F}_i^{\text{diff}} \cdot \mathbf{F}_i^{\text{tot}} \right) \Phi(\mathbf{r}^N, t). \end{aligned} \quad (2.43)$$

Comparing (2.42) with (2.43) shows that the $\langle \sum_i \mathbf{v}_i(t)^2 \rangle$ cannot be obtained from $\langle \sum_i (\mathbf{v}_i^{\text{BD}})^2 \rangle$ in general as the latter does not include the diffusive flux $\int d\mathbf{r}^N \sum_i \mathbf{F}_i^{\text{diff}} \cdot \mathbf{F}_i^{\text{tot}} \Phi(\mathbf{r}^N, t)$. However, parts of the diffusive flux can also be obtained from BD simulations as

$$\begin{aligned} \int d\mathbf{r}^N \sum_i \mathbf{F}_i^{\text{diff}} \cdot \mathbf{F}_i^{\text{tot}} \Phi(\mathbf{r}^N, t) &= \int d\mathbf{r}^N \sum_i \mathbf{F}_i^{\text{diff}} \cdot \left(\mathbf{F}_i^{\text{det}} + \mathbf{F}_i^{\text{diff}} \right) \Phi(\mathbf{r}^N, t) \\ &= \int d\mathbf{r}^N \sum_i \left(\mathbf{F}_i^{\text{diff}} \cdot \mathbf{F}_i^{\text{det}} + \mathbf{F}_i^{\text{diff}} \cdot \mathbf{F}_i^{\text{diff}} \right) \Phi(\mathbf{r}^N, t). \end{aligned} \quad (2.44)$$

Hence,

$$\left\langle \sum_i \mathbf{v}_i(t)^2 \right\rangle = \gamma^{-2} \int d\mathbf{r}^N \left[\sum_i \mathbf{F}_i^{\text{det}} \cdot (\mathbf{F}_i^{\text{det}} + 2\mathbf{F}_i^{\text{diff}}) + \sum_i \mathbf{F}_i^{\text{diff}} \cdot \mathbf{F}_i^{\text{diff}} \right] \Phi(\mathbf{r}^N, t). \quad (2.45)$$

In (2.45) only the last average $\langle \sum_i \mathbf{F}_i^{\text{diff}} \cdot \mathbf{F}_i^{\text{diff}} \rangle$ cannot be directly sampled from BD simulations, as comparing to (2.40) and (2.41) shows.

As a consequence, the full power functional R_t^0 cannot be sampled in general from Brownian dynamics simulations, but its deterministic part can be obtained. Note that the first term in (2.42) is given by the constant C in the definition (2.24). This situation is comparable to equilibrium statistical mechanics, where quantities such as the free energy F or the entropy S are not measurable directly as averages in simulations either, but have to be obtained, e.g., via thermodynamic integration [36].

Derivation of the sum rule in the Langevin picture, $I_t = 0$. Writing I_t defined by (2.33) in the same fashion as $\langle \sum_i (\mathbf{v}_i^{\text{BD}})^2 \rangle$ in (2.38) gives

$$I_t = \frac{1}{\gamma} \left\langle \sum_i \mathbf{F}_i^{\text{int}}(t_-)^2 \right\rangle + \frac{1}{\gamma} \left\langle \sum_i \mathbf{F}_i^{\text{int}}(t_-) \cdot \mathbf{F}_i^{\text{ext}}(t_-) \right\rangle + \frac{1}{2} \left\langle \sum_i \boldsymbol{\xi}(t_-) \cdot \mathbf{F}_i^{\text{int}}(t) \right\rangle, \quad (2.46)$$

where the constant C cancels out. Using the identity (2.39) in (2.46) yields

$$I_t = \frac{1}{\gamma} \left\langle \sum_i (\mathbf{F}_i^{\text{int}})^2 \right\rangle + \frac{1}{\gamma} \left\langle \sum_i \mathbf{F}_i^{\text{int}} \cdot \mathbf{F}_i^{\text{ext}} \right\rangle + D_{\text{trans}} \left\langle \sum_i \nabla_i \cdot \mathbf{F}_i^{\text{int}} \right\rangle. \quad (2.47)$$

Analogous to (2.40), (2.47) can be transferred to the Smoluchowski picture and written as

$$I_t = \frac{1}{\gamma} \int d\mathbf{r}^N \sum_i \mathbf{F}_i^{\text{int}} \cdot (\mathbf{F}_i^{\text{int}} + \mathbf{F}_i^{\text{ext}} - k_B T \nabla_i \ln \Phi) \Phi(\mathbf{r}^N, t). \quad (2.48)$$

The term in brackets in (2.48) is the velocity \mathbf{v}_i of particle i following from the definition of the velocity operator (1.8). As the internal force is given by the negative gradient of the interaction potential, $\mathbf{F}_i^{\text{int}} = -\nabla_i U(\mathbf{r}^N)$, (2.48) becomes

$$I_t = \frac{1}{\gamma} \int d\mathbf{r}^N \sum_i (-\nabla_i U) \cdot \mathbf{v}_i \Phi(\mathbf{r}^N, t). \quad (2.49)$$

Integration by parts yields

$$I_t = \frac{1}{\gamma} \int d\mathbf{r}^N \sum_i U (\nabla_i \cdot \mathbf{v}_i \Phi(\mathbf{r}^N, t)). \quad (2.50)$$

Using the Smoluchowski equation (1.7), the term in brackets in (2.50) gives the time derivative of the distribution function, $\partial \Phi(\mathbf{r}^N, t) / \partial t$, which vanishes in steady state. For this reason, I_t vanishes in steady state.

3 Overview of the publications

In this section we give an overview of the publications that contributed to this thesis. We approach the problem of motility-induced phase separation (MIPS) of active Brownian particles (ABP) in the first instance by describing the ABP model as an effective equilibrium system in Sec. 3.1 and the corresponding publication [1]. Thereby the interparticle interaction potential changes and repulsive interactions develop an attractive part. This is identified as the mechanism for MIPS. However this approach is only valid in the limit of small activity.

To overcome this problem a power functional theory (PFT) for ABP is developed in Sec. 3.2 and in the publications [2] and [3]. The theory is formally exact and is not restricted to any limit in the activity of the particles. Although many aspects of ABP systems can be described by PFT and the agreement with computer simulations is very good, the problem of MIPS is not finally solved.

This lack of explanation is the motivation to study the interface between coexisting phases in detail. The interface appears to be not only necessary to fully describe MIPS, but to be crucial to understand the physics of ABP because the active particles are orientated towards the liquid side of the interface making the interface polarized. This is fundamentally different from the bulk, where the orientations are evenly distributed and makes the study of the orientational dependency of the one-body density and current essential. A manuscript on the interface is in preparation [4]. Results obtained from computer simulations are shown in Sec. 4.

3.1 Effective interactions in active Brownian suspensions

In publication [1] we present one of the first studies in which the rotational equation of motion (2.4) is integrated out. By doing so the equations of motion reduce to one (translational) Langevin equation in three dimensions,

$$\dot{\mathbf{r}}_i(t) = \gamma^{-1} \mathbf{F}_i^{\text{int}}(\mathbf{r}^N) + \boldsymbol{\xi}_i(t) + \boldsymbol{\chi}_i(t), \quad (3.1)$$

where $\mathbf{F}_i^{\text{int}}(\mathbf{r}^N)$ is the interparticle interaction force. In (3.1) the self-propulsion force does not appear directly, as it does in (2.3), because the orientations have been integrated out. The activity is contained in the colored noise $\boldsymbol{\chi}_i(t)$, and $\boldsymbol{\xi}_i(t)$ describes Gaussian white noise as given by (2.5). The colored noise $\boldsymbol{\chi}_i(t)$ has zero mean and the time correlation function

$$\langle \boldsymbol{\chi}_i(t) \boldsymbol{\chi}_j(t') \rangle = \frac{s^2}{3} \exp(-2D_{\text{rot}}|t-t'|) \mathbf{1}\delta_{ij}. \quad (3.2)$$

In [1] we used an approach by Fox [41, 42] that is based on an expansion in powers of the

correlation time, which is proportional to $1/D_{\text{rot}}$ here. The technical details of the calculation can be found in the Appendix of [1]. The result is a Fokker-Planck equation for the configurational probability distribution,

$$\frac{\partial \Phi(\mathbf{r}^N, t)}{\partial t} = \sum_{i=1}^N \nabla_i \cdot D_i(\mathbf{r}^N) \left(\nabla_i - \beta \mathbf{F}_i^{\text{eff}}(\mathbf{r}^N) \right) \Phi(\mathbf{r}^N, t), \quad (3.3)$$

where $\beta \equiv 1/(k_B T)$. The diffusion coefficient therein is

$$D_i(\mathbf{r}^N) = D_{\text{trans}} + \frac{s^2}{6D_{\text{rot}}} \left(1 + \frac{\tau \nabla_i \cdot \beta \mathbf{F}_i^{\text{int}}(\mathbf{r}^N)}{1 - \tau \nabla_i \cdot \beta \mathbf{F}_i^{\text{int}}(\mathbf{r}^N)} \right) \quad (3.4)$$

where $\tau = D_{\text{trans}}/(2D_{\text{rot}}\sigma^2)$, and the effective force is

$$\mathbf{F}_i^{\text{eff}}(\mathbf{r}^N) = \frac{D_{\text{trans}}}{D_i(\mathbf{r}^N)} \left(\mathbf{F}_i^{\text{int}} - k_B T \nabla_i \frac{D_{\text{trans}}}{D_i(\mathbf{r}^N)} \right). \quad (3.5)$$

Assuming that the interparticle interaction is a pair interaction, i.e. $\mathbf{F}_i^{\text{int}}(\mathbf{r}^N) = -\frac{1}{2} \nabla_i \sum_{i \neq j} \phi(r_{ij})$, gives an effective pair potential

$$\phi^{\text{eff}}(r) = k_B T \int_r^\infty dr' \left(\frac{\beta |-\nabla \phi(r')| D_{\text{trans}}}{D(r')} - \frac{\partial}{\partial r'} \ln \frac{D(r')}{D_{\text{trans}}} \right), \quad (3.6)$$

where $r \equiv r_{ij}$. The activity of the particles in (3.6) is controlled by the radial diffusivity

$$D(r) = D_{\text{trans}} + \frac{s^2}{6D_{\text{rot}}} \left(1 - \frac{\tau \nabla^2 \beta \phi(r)}{1 + \tau \nabla^2 \beta \phi(r)} \right), \quad (3.7)$$

in which the activity parameters s , D_{rot} , and τ enter directly. The effective force between two particles follows straightforwardly as $\mathbf{F}^{\text{eff}}(r) = -\nabla \phi^{\text{eff}}(r)$. Therefore

$$\mathbf{F}^{\text{eff}}(r) = \frac{D_{\text{trans}}}{D(r)} \left(-\nabla \phi(r) - k_B T \nabla \frac{D(r)}{D_{\text{trans}}} \right). \quad (3.8)$$

We show in [1] in detail how these equations are derived. Increasing the activity leads to the development of an attractive tail in the (effective) interaction potential (see Fig. 1 in [1]). As particles (effectively) attract each other a phenomenon comparable to spinodal decomposition is observed, where the system separates into a dilute and a dense phase. We use the soft mean-spherical approximation integral equation theory [43] to obtain the spinodals associated with the phase separation for different values of activity. We conclude that MIPS can be explained by an effective attractive interaction between the particles. Furthermore the pair correlation function, $g(r)$, is calculated within the theory. These results are tested against many-body computer simulation, where the translational and rotational equation of motion, (2.3) and (2.4), respectively, are integrated in time directly. Hence the computer simulations generate the “real” dynamics, structure, and phase behavior of the active system. The simulation data and the effective interaction approach agree very well showing the validity of the effective interaction

approach.

Similar considerations have been done for particles that passively show an attraction, such as the Lennard-Jones particles. An increase of the activity first decreases the magnitude of attraction (see Fig. 2 in [1]). Increasing the activity further again increases the attraction on length scales $r \approx \sigma$. Furthermore the development of an repulsive bump is observed at $r \approx 1.4\sigma$. Therefore a reappearance of phase separation behavior can be observed. These results are in good agreement with work by Redner *et al.* who studied the reentrant phase behavior with a kinetic model and computer simulations [44].

Although the effective interaction approach gives very good quality results, its range of possible application is limited. First, the approximation to get the Fokker-Planck equation only works for active motion with a small persistence time, i.e. small reorientation time or high rotational diffusion coefficient [45]. What is meant quantitatively by small persistence time in this context is not well defined. Qualitatively, small persistence is associated with a high rotational diffusion coefficient. Second, the assumption of the many-body interparticle interaction being a pair interaction for finite bulk densities is only validated by the comparison of the pair correlation function of the theory with BD simulations, as a priori this is only clear in the low density limit. The method is often referred to as effective equilibrium, because the activity only determines the form of the interaction between the particles. Therefore it is possible to approach the problem with methods from equilibrium statistical physics, such as free energy functionals.

Apart from Fox's approximation for colored noise, there exists a second prominent approximation, the unified colored noise approximation (UCNA) [46, 47]. Both approaches produce comparable results.

The development of the effective equilibrium description opened an individual branch in the studies of active particles that uses and develops systematically methods for the description of ABP closely related to known approaches for passive Brownian particles. For example a density functional theory (DFT) and a dynamical density functional theory (DDFT) for ABP were formulated by Brader and Wittmann using the effective equilibrium approach [48]. They studied inhomogenous situations, such as wetting and capillary evaporation. Therein the effective external potential, $V_{\text{ext}}^{\text{eff}}(z)$, depends on z , the distance to the wall. The effective free energy functional is then

$$F^{\text{eff}}[\rho] = F_{\text{id}}[\rho] + F_{\text{exc}}^{\text{eff}}[\rho] + \int d\mathbf{r} \rho(\mathbf{r}) V_{\text{ext}}^{\text{eff}}(z), \quad (3.9)$$

where $F_{\text{id}}[\rho]$ is the familiar ideal gas contribution (1.6). The effective excess free energy, $F_{\text{exc}}^{\text{eff}}[\rho]$ consists of a hard-sphere reference system plus an attractive perturbation that is given by the effective interaction potential in a mean-field fashion. Taking the adiabatic assumption for the dynamics into account, (1.12), yields the effective DDFT equation

$$\frac{\partial \rho(\mathbf{r}, t)}{\partial t} = D_{\text{trans}} \nabla \cdot \left(\rho(\mathbf{r}, t) \nabla \frac{\delta \beta F^{\text{eff}}[\rho]}{\delta \rho(\mathbf{r}, t)} \right), \quad (3.10)$$

that allows the study of (effective) dynamics, statics, and thermodynamics in ABP systems.

For a detailed discussion about thermodynamic aspects, such as the pressure or the surface tension in both, the Fox approach and the UCNA are given in Refs. [49, 50]. Therein both approaches are compared in detail and thoroughly.

For the sake of completeness, there exist a number of approaches that construct a local effective free energy functional based phenomenological considerations [51, 52].

3.2 Power functional theory for active Brownian particles

For active Brownian particles (ABP) not only the $\{\mathbf{r}_1 \dots \mathbf{r}_N\} \equiv \mathbf{r}^N$ positions of the N particles have to be considered, but their orientations $\{\boldsymbol{\omega}_1 \dots \boldsymbol{\omega}_N\} \equiv \boldsymbol{\omega}^N$ along which the particles are self-propelled with speed s , as well. The Smoluchowski equation for the time-dependent probability distribution $\Phi(\mathbf{r}^N, \boldsymbol{\omega}^N, t)$ of an ensemble of interacting ABP is

$$\frac{\partial}{\partial t} \Phi(\mathbf{r}^N, \boldsymbol{\omega}^N, t) + \sum_i (\nabla_i \cdot \hat{\mathbf{v}}_i + \nabla_i^\omega \cdot \hat{\mathbf{v}}_i^\omega) \Phi(\mathbf{r}^N, \boldsymbol{\omega}^N, t) = 0, \quad (3.11)$$

where ∇_i^ω indicates the derivative on the unit sphere with respect to $\boldsymbol{\omega}_i$; $\hat{\mathbf{v}}_i$ and $\hat{\mathbf{v}}_i^\omega$ are the translational and rotational velocity operators, respectively. They are given by

$$\gamma \hat{\mathbf{v}}_i = -(\nabla_i U(\mathbf{r}^N, \boldsymbol{\omega}^N)) - (\nabla_i V^{\text{ext}}(\mathbf{r}_i, \boldsymbol{\omega}_i, t)) + \mathbf{X}(\mathbf{r}_i, t) + \gamma s \boldsymbol{\omega}_i - k_B T \nabla_i, \quad (3.12)$$

$$\gamma^\omega \hat{\mathbf{v}}_i^\omega = -(\nabla_i^\omega U(\mathbf{r}^N, \boldsymbol{\omega}^N)) - (\nabla_i^\omega V^{\text{ext}}(\mathbf{r}_i, \boldsymbol{\omega}_i, t)) + \mathbf{X}^\omega(\mathbf{r}_i, t) - k_B T \nabla_i^\omega, \quad (3.13)$$

where \mathbf{X}^ω is the external non-conservative torque. The many-body expression of the power functional is minimal (indicated by the superscript 0) at the physical dynamics and has the form

$$\mathcal{R}_t^0 = -\frac{1}{2} \int d\mathbf{r}^N d\boldsymbol{\omega}^N \sum_i (\gamma \mathbf{v}_i^2 + \gamma^\omega (\mathbf{v}_i^\omega)^2) \Phi(\mathbf{r}^N, \boldsymbol{\omega}^N, t), \quad (3.14)$$

where \mathbf{v}_i is the eigenvalue of the velocity operator at a given time t according to $\hat{\mathbf{v}}_i \Phi(\mathbf{r}^N, \boldsymbol{\omega}^N, t) = \mathbf{v}_i \Phi(\mathbf{r}^N, \boldsymbol{\omega}^N, t)$ and \mathbf{v}_i^ω is the rotational velocity given by $\hat{\mathbf{v}}_i^\omega \Phi(\mathbf{r}^N, \boldsymbol{\omega}^N, t) = \mathbf{v}_i^\omega \Phi(\mathbf{r}^N, \boldsymbol{\omega}^N, t)$. At the minimum this is equivalent to the velocity of the particle i .

The many-body theory is connected to the one-body level by a constrained Levy search [53, 54] by which $\mathcal{R}_t \rightarrow R_t[\rho, \mathbf{J}, \mathbf{J}^\omega]$. The power functional, $R_t[\rho, \mathbf{J}, \mathbf{J}^\omega]$, thus becomes a functional of $\rho(\mathbf{r}, \boldsymbol{\omega}, t)$, $\mathbf{J}(\mathbf{r}, \boldsymbol{\omega}, t)$, and $\mathbf{J}^\omega(\mathbf{r}, \boldsymbol{\omega}, t)$. The one-body density distribution for ABP is then given by

$$\rho(\mathbf{r}, \boldsymbol{\omega}, t) = \left\langle \sum_{i=1}^N \delta(\mathbf{r} - \mathbf{r}_i(t)) \delta^\omega(\boldsymbol{\omega} - \boldsymbol{\omega}_i(t)) \right\rangle, \quad (3.15)$$

where $\delta(\cdot)$ is the Dirac distribution, $\delta^\omega(\cdot)$ is the Dirac distribution on the unit sphere, and the brackets indicate an – in general nonequilibrium – average. Consequently the one-body

translational and rotational current distributions are

$$\mathbf{J}(\mathbf{r}, \boldsymbol{\omega}, t) = \left\langle \sum_{i=1}^N \delta(\mathbf{r} - \mathbf{r}_i(t)) \delta^\omega(\boldsymbol{\omega} - \boldsymbol{\omega}_i(t)) \hat{\mathbf{v}}_i(t) \right\rangle, \quad (3.16)$$

$$\mathbf{J}^\omega(\mathbf{r}, \boldsymbol{\omega}, t) = \left\langle \sum_{i=1}^N \delta(\mathbf{r} - \mathbf{r}_i(t)) \delta^\omega(\boldsymbol{\omega} - \boldsymbol{\omega}_i(t)) \hat{\mathbf{v}}_i^\omega(t) \right\rangle, \quad (3.17)$$

respectively. The physical time evolution is obtained when R_t is minimized with respect to the currents, while the density is kept constant:

$$\frac{\delta R_t[\rho, \mathbf{J}, \mathbf{J}^\omega]}{\delta \mathbf{J}(\mathbf{r}, \boldsymbol{\omega}, t)} = 0, \quad (3.18)$$

$$\frac{\delta R_t[\rho, \mathbf{J}, \mathbf{J}^\omega]}{\delta \mathbf{J}^\omega(\mathbf{r}, \boldsymbol{\omega}, t)} = 0. \quad (3.19)$$

The evolution of the density follows then straight-forwardly from the continuity equation,

$$\frac{\partial \rho(\mathbf{r}, \boldsymbol{\omega}, t)}{\partial t} = -\nabla \cdot \mathbf{J}(\mathbf{r}, \boldsymbol{\omega}, t) - \nabla^\omega \cdot \mathbf{J}^\omega(\mathbf{r}, \boldsymbol{\omega}, t). \quad (3.20)$$

The splitting introduced by (1.28) still holds for ABP, but now the dissipation functionals and the external functional are also functionals of the orientational current. Hence,

$$R_t[\rho, \mathbf{J}, \mathbf{J}^\omega] = \dot{F}_{\text{id}}[\rho] + \dot{F}_{\text{exc}}[\rho] + P_t^{\text{id}}[\rho, \mathbf{J}, \mathbf{J}^\omega] + P_t^{\text{exc}}[\rho, \mathbf{J}, \mathbf{J}^\omega] - X_t[\rho, \mathbf{J}, \mathbf{J}^\omega], \quad (3.21)$$

where

$$\dot{F}_{\text{id}}[\rho] = k_{\text{B}}T \int d\mathbf{r} d\boldsymbol{\omega} (\mathbf{J} \cdot \nabla + \mathbf{J}^\omega \cdot \nabla^\omega) \ln \rho, \quad (3.22)$$

$$\dot{F}_{\text{exc}}[\rho] = \int d\mathbf{r} d\boldsymbol{\omega} (\mathbf{J} \cdot \nabla + \mathbf{J}^\omega \cdot \nabla^\omega) \frac{\delta F^{\text{exc}}[\rho]}{\delta \rho}, \quad (3.23)$$

$$P_t^{\text{id}}[\rho, \mathbf{J}, \mathbf{J}^\omega] = \int d\mathbf{r} d\boldsymbol{\omega} \frac{\gamma \mathbf{J}^2 + \gamma^\omega (\mathbf{J}^\omega)^2}{2\rho}, \quad (3.24)$$

$$X_t[\rho, \mathbf{J}, \mathbf{J}^\omega] = \int d\mathbf{r} d\boldsymbol{\omega} [\mathbf{J} \cdot (-\nabla V^{\text{ext}} + \mathbf{X} + \gamma s \boldsymbol{\omega}) + \mathbf{J}^\omega \cdot (-\nabla^\omega V^{\text{ext}} + \mathbf{X}^\omega)]. \quad (3.25)$$

Applying the variational principles (3.18) and (3.19) to (3.21) yields the following equations of motion,

$$\frac{\gamma \mathbf{J}(\mathbf{r}, \boldsymbol{\omega}, t)}{\rho(\mathbf{r}, \boldsymbol{\omega}, t)} = \gamma s \boldsymbol{\omega} - \nabla V^{\text{ext}}(\mathbf{r}, \boldsymbol{\omega}, t) + \mathbf{X}(\mathbf{r}, \boldsymbol{\omega}, t) - \nabla \frac{\delta F[\rho]}{\delta \rho(\mathbf{r}, \boldsymbol{\omega}, t)} - \frac{\delta P_t^{\text{exc}}[\rho, \mathbf{J}, \mathbf{J}^\omega]}{\delta \mathbf{J}(\mathbf{r}, \boldsymbol{\omega}, t)}, \quad (3.26)$$

$$\frac{\gamma \mathbf{J}^\omega(\mathbf{r}, \boldsymbol{\omega}, t)}{\rho(\mathbf{r}, \boldsymbol{\omega}, t)} = -\nabla^\omega V^{\text{ext}}(\mathbf{r}, \boldsymbol{\omega}, t) + \mathbf{X}^\omega(\mathbf{r}, \boldsymbol{\omega}, t) - \nabla^\omega \frac{\delta F[\rho]}{\delta \rho(\mathbf{r}, \boldsymbol{\omega}, t)} - \frac{\delta P_t^{\text{exc}}[\rho, \mathbf{J}, \mathbf{J}^\omega]}{\delta \mathbf{J}^\omega(\mathbf{r}, \boldsymbol{\omega}, t)}. \quad (3.27)$$

Evaluating the power functional at the physical time evolution yields

$$\mathcal{R}_t^0 \equiv R_t^0. \quad (3.28)$$

Starting from this general and exact expressions a discussion of the steady-state properties for ABP is given in [2] and in more detail in [3]. Therein we consider systems where no external fields or forces are present, i.e., $V^{\text{ext}} = 0$ and $\mathbf{X} = \mathbf{X}^\omega = 0$. Additionally, $\dot{F} = 0$ in steady state. Furthermore, we propose an excess dissipation functional of the form,

$$P_t^{\text{exc}}[\rho, \mathbf{J}] = \frac{\gamma}{2} \int d\mathbf{r} d\boldsymbol{\omega} d\mathbf{r}' d\boldsymbol{\omega}' \rho(\mathbf{r}, \boldsymbol{\omega}) \rho(\mathbf{r}', \boldsymbol{\omega}') \left(\frac{\mathbf{J}(\mathbf{r}, \boldsymbol{\omega})}{\rho(\mathbf{r}, \boldsymbol{\omega})} - \frac{\mathbf{J}(\mathbf{r}', \boldsymbol{\omega}')}{\rho(\mathbf{r}', \boldsymbol{\omega}')} \right)^2 M(\mathbf{r}, \boldsymbol{\omega}, \mathbf{r}', \boldsymbol{\omega}'), \quad (3.29)$$

where $M(\mathbf{r}, \boldsymbol{\omega}, \mathbf{r}', \boldsymbol{\omega}')$ is a convolution kernel. The assumptions are such that (3.29) models a homogeneous bulk steady state. From this a simple expression for the power functional at the minimum, R_t^0 , can be obtained. With our power sampling method, c.f. Sec. 2, we compare the results from theory with many-body computer simulations. The agreement, as shown in Fig. 1 and Fig. 2 in [2] is very good. As argued in [2], the simulations show a clear separation in dilute and dense bulk phases. Remarkably, imposing the excess dissipation functional designed for homogeneous situations, (3.29), the power functional matches the sampled data well, even in the inhomogeneous state, where both phases coexist.

The value of the power functional at the physical dynamics may be split into internal and external parts,

$$R_t^0 = -\mathcal{I}_t/2 - \mathcal{X}_t/2. \quad (3.30)$$

The internal part \mathcal{I}_t and the external part \mathcal{X}_t are given by (2.27) and (2.28), respectively, and can be thus be sampled from Brownian dynamics simulations (c.f. Sec. 2.2). Numerical results of the power sampling presented in [2] suggest that the sampled quantity matches with the external power in the Langevin picture, $X_t/2$. In [3] we present the derivation of the sum rule obtained from first principles on the many-body level. As the sum rule gives $R_t^0 = -\mathcal{X}_t/2$, the results in [2] show that the power sampling technique gives the power functional in steady state. This suggests that power sampling indeed gives the power functional at the minimum, at least in steady state. Additionally, it is shown that the excess dissipation functional (3.29) satisfies the sum rule, acting as a further justification for P_t^{exc} .

Furthermore, we have demonstrated how PFT can be used to describe phase coexistence of out-of-equilibrium stationary states. Therein we assumed that the Lagrange multiplier α in (1.23) vanishes. This leads to a Maxwell construction which gives the densities of the coexisting phases in principle. As further studied showed [14], this treatment is not suitable for ABP. However, different approaches that use a Maxwell equal area construction cannot predict the coexisting densities either [14, 55]. This leaves MIPS an unsolved problem.

By describing and fully modeling the interface between the two phases with PFT we hope to solve the problem of MIPS as discussed in Sec. 4.

4 Structure of the fluid-fluid interface in phase-separated active Brownian suspensions

In this section we present results for the free interface between two bulk phases in a phase separating system of active Brownian particles (ABP). Phase separation is fully driven by the activity of the particles and called motility-induced phase separation (MIPS) and is of particular interest as MIPS is stable in systems of purely repulsive particles. The nonequilibrium character of ABP systems make the theoretical description and modeling of MIPS a challenging problem, and a variety of approaches exist including effective equilibrium models, c.f. Sec. 3.1 and [1], continuum theories [52], microscopic many-body theories [51, 56], mechanical theories [57], and kinetic approaches [58]. Based on these ideas special interest lies on the thermodynamics of active matter [55, 57, 59, 60] and thermodynamic variables such as temperature [61], pressure [62–67], chemical potential [14, 68], and interfacial tension [69] (that remarkably is found to be negative), in order to determine phase coexisting conditions for MIPS. This negative value violates physical intuition and the authors of Ref. [14] point out that a correct treatment of the active interface is crucial for describing MIPS. Often theoretical approaches are supported by computer simulations as a direct and practical test.

Here, we use Brownian dynamics computer simulations in order to investigate the inhomogeneous one-body density and current distribution at the fluid-fluid interface of phase separating ABP. The simulations are performed in an elongated box in a center of mass reference system, i.e. the center of mass of the system lies in the center of the box during the complete sampling time. This guarantees a stationary interface and thus good sampling statistics. Our directly sampled results are used to calculate a variety of characteristics of the interface, such as density and polarization profiles. We compare these results with the current state of literature. Polarization in systems of self-propelled Brownian particles for example is a widely-known phenomena. It can be observed in systems where ABP are under the influence of external fields, such as a harmonic potential [70] or gravity [15]. In the context of interfaces and pressure of ABP, polarization effects play an important role [14, 59, 67]. But for bulk theories the polarization is an important input for stability analysis, which are used to predict MIPS [51, 56, 71]. For the density profile as a function of the coordinate along the long side of the box, tanh fit functions are commonly used to describe the data [14, 69, 72]. Comparisons with these results of the literature validates our simulation data as good reference data for an analytic model of the interface. We additionally give a Fourier decomposition of the angular components of the one-body density and calculate the first five Fourier coefficients. The decomposition can be used to determine the symmetry of the density distribution and identify physical effects that emerge at the interface. An outlook on

possible future work is given that will include a detailed theoretical model which goes beyond the scope of this thesis.

4.1 Brownian dynamics simulations

We consider N active particles with positions $\mathbf{r}^N = \{\mathbf{r}_1 \dots \mathbf{r}_N\}$ that are self-propelled with speed s along their orientations $\boldsymbol{\omega}^N = \{\boldsymbol{\omega}_1 \dots \boldsymbol{\omega}_N\}$, to be contained in a square simulation box with an elongated geometry, i.e. the aspect ratio of the box is $L_x/L_y = \mathcal{A}$, in two dimensions with lengths L_x and L_y . The total ‘‘volume’’ of the box is $V = L_x L_y$ and is adjusted to fit the overall bulk density ρ_b according to $V = N/\rho_b$. In practice we choose $L_x > L_y$ and hence $\mathcal{A} > 1$. The interface is expected to be parallel to the short side of the box, making the system translational invariant in the y -direction. Therefore most spatial dependencies reduce to a dependency on the x -coordinate. For a bulk steady state the one-body density distribution becomes a constant, $2\pi\rho(\mathbf{r}, \boldsymbol{\omega}, t) = \rho_b = N/V$ and the current reduces to $\mathbf{J} = J_b \boldsymbol{\omega}$ [2],[3]. The dynamics of the system in two dimensions is described by the over-damped Langevin equations (c.f. (2.3) and (2.4))

$$\dot{\mathbf{r}}_i(t) = s\boldsymbol{\omega}_i(t) + \gamma^{-1}\mathbf{F}_i^{\text{int}}(\mathbf{r}^N) + \boldsymbol{\xi}_i(t), \quad (4.1)$$

$$\dot{\varphi}_i(t) = \eta_i(t), \quad (4.2)$$

where the orientation is given by $\boldsymbol{\omega}_i = (\cos \varphi_i, \sin \varphi_i)$ and φ_i is measured against the x -axis. The stochastic vector $\boldsymbol{\xi}_i$ and the stochastic scalar variable η_i both describe Gaussian white noise with zero mean and auto-correlations given by

$$\langle \boldsymbol{\xi}_i(t) \boldsymbol{\xi}_j(t') \rangle = 2D_{\text{trans}} \mathbf{1} \delta_{ij} \delta(t - t'), \quad (4.3)$$

$$\langle \eta_i(t) \eta_j(t') \rangle = 2D_{\text{rot}} \delta_{ij} \delta(t - t'). \quad (4.4)$$

Here, $D_{\text{trans}} = k_B T/\gamma$ and $D_{\text{rot}} = k_B T/\gamma^\omega$ are the translational and the rotational diffusion coefficient with friction coefficients γ and γ^ω , respectively, and $\mathbf{1}$ is the unit matrix. We consider (conservative) interparticle interactions of a pairwise form, generated from the Weeks-Chandler-Anderson potential (WCA) as given by (2.13),

$$\phi_{\text{WCA}}(r_{ij}) = \begin{cases} 4\epsilon \left[\left(\frac{\sigma}{r_{ij}} \right)^{12} - \left(\frac{\sigma}{r_{ij}} \right)^6 \right] + \epsilon, & \text{for } r_{ij} < 2^{1/6}\sigma, \\ 0, & \text{otherwise.} \end{cases} \quad (4.5)$$

by

$$\mathbf{F}_i^{\text{int}}(r_{ij}) = -\nabla_i \sum_{j, j \neq i} \phi_{\text{WCA}}(r_{ij}), \quad (4.6)$$

where $r_{ij} = |\mathbf{r}_i - \mathbf{r}_j|$ is the distance between particles i and j , ∇_i is the derivative with respect to \mathbf{r}_i , ϵ is the fundamental unit of energy, and σ is the associated particle diameter. As the WCA potential is a Lennard-Jones potential that is cut and shifted at the minimum, it generates

a soft-core repulsive interaction of finite range without any force artifacts at the cut-off. A common measure for activity is given by the dimensionless Peclet number defined as [52]

$$\text{Pe} = \frac{3s}{D_{\text{rot}}\sigma}. \quad (4.7)$$

We carry out Brownian dynamics simulations for $N = 2000$ particles in two spatial dimensions by solving the equations of motion (4.1) and (4.2) with a forward Euler algorithm, where periodic boundary conditions are implemented in both space dimensions of the elongated box. The time between two steps is $\Delta t = 10^{-5}\tau_0$, where $\tau_0 = \sigma^2\gamma/\epsilon$ is the fundamental unit of time expressed in the natural units of the system ϵ , σ , which are both set up by the potential (4.5), and the friction coefficient γ .

The simulations are performed in the center of mass system, i.e. the system is prepared such that the x -component of the center of mass remains in the center of the simulation box. This global shift does not affect the forces on the particles as all distances between the particles remain the same. The shift is important to establish a stationary interface. We initialize the system with random positions and orientations of the particles and let it reach a steady state for $n_{\text{equi}} = 10^7$ steps. Afterwards, data is sampled for $n_{\text{samp}} = 10^8$ steps. We fix $D_{\text{rot}}/D_{\text{trans}} = 3\sigma^{-2}$ for all simulations. With this choice of parameters the Peclet number given by (4.7) is $\text{Pe} = \gamma\sigma s/(k_{\text{B}}T)$. It is fixed to $\text{Pe} = 120$ in order to ensure MIPS happening in the system (see e.g. the phase diagrams in Refs. [44, 52] and [2]). We perform simulations for bulk densities $\rho_b\sigma^2 = 0.4$ to 1 in steps of 0.1, for aspect ratios of $\mathcal{A} = 2.5, 5, \text{ and } 10$. The temperature and swim speed is varied in a way that $\text{Pe} = 120$. The values carried out are $(k_{\text{B}}T/\epsilon, s\tau_0/\sigma) = (1, 120), (0.5, 60), (0.25, 30)$, and $(0.1, 12)$.

4.2 Results

4.2.1 One-body density, current, and velocity

Density

Figure 4.1 shows the density as a function of position x and angle φ for a phase-separating system with $s\tau_0/\sigma = 60$, $k_{\text{B}}T/\epsilon = 0.5$, $\mathcal{A} = 5$, and $\rho_b = 0.7$. The values $\varphi = 0$ and $\varphi = \pi$ correspond to swimming in the positive and negative x -direction, respectively. Each of the two interfaces that separate the dilute and the dense phase are clearly visible by the white color. At $x/\sigma \approx -20$ – the “left” interface from gas to liquid – the density is maximal for $\varphi = 0$, where the particles swim against the interface in positive x -direction. This means that the interface is polarized; at the interface the orientation vectors of the particles, $\boldsymbol{\omega}$, point towards the dense phase [14, 67]. The polarization will be discussed in detail in Sec. 4.2.3. Likewise the density of particles which point towards the dilute phase is significantly smaller, as those particles just swim away from the interface in a rather unhindered fashion.

In Fig. 4.2 we show the density profiles along the x -direction, i.e. the integral of the density field

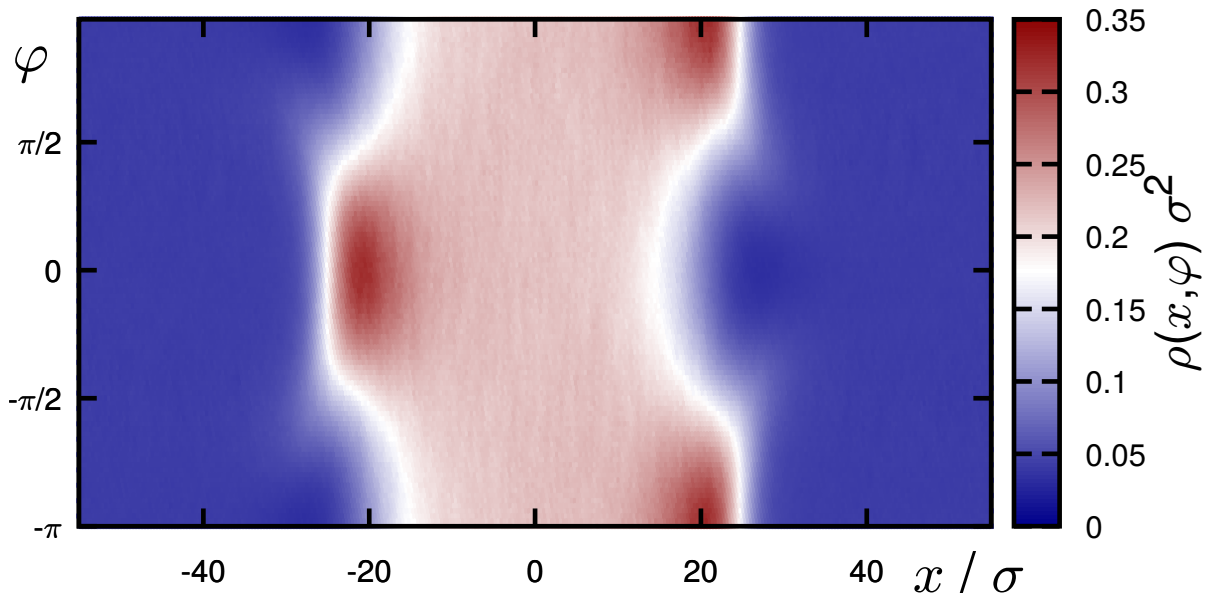


Figure 4.1: Density profile as a function of x and φ for $s\tau_0/\sigma = 60$, $k_B T/\epsilon = 0.5$, $\mathcal{A} = L_x/L_y = 5$, and $\rho_b = 0.7$. Blue regions indicate areas with low density, while red regions indicate areas with high density. The middle of the color scale is given by white color and therefore the interface roughly coincide with white regions.

over all orientations

$$\bar{\rho}(x) = \int_0^{2\pi} d\varphi \rho(x, \varphi). \quad (4.8)$$

Figure 4.2(a) shows the dependency of the density profile on the temperature, while $\mathcal{A} = 5$ and $\rho_b \sigma^2 = 0.7$ is fixed. As $Pe=120$ is kept constant, different temperatures mean different swim speeds, too. We find that the density in both the dilute and the dense phase increases with temperature. Likewise the area of the dilute phase decreases with temperature such that the normalization $N = \int \bar{\rho}(x) dx$ holds. The magnitude of the polarization effect increases with swim speed as the particles push harder against the interface, hence an increase in s (and therefore in T due to the constant Pe number) gives a larger compression of the dense phase. Therefore we observe an increase of the bulk density of the dense phase at high temperatures.

In Fig. 4.2(b) we show $\bar{\rho}(x)$ for different values of bulk density ρ_b , as indicated by color and pointstyle, while $s\tau_0/\sigma = 60$, $k_B T/\epsilon = 0.5$ and $\mathcal{A} = 5$ are fixed. For $\rho_b \sigma^2 = 0.5$ the system does not separate in two phases and $\bar{\rho}(x) = \text{const} = \rho_b$. Increasing the bulk density leads to phase separation. Clearly, the coexisting densities are independent of the bulk densities, but the area fraction of the dense phase increases, because the total volume of the simulation box decreases with ρ_b .

Panel (c) of Fig. 4.2 shows the dependence on the aspect ratio. Here $k_B T/\epsilon = 0.5$, $s\tau_0/\sigma = 60$, and $\rho_b \sigma^2 = 0.7$ are fixed. For $\mathcal{A} = 2.5$ and $\mathcal{A} = 5$ the density profiles share the same overall shape and the coexisting bulk densities in gas and liquid are the same. Increasing the aspect ratio further to $\mathcal{A} = 10$, i.e. making the simulation box narrower, this shape is not fully retained. We

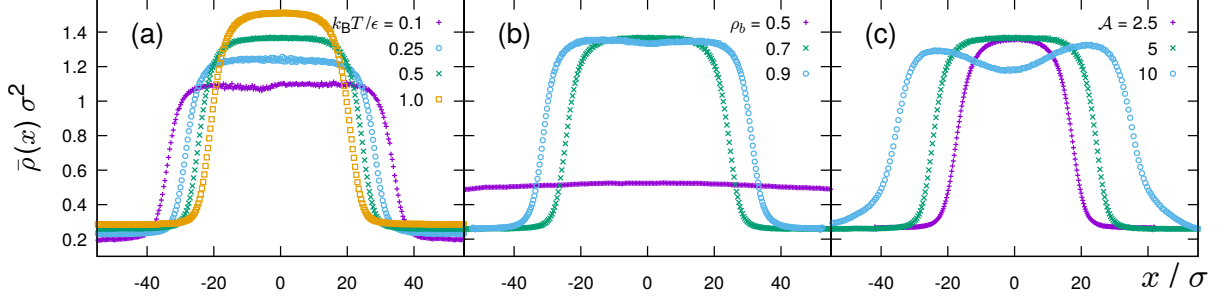


Figure 4.2: Density profiles $\bar{\rho}(x)$ along the x axis. (a) For different temperatures $k_B T / \epsilon = 0.1, 0.25, 0.5,$ and 1.0 . The corresponding swim speeds are $s\tau_0 / \sigma = 12, 30, 60,$ and 120 . The parameters $\mathcal{A} = 5$ and $\rho_b \sigma^2 = 0.7$ are fixed. (b) For different bulk densities $\rho_b \sigma^2 = 0.5, 0.7,$ and 0.9 , while $\mathcal{A} = 5$ and $k_B T / \epsilon = 0.5$ are fixed. (c) For different aspect ratios $\mathcal{A} = 2.5, 5,$ and 10 , while $k_B T / \epsilon = 0.5$ and $\rho_b \sigma^2 = 0.7$ are fixed.

assume that finite size effects due to the short length L_y are responsible for this. Nevertheless, the density profile suggests that the bulk densities in the gas and the liquid phase are the same for all aspect ratios considered.

Current

The one-body current distributions \mathbf{J} and \mathbf{J}^ω are calculated as given by (3.16) and (3.17), respectively, where the corresponding velocity operator is evaluated at the physical time evolution and thus is given by the velocity of the particles. In two spatial dimensions the components of the current \mathbf{J} are J_x, J_y , and \mathbf{J}^ω reduces to a scalar denoted by J_φ . These are shown in Fig. 4.3 (a), (b), and (c), respectively, where the rotational current J_φ is magnified by a factor of 10 to fit the scale. For the bulk currents in dilute and dense phases the dependence on position and angle are as expected. For example, J_x is positive for $-\pi/2 < \varphi < \pi/2$ with a maximum at $\varphi = 0$ as the particles swim in positive x -direction along their built-in orientation. Consequently the minimum of J_x is at $\varphi = \pi$. At $\varphi = -\pi/2$ and $\pi/2$ the particles swim in the negative and the positive y -direction respectively and $J_x = 0$ in bulk. At these angles the bulk value of J_y is maximal ($\varphi = \pi/2$), or rather minimal ($\varphi = -\pi/2$), as these orientations are associated with swimming in positive y -direction (“upwards”), or in negative y -direction (“downwards”), respectively. In bulk the rotational current is zero, as no torques act on the particles and the density is constant.

At the interface the behavior of J_x, J_y and J_φ becomes more complex: In general the current is high in the dilute phase and low in the dense phase. The value of J_x drops drastically at the interface, as does the value of J_y . The reason is that swimming along the orientation of the particles is hindered in the dense phase due to the high density and thus the collisions with other particles. In addition, the regions where J_x changes sign deform. For the “left” interface ($x/\sigma \approx -20$) for example the, J_x is negative for $\varphi = \pi/2$. Hence the particles do not swim along their orientation. Regarding J_y we observe an increase of the value of J_y compared to the bulk value. Furthermore, at the interface a rotational current J_φ is observed indicating a directed

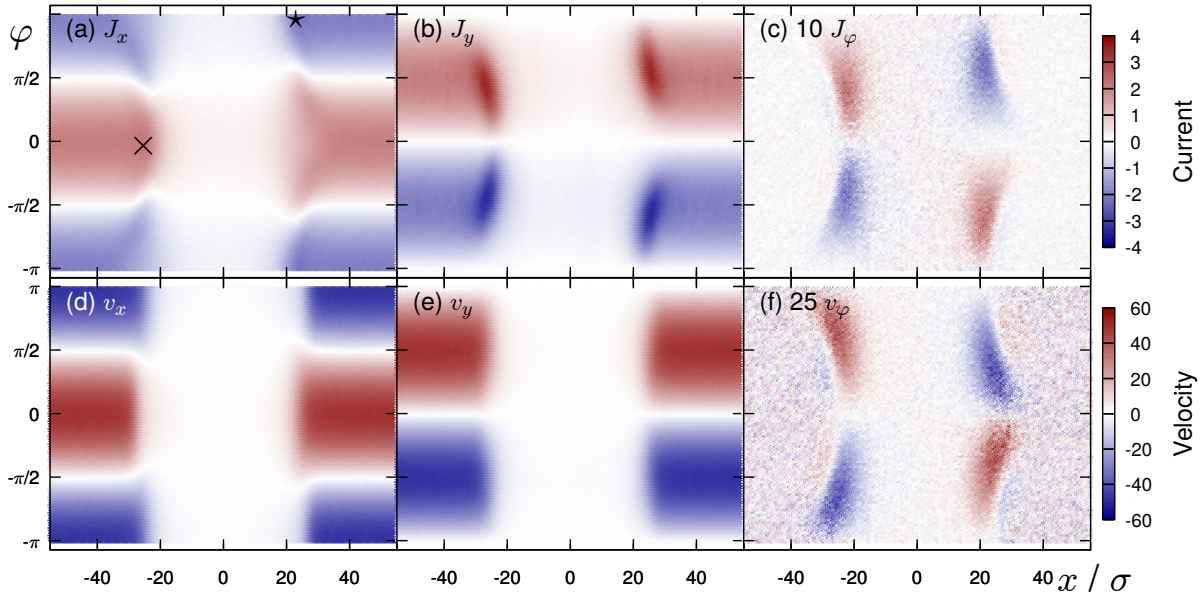


Figure 4.3: Components of the current, (a) – (c), and velocity, (d) – (f) as a function of x and φ for $s\tau_0/\sigma = 60$, $k_B T/\epsilon = 0.5$, $\mathcal{A} = L_x/L_y = 5$, and $\rho_b = 0.7$. Blue areas indicate regions with negative components, red areas indicate regions where the components are positive. In the white regions the value of the components is small with completely white indicating zero. For clarity the rotational components in (d) and (f) are magnified by a factor of 10 and 25, respectively. The cross (\times) and the star (\star) in (a) indicate corresponding points with respect to symmetry.

rotational movement at the interface.

At the interface we picture the trajectory of the particles as shown in Fig. 4.4 by the dashed arrow. The tagged (red) particle approaches the interface that cannot be penetrated in (a). The orientation of the particle changes over time by diffusion and becomes parallel to the interface in (b) and the particle moves parallel to the interface (c) until the orientations changes again in the direction away from the interface in (d). Based on similar ideas, the authors of Ref. [58] formulated a kinetic theory for phase-separating system of ABP. This explains the increase of J_y at the interface, as well as the occurrence of the rotational current J_φ , both shown in Fig. 4.3. The current in y -direction has its origin in the movement of the particles parallel to the interface. Due to the interface this movement in y -direction is increased compared to the “regular” movement in this direction in the dilute phase, resulting in an increase of J_y at the interface, compared to the dilute phase. The sign of the current is positive for $\varphi > 0$. As the angle is measured against the x -axis, $\varphi > 0$ is equivalent to swimming “upwards”, i.e. in positive y -direction. For $\varphi < 0$ the same arguments explain $J_y < 0$. The orientational current J_φ is generated because the particles have to re-orientate at the interface in order to not be absorbed by it. The value of J_φ is one order of magnitude smaller than the other components, suggesting that the reorientation is slower than other processes at the interface. However, this is not surprising as the reorientation is completely driven by diffusion and is therefore determined by stochastic processes only. Nevertheless a measurable current exists. Furthermore, the density clearly shows a dependence on φ at the interface, c.f. Fig. 4.1. Taking into account the rotational

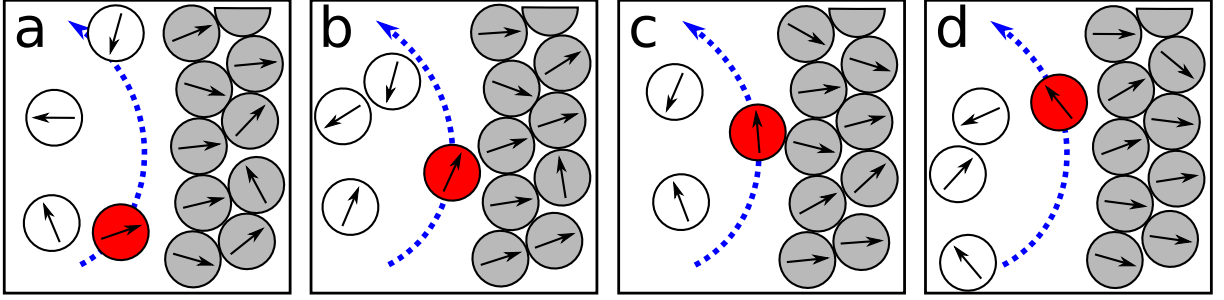


Figure 4.4: Sketch of the behavior of a particle at the interface. The particle in the dense phase are colored in gray, in the dilute phase the particles are white and the tagged particle is red. The arrows indicate the direction of the orientation of the particles, and the dashed line indicates the total path of the tagged particle. (a) The tagged particle approaches the interface. (b) The particle cannot penetrate the interface and the orientational diffusion orientates the particle parallel to the interface. (c) The particles moves parallel to the interface. (d) The orientation diffuses away from the interface and the tagged particle moves in the dilute phase.

equation of motion given in Sec. 3.2 by (3.27) with no external torques and particle-particle interaction for the orientation in the given geometry it yields

$$\gamma^\omega J_\varphi = -k_B T \frac{\partial \rho(x, \varphi)}{\partial \varphi}. \quad (4.9)$$

Therefore the polarization of the interface itself causes the particles to re-orientate and perform the motion sketched in Fig. 4.4.

An additional explanation for J_φ is given by treating the ABP systems as a mixture of an infinite number of species labeled by the orientation, i.e by φ . Due to its polarization the interface is a region rich in particles of species $\varphi \approx 0$. Therefore particles in the dilute phase reorientate at the interface in order to compensate the excess of particles with $\varphi \approx 0$. The effect is thus driven by mixing entropy with respect to the orientations.

The interface from dilute to dense phase ($x < 0$) appears differently from the interface from the dense to the dilute phase ($x > 0$) in Fig. 4.3 and suggests that the system is surprisingly not symmetric, as one expects because the same physical effects should occur at both interfaces. The reason is that not only the symmetry with respect to $x \rightarrow -x$, but also the symmetry with respect to $\omega \rightarrow -\omega$ has to be considered. In two dimensions this corresponds to changing the orientation angle $\varphi \rightarrow \varphi + \pi$. Therefore the point corresponding to e.g. $x/\sigma = -20, \varphi = 0$ is $x/\sigma = 20, \varphi = \pi$ as indicated in Fig. 4.3(a) by the cross (\times) and the star (\star), respectively. As the sign of J_x at these two points is opposite the component J_x can be called an odd quantity. This is clear with the arguments from above, as at $\varphi = \pi$ the orientation of the particles points in negative x -direction which means $J_x < 0$. In contrast, the component J_φ and the density $\rho(x, \varphi)$ (c.f. Fig. 4.1) for example are even quantities. This symmetry argument can be used for all quantities and is an important part of our interfacial model that will be presented in a future paper [4].

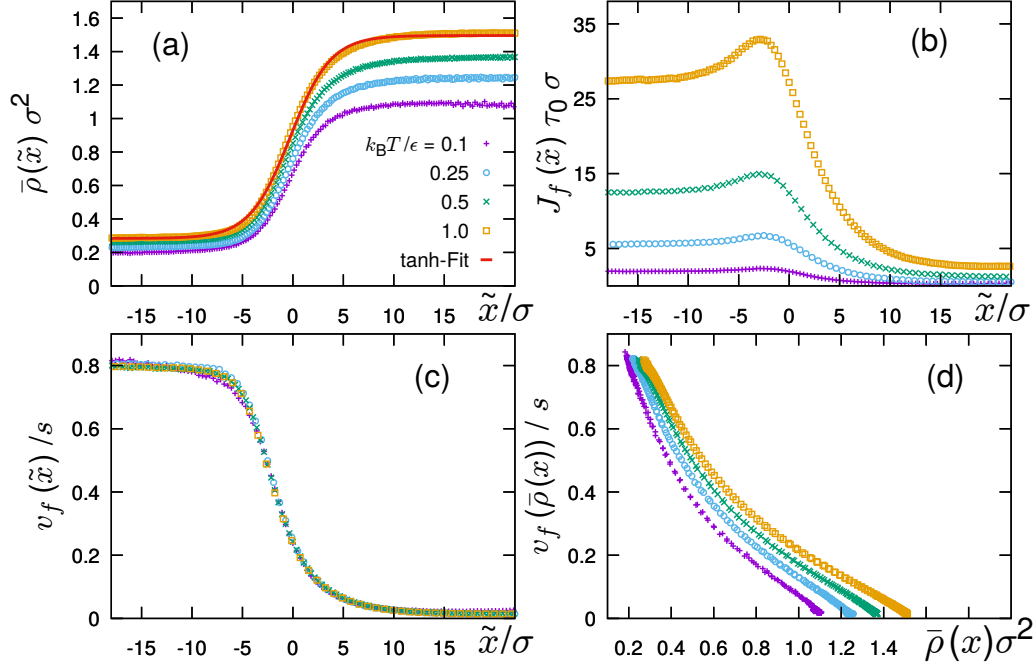


Figure 4.5: (a) Density profile as in Fig. 4.2 (a) with the fit (4.13). (b) Forward current J_f for different temperatures $k_B T/\epsilon = 0.1, 0.25, 0.5, 1$. The corresponding swim speeds are $s\tau_0/\sigma = 12, 30, 60,$ and 120 . The parameters $\mathcal{A} = 5$ and $\rho_b\sigma^2 = 0.7$ are fixed. (c) Same as (b), but the forward velocity is displayed. All quantities are centered around the Gibbs dividing surface and are therefore displayed as a function of $\tilde{x} = x - x_{\text{GDS}}$. (d) Forward velocity as a function of density. Colors corresponds to the legend in (a).

Velocity

The velocity field, as defined via

$$\mathbf{v}(x, \varphi) = \frac{\mathbf{J}(x, \varphi)}{\rho(x, \varphi)} \quad (4.10)$$

is shown in Fig. 4.3 (d) – (f) componentwise. The dependence of \mathbf{v} on x and φ is the same in most areas as for \mathbf{J} (c.f. Fig. 4.3 (a) – (c)). But some of the structures \mathbf{J} shows at the interface are not present in \mathbf{v} . For instance the characteristic feature of J_y , the increase at the interface, is not present in v_y . An angular velocity at the interface, v_φ , is observed at the interface, as expected from the existence of J_φ . But the magnification factor of v_φ to fit the scale of the other components is much higher compared to the magnification factor of J_φ .

4.2.2 Density, current, and velocity profiles with respect to the Gibbs dividing surface

The results in the following are displayed as a function of the position with respect to the Gibbs dividing surface (GDS) [73] of the interface at the crossover from dilute to dense phase. A common way to set the GDS is to take the liquid and the gas absorption into account,

respectively defined by

$$\Gamma_g(x_0) = \int_{-\infty}^{x_0} dx (\bar{\rho}(x) - \rho_g), \quad \Gamma_l(x_0) = \int_{x_0}^{\infty} dx (\bar{\rho}(x) - \rho_l), \quad (4.11)$$

where x_0 denotes the (arbitrary) location of the interface [19]. The densities ρ_g and ρ_l respectively denote the bulk density in the dilute and the dense phase. The location of the dividing surface, x_{GDS} , is then given such that

$$\Gamma_g(x_{\text{GDS}}) + \Gamma_l(x_{\text{GDS}}) = 0. \quad (4.12)$$

With this, the x -coordinate is shifted in the following according to $\tilde{x} = x - x_{\text{GDS}}$.

In Fig. 4.5(a) we show the same density profiles as in Fig. 4.2(a), but centered around the GDS. Note that x_{GDS} is different for every temperature and has to be calculated for each value of temperature separately. Additionally a fit is shown of the form

$$\bar{\rho}_{\text{fit}}(\tilde{x}) = \alpha + \beta \tanh\left(\frac{\tilde{x}}{\nu}\right), \quad (4.13)$$

where ν determines the width of the interface. The fit parameters α and β can be related to the coexisting densities according to

$$\alpha = \frac{\rho_l + \rho_g}{2}, \quad \beta = \frac{\rho_l - \rho_g}{2}. \quad (4.14)$$

The fit function (4.13) is commonly used in the literature [14, 69, 72] and matches the data remarkably well.

In Fig. 4.5(b) the orientation-averaged forward current

$$\begin{aligned} J_f(x) &= \int d\boldsymbol{\omega} \boldsymbol{\omega} \cdot \mathbf{J}(\mathbf{r}, \boldsymbol{\omega}) \\ &= \int_0^{2\pi} d\varphi (\cos(\varphi) J_x(x, \varphi) + \sin(\varphi) J_y(x, \varphi)) \end{aligned} \quad (4.15)$$

is shown with respect to the GDS. In the figure the forward current is given for systems with fixed $\rho_b \sigma^2 = 0.7$ and $\mathcal{A} = 5$, while $k_{\text{B}}T$ is varied as indicated. As at low temperature, s decreases due to the constant Pe , the bulk values for J_f decrease with temperature. However, the increase of J_f at the interface is observed for all temperatures. We assume that this maximum is associated with the increase of J_y at the interface as discussed above.

Interestingly the components of the average velocity in orientation direction, i.e. the forward velocity $v_f(x) = J_f(x)/\bar{\rho}(x)$, does not show the increase of value at the interface such as the forward current, as shown by Fig. 4.5 (c). The maximum of J_f is compensated by the density profile, as the crossover from the dilute to dense (bulk) value in J_f is much smoother than in $\bar{\rho}$. Due to the scaling of v_f to the swim speed s and the centering around the GDS all curves lie on top of each other, suggesting that the forward velocity is not solely determined by either the temperature or the swim speed, but by Pe . We investigate a dramatic decrease in forward

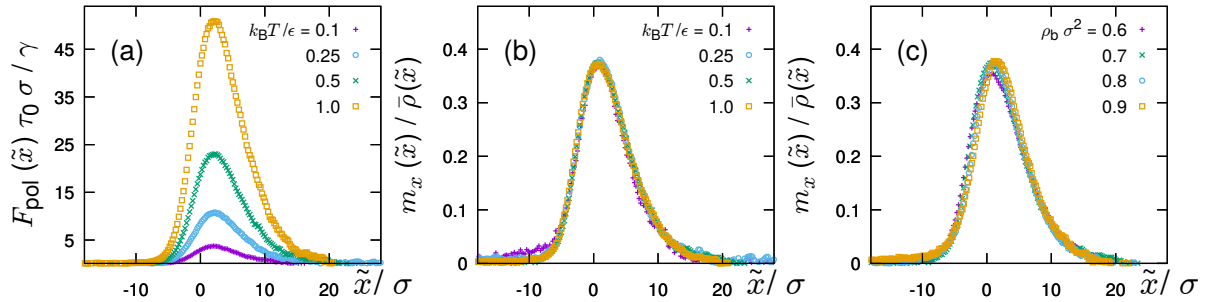


Figure 4.6: (a) Polarization force per unit area $F_{\text{pol}}(x) = \gamma s m_x(x)$ for different temperatures $k_B T / \epsilon = 0.1, 0.25, 0.5, 1$. The corresponding swim speeds are $s \tau_0 / \sigma = 12, 30, 60$, and 120 . The parameters $\mathcal{A} = 5$ and $\rho_b \sigma^2 = 0.7$ are fixed. (b) same as (a) but the Polarization $m_x(x) / \bar{\rho}(x)$ is shown. (c) same as (b) but for different bulk densities $\rho_b \sigma^2 = 0.6, 0.7, 0.8$, and 0.9 , while $\mathcal{A} = 5$ and $k_B T / \epsilon = 0.5$ are fixed. All quantities are centered around the GDS.

swimming at the interface as the high density in the dense phase reduces the motility of the swimmers drastically.

Combining the results for $\bar{\rho}(x)$ and $v_f(x)$ lets us display the forward velocity as a function of $\bar{\rho}(x)$ as shown in Fig. 4.5 (d). As described above the forward velocity decreases with increasing density. The velocity of the ABP in direction of their orientation as a function of density, $v(\rho)$ (which is comparable to $v_f(\rho)$ here), is of particular interest for some approaches phenomenologically explaining MIPS [51, 52]. The authors of Ref. [51] introduce the density-dependent swim speed in order to approximate the two-body density and give a linear relation for $v(\rho)$, whereas Stenhammar *et al.* estimate $v(\rho)$ by taking the free path of individual ABP between collisions into account [52]. Despite their approximation also gives a linear dependency, a non-linear behavior is observed for high Pe in computer simulations, c.f. supplementary material of Ref. [52]. We find clearly a non-linear dependency of v_f on $\bar{\rho}$. It is comparable to our findings in [2] and [3], but the sampling therein is fundamentally different from here because each data point represents a whole simulation of a bulk system. Whether these results both origin in the same physical mechanisms or not must be demonstrated in future studies, as well as if a linear function $v(\rho)$ is sufficient to describe MIPS.

4.2.3 Polarization profile

The polarization of the particles is measured by [14, 51, 56, 59, 67, 71]

$$\mathbf{m}(\mathbf{r}, t) = \int d\omega \omega \rho(\mathbf{r}, \omega, t). \quad (4.16)$$

In two dimensions and in the elongated geometry only the x -component is not vanishing. It yields in steady state

$$m_x(x) = \int_0^{2\pi} d\varphi \cos(\varphi) \rho(x, \varphi). \quad (4.17)$$

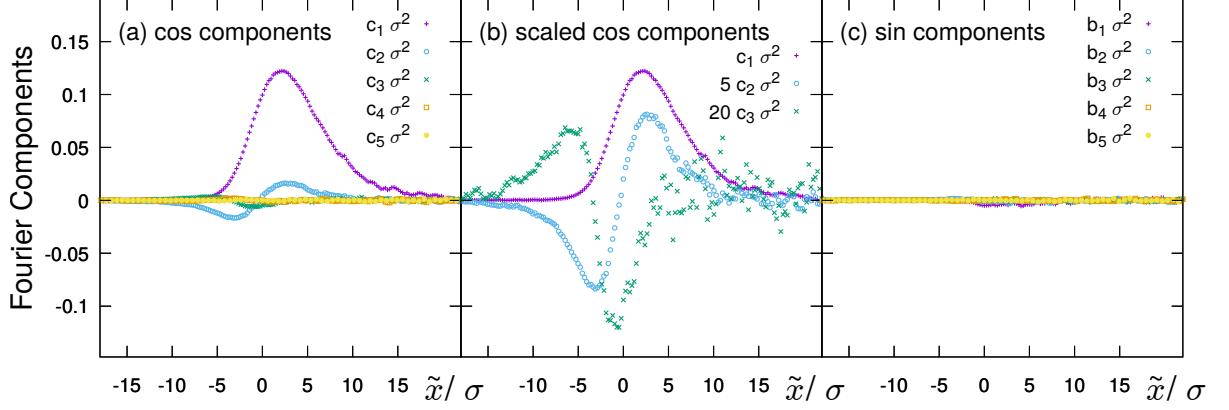


Figure 4.7: Fourier components of the one-body density $\rho(x, \varphi)$ for a system with $\rho_b \sigma^2 = 0.7$, $k_B T / \epsilon = 0.5$, and $\mathcal{A} = 5$, centered around the GDS. In (a) cos-components as given by (4.21). In cos-components c_1 , c_2 and c_3 as in (a) but scaled. In (c) sin-components as given by (4.22).

As polarized particles swim collectively in one direction, there is a polarization force density that is associated with polarization:

$$F_{\text{pol}}(x) = \gamma s m_x(x). \quad (4.18)$$

Figure 4.6 (a) shows this polarization force density as obtained from computer simulations centered around the Gibbs dividing surface for different temperatures and hence different swim speeds s , while the bulk density $\rho_b \sigma^2 = 0.7$ and the aspect ratio $\mathcal{A} = 5$ are fixed. As the swim speed increases with temperature, it is clear that the polarization force at the interface increases with temperature, too. The physical interpretation is that a larger swimming velocity pushes the particles harder against the interface and thus the polarization effect is increased.

Figure 4.6 (b) shows the polarization m_x . Clearly all curves lie on top of each other which again indicates that the temperature is not important for the fundamental physical processes at the interface, as long as Pe is kept constant. A direct comparison to the work of Paliwal *et al.*, c.f. Fig. 5 (a) in Ref. [14], shows very good agreement. As $\text{Pe}=50$ there and the polarization is displayed in the same way there as here, a comparison between our work and Ref. [14] is reasonable and the good agreement shows the validity of our simulation results.

In Fig. 4.6 (c) we show the polarization for different bulk densities and $k_B T / \epsilon = 0.5$ and $\mathcal{A} = 5$ fixed. Surprisingly, the maximum of the polarization for $\rho_b \sigma^2$ is decreased compared to the other bulk density. We explain this by the fact that $\rho_b \sigma^2$ is close to the critical point and finite size effect may play an important role there.

4.2.4 Angular Fourier decomposition of the density distribution

The orientation of the active particles is evenly distributed in the two bulk phases, but not at the interface as shown by e.g. Fig. 4.1. Therefore integration over the orientation is useful to understand the physics of the interface such as the emergence of polarization. In order to generalize and study the interface more systematically we perform a Fourier decomposition of

the angular dependence of the one-body density. The Fourier expansion is given by

$$\rho(x, \varphi) = c_0(x) + \sum_{k=1}^{\infty} (c_k(x) \cos(k\varphi) + b_k(x) \sin(k\varphi)) \quad (4.19)$$

with the components

$$c_0(x) = \frac{1}{2\pi} \int_0^{2\pi} \rho(x, \varphi) d\varphi, \quad (4.20)$$

$$c_k(x) = \frac{1}{\pi} \int_0^{2\pi} \rho(x, \varphi) \cos(k\varphi) d\varphi, \quad (4.21)$$

$$b_k(x) = \frac{1}{\pi} \int_0^{2\pi} \rho(x, \varphi) \sin(k\varphi) d\varphi. \quad (4.22)$$

The components c_0 and c_1 can thus be identified as $2\pi c_0 = \bar{\rho}$ and $\pi c_1 = m_x$.

Figure 4.7 shows the first five Fourier components, $c_1 - c_5$ in (a), c_1, c_2 , and c_3 scaled in (b), and $b_1 - b_5$ in (c), of the density obtained from a simulation with $\rho_b \sigma^2 = 0.7$, $k_B T / \epsilon = 0.5$, and $\mathcal{A} = 5$, centered around the GDS. Clearly c_1 is proportional to the polarization m_x , c.f. Fig. 4.6 (b). The components c_2 and c_3 are different from zero, indicating higher order anisotropy effects. The scaled representation of c_2 and c_3 shows that these are measurable. Especially c_2 is antisymmetric with respect to the GDS, and c_3 is minimal close to the interface. Whether c_3 shows some symmetry as well is not clear because of the noise in the dense phase. Higher components seem to be negligible in $\rho(x, \varphi)$ as they decay fast and $c_4 = c_5 \approx 0$. However, a more detailed study is necessary to validate that. Differently to the cos-coefficients, the sin-coefficients vanish for all k , as presented by Fig. 4.7 (c). As these components are associated with the odd part of $\rho(x, \varphi)$ with respect to inversion of the orientation, we expected this result because the density is clearly an even function with respect to the orientation. Hence a Fourier decomposition for other quantities that depend on the orientation angle, e.g. the current of the velocity, are reasonable to determine their symmetry and to extract information about the physics behind them. This procedure may be also generalized to higher spatial dimensions or bulk systems by decomposition in powers of the orientation instead of angular Fourier components. In such case the forward current is given by the first moment of the current and the polarization \mathbf{m} is given by the first moment of the density, c.f. (4.15) and (4.16), respectively.

Despite c_1 , i.e. the polarization, no detailed study of the Fourier components exists to our best knowledge, apart from a paper by Speck and Jack for an ideal system [67]. Therein the authors use the second moment of the orientation to study the mechanical pressure on a wall. Therefore the Fourier decomposition and the symmetry of the physical quantities leave room for proper theoretical description and offer the opportunity for qualitative and quantitative validation of such a model.

5 Conclusion and outlook

In this thesis we investigated the physics and especially the phenomenon of motility-induced phase separation (MIPS) of active Brownian particles by two different theoretical approaches and computer simulations. We formulated an effective equilibrium approach in [1] that is briefly summarized in Sec. 3.1. The approach allows the derivation of an effective activity-dependent pair interaction potential between the Brownian particles by integrating out the orientation of the particles. The activity only determines the form of the interaction potential which allows the study of the active matter as a passive system with a modified, i.e., the effective interaction potential. The mechanism that leads to MIPS is identified as explicit repulsive interactions develop an attractive part in the effective potential. It has been demonstrated that the approach can be extended to external fields [48] and is useful to calculate a whole range of thermodynamic quantities for active systems [49, 50]. Because the effective equilibrium mapping allows the usage of well-known methods from equilibrium statistical, even more applications are thinkable.

The effective equilibrium approach is limited to cases with low activity due to assumptions that has to be taken in the derivation of the effective interaction. In order to overcome these limitations, we developed a power functional theory (PFT) for active particles. In [2] we formulated the basic idea of a variational principle for active systems, presented a well-justified approximation for the power functional, and introduced new sampling methods for Brownian dynamics simulations. A more detailed derivation of the theory is given in [3]. Therein a nonequilibrium sum rule is presented that allows the calculation of the power functional by only considering external driving forces in steady state. An overview of both publications is given in Sec. 3.2. With this work we demonstrated how power functional theory is used to describe a concrete out-of-equilibrium system, how powerful the approach in application is, and how good the agreement to numerical simulations is when a rather simple approximation for the P_t^{exc} functional is considered. PFT is therefore a natural choice to describe other open problems in nonequilibrium statistical physics, such as the laning transition [34, 74].

In order to fully describe MIPS with PFT the simple form of P_t^{exc} described in [2] and [3] is not sufficient as the fluid-fluid interface has to be considered explicitly. The planned publication [4] will give a detailed treatment of the interface. In Sec. 4 we presented a detailed simulation study of the free interface that will be also included in [4]. We investigated the one-body density distribution, the one-body current distribution, and the velocity as a function of spatial coordinates and the orientation. In accordance with previous work we find that the interface is polarized. The polarization is furthermore identified as the prime effect for additional and a priori unknown effects at the interface, such as the maximum in the forward current and the rotational current. The angular Fourier decomposition is useful to determine the symmetry of

quantities with respect to inversion of the orientation. We also presented the higher Fourier coefficients of the density. Thereby the polarization and the density profile emerges naturally within the decomposition. Our numerical findings are compared to work by other authors and show good agreement. We take this as a validation of our data.

In order to gain a full understanding of the interface and hence the phase separation of active particles an analytical model would be very valuable. In a future publication we will present a new approach for modeling the interface, based on previous results [2],[3] and new findings such as the symmetry character of the one-body currents and the one-body density and their anisotropy at the interface. Furthermore, we want to apply and extend the bulk functional P_t^{exc} , given by (3.29), to the interface to obtain a power functional theory that covers the behavior of the particles at the interface. The functional should not only give dissipative forces but also nonequilibrium forces that are responsible for structural formation processes. It gives thus all nonequilibrium (superadiabatic) forces that are important to describe the nonequilibrium phenomena of MIPS. By doing so, a big step in establishing full picture of the physics of phase separation in active Brownian systems is provided. The numerical results presented here are very important not only as a validity check of the theory, but also as a feedback in the formulation of new ideas. All this work goes beyond the scope of this thesis. But the full study will be presented as a paper.

References

- [1] T. F. F. Farage, P. Krinninger, and J. M. Brader, *Phys. Rev. E* **91**, 042310 (2015).
 - [2] P. Krinninger, M. Schmidt, and J. M. Brader, *Phys. Rev. Lett.* **117**, 208003 (2016); Erratum: **119**, 029902 (2017), 208003.
 - [3] P. Krinninger and M. Schmidt, *submitted* (2018).
 - [4] P. Krinninger, S. Hermann, D. de las Heras, and M. Schmidt, *in preparation* (2018).
-
- [5] M. Alexander, L. F. Rojas-Ochoa, M. Leser, and P. Schurtenberger, *J. Colloid Interface Sci.* **253**, 35 (2002).
 - [6] H. D. Goff, *Int. Dairy J.* **7**, 363 (1997).
 - [7] D. Brutin, B. Sobac, B. Loquet, and J. Sampaol, *J. Fluid Mech.* **667**, 85 (2011).
 - [8] K. B. Singh, L. R. Bhosale, and M. S. Tirumkudulu, *Langmuir* **25**, 4284 (2009).
 - [9] M. Ballerini, N. Cabibbo, R. Candelier, A. Cavagna, E. Cisbani, I. Giardina, V. Lecomte, A. Orlandi, G. Parisi, A. Procaccini, M. Viale, and V. Zdravkovic, *Proc. Nat. Aca. Sci.* **105**, 1232 (2008).
 - [10] R. Lukeman, Y.-X. Li, and L. Edelstein-Keshet, *Proc. Nat. Aca. Sci.* **107**, 12576 (2010).
 - [11] Y. Sumino, K. H. Nagai, Y. Shitaka, D. Tanaka, K. Yoshikawa, H. Chaté, and K. Oiwa, *Nature* **483**, 448 (2012).
 - [12] H. P. Zhang, A. Be'er, E.-L. Florin, and H. L. Swinney, *Proc. Nat. Aca. Sci.* **107**, 13626 (2010).
 - [13] I. Buttinoni, J. Bialké, F. Kümmel, H. Löwen, C. Bechinger, and T. Speck, *Phys. Rev. Lett.* **110**, 238301 (2013).
 - [14] S. Paliwal, J. Rodenburg, R. van Roij, and M. Dijkstra, *New J. Phys.* **20**, 015003 (2018).
 - [15] S. Hermann and M. Schmidt, *Soft Matter* **14**, 1614 (2018).
 - [16] M. E. Cates and J. Tailleur, *Ann. Rev. Cond. Matter Phys.* **6**, 219 (2015).
 - [17] R. Evans, M. Oettel, R. Roth, and G. Kahl, *J. Phys. Condens. Matter* **28**, 240401 (2016).
 - [18] R. Evans, *Adv. Phys.* **28**, 143 (1979).
 - [19] J.-P. Hansen and I. R. McDonald, *Theory of Simple Liquids* (Academic Press, Oxford, 2013).
 - [20] J. K. Percus, *J. Stat. Phys.* **15**, 505 (1976).

- [21] A. J. Archer, B. Chacko, and R. Evans, *J. Chem. Phys.* **147**, 034501 (2017).
- [22] Y. Rosenfeld, *Phys. Rev. Lett.* **63**, 980 (1989).
- [23] Y. Rosenfeld, M. Schmidt, H. Löwen, and P. Tarazona, *Phys. Rev. E* **55**, 4245 (1997).
- [24] R. Roth, K. Mecke, and M. Oettel, *J. Chem. Phys.* **136**, 081101 (2012).
- [25] H. Hansen-Goos, M. Mortazavifar, M. Oettel, and R. Roth, *Phys. Rev. E* **91**, 052121 (2015).
- [26] R. Zwanzig, *Nonequilibrium Statistical Mechanics* (Oxford University Press, New York, 2001).
- [27] U. M. B. Marconi and P. Tarazona, *J. Phys.: Cond. Matt.* **110**, 8032 (1999).
- [28] A. J. Archer and R. Evans, *J. Chem. Phys.* **121**, 4246 (2004).
- [29] M. Schmidt and J. M. Brader, *J. Chem. Phys.* **138**, 214101 (2013).
- [30] J. M. Brader and M. Schmidt, *J. Chem. Phys.* **139**, 104108 (2013).
- [31] M. Schmidt, *J. Chem. Phys.* **148**, 044502 (2018).
- [32] M. Schmidt, *J. Chem. Phys.* **143**, 174108 (2015).
- [33] D. de las Heras and M. Schmidt, *Phys. Rev. Lett.* **120**, 028001 (2018).
- [34] T. Geigenfeind, D. de las Heras, and M. Schmidt, *to be published* (2018).
- [35] A. Fortini, D. de las Heras, J. M. Brader, and M. Schmidt, *Phys. Rev. Lett.* **113**, 167801 (2014).
- [36] D. Frenkel and B. Smit, *Understanding Molecular Simulation* (Academic Press, London, 2002).
- [37] M. P. Allen and D. J. Tildesley, *Computer Simulations of Liquids* (Oxford University Press, New York, 2009).
- [38] J. D. Weeks, D. Chandler, and H. C. Andersen, *J. Chem. Phys.* **54**, 5237 (1971).
- [39] T. Schindler and M. Schmidt, *J. Chem. Phys.* **145**, 064506 (2016).
- [40] J. Bleibl and M. Oettel, *private communication*.
- [41] R. F. Fox, *Phys. Rev. A* **33**, 467 (1986).
- [42] R. F. Fox, *Phys. Rev. A* **34**, 4525 (1986).
- [43] W. G. Madden and S. A. Rice, *J. Chem. Phys.* **72**, 4208 (1980).
- [44] G. S. Redner, A. Baskaran, and M. F. Hagan, *Phys. Rev. E* **88**, 012305 (2013).
- [45] M. Rein and T. Speck, *Eur. Phys. J. E* **39**, 84 (2016).
- [46] P. Jung and P. Hänggi, *Phys. Rev. A* **35**, 4464 (1987).
- [47] P. Jung and P. Hänggi, in *Advances in chemical physics, volume 89*, edited by I. Prigogine and S. A. Rice (Wiley & Sons Inc., 2007) Chap. Colored Noise in Dynamical Systems.
- [48] R. Wittmann and J. M. Brader, *Europhys. Lett.* **114**, 68004 (2016).

- [49] R. Wittmann, C. Maggi, A. Sharma, A. Scacchi, J. M. Brader, and U. M. B. Marconi, *J. Stat. Mech.*, 113207 (2017).
- [50] R. Wittmann, U. M. B. Marconi, C. Maggi, and J. M. Brader, *J. Stat. Mech.*, 113208 (2017).
- [51] J. Bialké, H. Löwen, and T. Speck, *Europhys. Lett.* **103**, 30008 (2013).
- [52] J. Stenhammar, A. Tiribocchi, R. J. Allen, D. Marenduzzo, and M. E. Cates, *Phys. Rev. Lett.* **111**, 145702 (2013).
- [53] M. Levy, *Proc. Nat. Acad. Sci.* **76**, 6062 (1979).
- [54] W. S. B. Dwandaru and M. Schmidt, *Phys. Rev. E* **83**, 061133 (2011).
- [55] A. P. Solon, J. Stenhammar, M. E. Cates, Y. Kafri, and J. Tailleur, *Phys. Rev. E* **97**, 020602(R) (2018).
- [56] T. Speck, A. M. Menzel, J. Bialké, and H. Löwen, *J. Chem. Phys.* **142**, 224109 (2015).
- [57] S. C. Takatori and J. F. Brady, *Soft Matter* **11**, 7920 (2015).
- [58] G. S. Redner, M. F. Hagan, and A. Baskaran, *Phys. Rev. Lett.* **110**, 055701 (2013).
- [59] T. Speck, *Europhys. Lett.* **114**, 30006 (2016).
- [60] S. C. Takatori and J. F. Brady, *Phys. Rev. E* **91**, 032117 (2015).
- [61] J. Palacci, C. Cottin-Bizonne, C. Ybert, and L. Bocquet, *Phys. Rev. Lett.* **105**, 088304 (2010).
- [62] A. P. Solon, J. Stenhammar, R. Wittkowski, M. Kardar, Y. Kafri, M. E. Cates, and J. Tailleur, *Phys. Rev. Lett.* **114**, 198301 (2015).
- [63] V. Prymidis, S. Paliwal, M. Dijkstra, and L. Fillion, *J. Chem. Phys.* **145**, 124904 (2016).
- [64] U. M. B. Marconi, C. Maggi, and S. Melchionna, *Soft Matter* **12**, 5727 (2016).
- [65] A. P. Solon, Y. Fily, A. Baskaran, M. E. Cates, Y. Kafri, M. Kardar, and J. Tailleur, *Nature Physics* **11**, 673 (2015).
- [66] W. Yan and J. F. Brady, *J. Fluid Mech.* **785**, R1 (2015).
- [67] T. Speck and R. L. Jack, *Phys. Rev. E* **93**, 062605 (2016).
- [68] B. van der Meer, V. Prymidis, M. Dijkstra, and L. Fillion, arXiv 1609.03867 (2016).
- [69] J. Bialké, J. T. Siebert, H. Löwen, and T. Speck, *Phys. Rev. Lett.* **115**, 098301 (2015).
- [70] A. Pototsky and H. Stark, *Europhys. Lett.* **98**, 50004 (2012).
- [71] T. Speck, *Eur. Phys. J. Special Topics* **225**, 2287 (2016).
- [72] S. Paliwal, V. Prymidis, L. Fillion, and M. Dijkstra, *J. Chem. Phys.* **147**, 084902 (2017).
- [73] J. W. Gibbs, *The collected works of J. Willard Gibbs* (Longmans, Green and Co., New York, 1928).
- [74] T. Glanz and H. Löwen, *J. Phys.: Condens. Matter* **24**, 464114 (2012).

6 Publications

This section contains chronologically all publications that contributed to this thesis. A fourth paper concerning interfaces in systems of phase-separated active Brownian particles is in preparation [4] and an abstract is included here on page 88. First results obtained from computer simulations are presented in Sec. 4.

[1]	<i>Effective interactions in active Brownian suspensions.</i> T. F. F. Farage, P. Krinninger, and J. M. Brader, Physical Review E 93 , 042310 (2015)	59
[2]	<i>Nonequilibrium Phase Behavior from Minimization of Free Power Dissipation.</i> P. Krinninger, M. Schmidt, and J. M. Brader, Physical Review Letters 117 , 208003 (2016); Erratum: 119 , 029902 (2017)	69
[3]	<i>Power functional theory for active Brownian particles: general formulation and power sum rules.</i> P. Krinninger and M. Schmidt, <i>submitted</i> (2018)	75

Effective interactions in active Brownian suspensionsT. F. F. Farage,¹ P. Krinninger,² and J. M. Brader¹¹*Department of Physics, University of Fribourg, CH-1700 Fribourg, Switzerland*²*Theoretische Physik II, Physikalisches Institut, Universität Bayreuth, D-95440 Bayreuth, Germany*

(Received 14 January 2015; published 16 April 2015)

Active colloids exhibit persistent motion, which can lead to motility-induced phase separation (MIPS). However, there currently exists no microscopic theory to account for this phenomenon. We report a first-principles theory, free of fit parameters, for active spherical colloids, which shows explicitly how an *effective* many-body interaction potential is generated by activity and how this can rationalize MIPS. For a passively repulsive system the theory predicts phase separation and pair correlations in quantitative agreement with simulation. For an attractive system the theory shows that phase separation becomes suppressed by moderate activity, consistent with recent experiments and simulations, and suggests a mechanism for reentrant cluster formation at high activity.

DOI: [10.1103/PhysRevE.91.042310](https://doi.org/10.1103/PhysRevE.91.042310)

PACS number(s): 82.70.Dd, 64.75.Xc, 05.40.−a

I. INTRODUCTION

Active colloidal particles in suspension are currently the subject of considerable attention, due largely to their ability to model self-organization phenomena in biological systems, but also as a new branch of fundamental research in nonequilibrium statistical mechanics: assemblies of active colloids are intrinsically out-of-equilibrium systems. In contrast to their passive counterparts, active colloids undergo both solvent-induced Brownian motion and a self-propulsion which requires a continual consumption of energy from the local environment. Several idealized experimental model systems have been developed, such as catalytic Janus particles [1–3], colloids with artificial flagella [4], and light-activated particles [5]. The understanding of active systems has been further aided by the development of simple theoretical models, which aim to capture the essential physical mechanisms and which have been used to study, e.g., bacteria, cells, or filaments in the cytoskeleton [6–9].

Active particles are characterized by a persistent motion, which can lead to “self-trapping” dynamics and a rich variety of related collective phenomena [6–10]. Even the simplest models of active spherical particles with purely repulsive interactions can display the phenomenon of motility-induced phase separation (MIPS) [10]. In many respects, MIPS resembles the equilibrium phase separation familiar from passive systems with an attractive component to the interaction potential (e.g., the Lennard-Jones potential) [11–15]. This apparent similarity has motivated several recent attempts to map an assembly of active particles onto a passive equilibrium system, interacting via an effective attraction (usually taken to be a very short range sticky-sphere potential [16,17]). Despite the intuitive appeal of mapping to an equilibrium system, there exists no systematic theoretical approach capable of predicting an effective equilibrium potential directly from the bare interactions.

Our current understanding of MIPS has largely been gained through either simulation [12–15,18] or phenomenological theory [10,11,13,19]. The phenomenological theory is based on an equation for the coarse-grained density, featuring a local speed and a local orientational relaxation time. Although the precise relationship between these one-body fields and the interparticle interaction potential remains to be clarified, some progress in this direction has been made [20]. On a

more microscopic level, it has recently been shown that a general system of active particles does not have an equation of state [21], due to the influence of the confining boundaries; however, one can be recovered for the special case of active Brownian spheres [21,22].

Here we report a first-principles theory for systems of active Brownian spheres, which demonstrates explicitly how an effective many-body interaction potential is induced by activity. An appealing feature of this approach is that intuition gained from equilibrium can be used to understand the steady-state properties of active systems. The required input quantities are the passive (“bare”) interaction potential, the rotational diffusion coefficient, and the particle propulsion speed. The theory generates as output the static correlation functions and phase behavior of the active system. For a repulsive bare interaction, activity generates an attractive effective pair potential, thus providing an intuitive explanation for the MIPS observed in simulations [12,15,23]. For an attractive bare potential, we find that increasing activity first reduces the effective attraction, consistent with the experiments of Schwarz-Linek *et al.* [16], before leading at higher activity to the development of a repulsive potential barrier. We speculate that this barrier may be related to the reentrant phase behavior observed in simulation by Redner *et al.* [14].

The paper will be structured as follows: In Sec. II we specify the microscopic dynamics and describe how to eliminate orientational degrees of freedom. From the resulting coarse-grained, non-Markovian Langevin equation we derive a Fokker-Planck equation for the positional degrees of freedom, from which we identify an effective pair potential. In Sec. III we employ the effective pair potential in an equilibrium integral equation theory and investigate the structure and phase behavior of both repulsive and attractive bare potentials. In the former case we predict MIPS, whereas in the latter case phase separation is suppressed by activity. Finally, in Sec. IV we discuss our findings and provide an outlook for future research.

II. THEORY**A. Microscopic dynamics**

We consider a three-dimensional system of N active, interacting, spherical Brownian particles with spatial coordinate

\mathbf{r}_i and orientation specified by an embedded unit vector \mathbf{p}_i . Each particle experiences a self-propulsion of speed v_0 in its direction of orientation. Omitting hydrodynamic interactions the particle motion can be modeled by the overdamped Langevin equations

$$\dot{\mathbf{r}}_i = v_0 \mathbf{p}_i + \gamma^{-1} \mathbf{F}_i + \boldsymbol{\xi}_i, \quad (1)$$

$$\dot{\mathbf{p}}_i = \boldsymbol{\eta}_i \times \mathbf{p}_i, \quad (2)$$

where γ is the friction coefficient and the force on particle i is generated from the total potential energy according to $\mathbf{F}_i = -\nabla_i U_N$. The stochastic vectors $\boldsymbol{\xi}_i(t)$ and $\boldsymbol{\eta}_i(t)$ are Gaussian distributed with zero mean and have time correlations $\langle \boldsymbol{\xi}_i(t) \boldsymbol{\xi}_j(t') \rangle = 2D_t \mathbf{1} \delta_{ij} \delta(t-t')$ and $\langle \boldsymbol{\eta}_i(t) \boldsymbol{\eta}_j(t') \rangle = 2D_r \mathbf{1} \delta_{ij} \delta(t-t')$, where D_t and D_r are the translational and rotational diffusion coefficients.

Equations (1) and (2) are convenient for simulation but are perhaps not the most suitable starting point for developing a first-principles microscopic theory. For a homogeneous system, averaging over the angular degrees of freedom generates a coarse-grained equation [12]

$$\dot{\mathbf{r}}_i(t) = \gamma^{-1} \mathbf{F}_i(t) + \boldsymbol{\xi}_i(t) + \boldsymbol{\chi}_i(t), \quad (3)$$

where $\boldsymbol{\chi}_i(t)$ is a Markov process with zero mean and where the time correlation function is given by

$$\langle \boldsymbol{\chi}_i(t) \boldsymbol{\chi}_j(t') \rangle = \frac{v_0^2}{3} e^{-2D_r|t-t'|} \mathbf{1} \delta_{ij}. \quad (4)$$

The average in Eq. (4) is over both noise and initial orientation. The distribution of $\boldsymbol{\chi}_i(t)$ is Gaussian to a good approximation. This point and further technical details of the coarse graining are discussed in Appendix A. Equation (3) provides a mean-field level of description, which deviates from the exact equations (1) and (2) by neglecting the coupling of fluctuations in orientation and positional degrees of freedom.

The Langevin equation (3) describes a non-Markovian process, which approximates the stochastic time evolution of the positional degrees of freedom. The persistent motion of active particles is here encoded by the exponential decay of the time correlation (4), with persistence time $\tau_p = (2D_r)^{-1}$. For small τ_p the time correlation becomes $\langle \boldsymbol{\chi}_i(t) \boldsymbol{\chi}_j(t') \rangle = 2D_a \mathbf{1} \delta_{ij} \delta(t-t')$, and the dynamics reduce to that of an equilibrium system with diffusion coefficient $D_t + D_a$, where $D_a = v_0^2/(6D_r)$. This limit is realized when τ_p is shorter than the mean free time between collisions, i.e., in a dilute suspension. To treat finite densities requires an approach which deals with persistent trajectories. With this aim, we adopt (3) as the starting point for constructing a closed theory.

B. Fokker-Planck equation

A stochastic process driven by colored noise, such as that described by Eq. (3), is always non-Markovian. Consequently it is not possible to derive an *exact* Fokker-Planck equation for the time evolution of the probability distribution [24]. Nevertheless, an approximate Fokker-Planck description capable of making accurate predictions can usually be found. The approximate Fokker-Planck equation implicitly defines a Markov process which best approximates the process of physical interest (although precisely what constitutes the

“best” approximation remains a matter of debate). From the extensive literature on this subject (see Refs. [24–26] and references therein) has emerged a powerful method due to Fox [27,28], in which a perturbative expansion in powers of correlation time is partially resummed using functional calculus. The resulting Fokker-Planck equation is most accurate for short correlation times (“off white” noise [25]) and for one-dimensional models makes predictions in good agreement with simulation data [26].

We now consider applying the method of Fox [27,28] to Eq. (3). This approach consists of first formulating the configurational probability distribution as a path (functional) integral and then making a time-local, Markovian approximation to this quantity. Technical details of the method are given in Appendix B. Fox’s approach was originally developed to treat one-dimensional problems [27,28]; however, the generalization to three dimensions is quite straightforward. This enables us to directly obtain the following Fokker-Planck equation:

$$\partial_t \Psi(\mathbf{r}^N, t) = - \sum_{i=1}^N \nabla_i \cdot \mathbf{J}_i(\mathbf{r}^N, t), \quad (5)$$

where $\Psi(\mathbf{r}^N, t)$ is the configurational probability distribution. Within the generalized Fox approximation the many-body current is given by

$$\mathbf{J}_i(\mathbf{r}^N, t) = -D_i(\mathbf{r}^N) [\nabla_i - \beta \mathbf{F}_i^{\text{eff}}(\mathbf{r}^N)] \Psi(\mathbf{r}^N, t), \quad (6)$$

where $\beta \equiv (k_B T)^{-1}$. The diffusion coefficient is given by

$$D_i(\mathbf{r}^N) = D_t + D_a \left[1 + \frac{\tau \nabla_i \cdot \beta \mathbf{F}_i(\mathbf{r}^N)}{1 - \tau \nabla_i \cdot \beta \mathbf{F}_i(\mathbf{r}^N)} \right], \quad (7)$$

where we have defined a dimensionless persistence time, $\tau = \tau_p D_t / d^2$. The effective force is given by

$$\mathbf{F}_i^{\text{eff}}(\mathbf{r}^N) = \frac{1}{\mathcal{D}_i(\mathbf{r}^N)} [\mathbf{F}_i(\mathbf{r}^N) - k_B T \nabla_i \mathcal{D}_i(\mathbf{r}^N)], \quad (8)$$

where $\mathcal{D}_i(\mathbf{r}^N) = D_i(\mathbf{r}^N) / D_t$ is a dimensionless diffusion coefficient. Either in the absence of interactions or in limit of large D_r the diffusivity (7) reduces to $D_t + D_a$ and the effective force becomes $D_t \mathbf{F}_i(\mathbf{r}^N) / (D_t + D_a)$. In this diffusion limit the system behaves as an equilibrium system at effective temperature $T_{\text{eff}} = T(1 + D_a/D_t)$.

For weakly persistent motion, $\tau \rightarrow 0$, Eqs. (5) to (8) become exact, and the theory provides the leading order correction to the diffusion approximation. However, the Fox approximation goes beyond this by including contributions to all orders in τ . Indeed, detailed studies of one-dimensional systems have demonstrated good results over a large range of τ values [26]. The only caveat is that the condition $1 - \tau \nabla_i \cdot \beta \mathbf{F}_i > 0$ must be satisfied [27,28]. The range of accessible τ values thus depends upon the specific form of the bare interaction potential.

Within our stochastic calculus approach, the effective many-body force (8) emerges in a natural way from the coarse-grained Langevin equation (3). The more standard route (adopted in all attempts made so far [20,29]) to approach this problem is to derive from the Markovian equations (1) the exact Fokker-Planck equation for the joint distribution

of positions and orientations, $P(\mathbf{r}^N, \mathbf{p}^N, t)$. However, coarse graining strategies based on integration of P over orientations generate intractable integral terms. By starting from (3) we are able to circumvent these difficulties. As we shall demonstrate below, our effective force accounts for several important collective phenomena in active systems.

C. Effective pair potential

In the low density limit we need only consider isolated pairs of particles. In this limit (5) reduces to an equation of motion for the radial distribution function, $g(r, t) \equiv \Psi(r, t) / \rho_b^2$, where ρ_b is the bulk density. This equation of motion, the pair Smolochowski equation, is given by

$$\partial_t g(r, t) = -\nabla \cdot \mathbf{j}(r, t), \quad (9)$$

where $r = |\mathbf{r}_{12}|$ is the particle separation and $\nabla = \nabla_{r_{12}}$. The pair current is given by

$$\mathbf{j}(r, t) = -2D(r)g(r, t)[\nabla \ln g(r, t) - \beta \mathbf{F}^{\text{eff}}(r)], \quad (10)$$

where the radial diffusivity

$$D(r) = D_t + D_a \left[1 - \frac{\tau \nabla^2 \beta u(r)}{1 + \tau \nabla^2 \beta u(r)} \right] \quad (11)$$

interpolates between the value D_t at small separations, where $u(r)$ is strongly repulsive, and $D_t + D_a$ at large separations. The effective interparticle force is given by

$$\mathbf{F}^{\text{eff}}(r) = \frac{1}{D(r)} [\mathbf{F}(r) - k_B T \nabla D(r)], \quad (12)$$

where the bare force is related to the pair potential by $\mathbf{F}(r) = -\nabla u(r)$. The symmetry of the two-body problem can be exploited to calculate from (12) an effective interaction potential

$$\beta u^{\text{eff}}(r) = \int_r^\infty dr' \left[\frac{\beta F(r')}{D(r')} - \frac{\partial}{\partial r'} \ln D(r') \right], \quad (13)$$

where $F(r) = |\mathbf{F}(r)|$. We have thus identified an effective interaction pair potential, which requires as input the bare potential and the activity parameters τ and D_a .

III. RESULTS

A. Motility-induced phase separation (MIPS)

To illustrate how activity can generate an effective attraction in a passively repulsive system we consider the nonspecific potential $\beta u(r) = r^{-12}$. In Fig. 1(a) we show the evolution of the effective potential (13) for fixed τ as a function of the dimensionless velocity $\text{Pe} = v_0 d / D_t$. For $\text{Pe} \gtrsim 10$ the effective potential develops an attractive tail. As Pe is increased the potential well deepens, the minimum moves to smaller separations and the radius of the soft repulsive core decreases. These trends are consistent with the intuitive picture that persistent motion drives soft particles into one another (the soft core radius reduces) and that they remain dynamically coupled (“trapped”) for longer than in the corresponding passive system. Within our equilibrium picture the trapping is accounted for by the effective attraction.

For systems at finite density the pair potential (13) is an approximation because three- and higher-body interactions

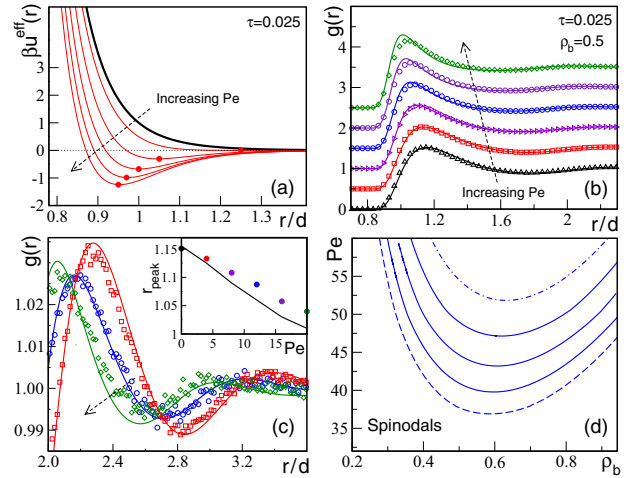


FIG. 1. (Color online) Activity induces effective attraction. Passive potential $\beta u(r) = r^{-12}$. (a) Increasing Pe (in steps of 8) from 0 to 40 generates an effective interparticle attraction. Points indicate the potential minima. (b) Radial distribution function, $g(r)$, from simulation (points) and theory (lines) for $\rho_b = 0.5$ and $\text{Pe} = 0$ to 20 (in steps of 4). Curves are shifted vertically for clarity. (c) As in (b), but focusing on larger separations for $\text{Pe} = 4$ (squares), 12 (circles), and 20 (diamonds). Inset: Position of the first peak in $g(r)$ as a function of Pe . (d) Spinodals for $\tau = 0.045$ (dot-dashed) to 0.065 (long dashed) in steps of 0.005.

will play a role [see Eq. (8)]. However, for simplicity we henceforth employ the pair potential (13) for all calculations, as we anticipate that this will provide the dominant contribution. Although corrections to this assumption can be made, they obscure the physical picture and come at the expense of a more complicated theory. The validity of the pair potential approximation is justified *a posteriori* by the comparison with simulation for the finite density pair correlations.

In Fig. 1(b) we show the steady-state (isotropic) radial distribution function for $\rho_b = 0.5$ for various values of Pe . We employ the effective pair potential (13) together with liquid state integral equation theory and compare theoretical predictions with direct Brownian dynamics simulation of Eqs. (1) and (2). The integral equation theory we employ is the soft mean-spherical approximation (SMSA) proposed by Madden and Rice [30]. This approximate closure of the Ornstein-Zernike equation is known to provide reliable results for the pair structure of Lennard-Jones-type potentials. Given the form of the effective pair potential shown in Fig. 1 the SMSA would seem to be a reasonable choice of closure. Details of the integral equation theory and the simulation procedure are given in Appendices C and D, respectively.

We find that as Pe is increased the main peak of $g(r)$ grows in height and shifts to smaller separations [see inset to Fig. 1(c)], reflecting the changes in the effective potential. In the main panel of Fig. 1(c) we focus on the second and third peaks. The quantitative accuracy of the theory in describing the decay of $g(r)$ is quite striking, in particular the phase shift induced by increasing activity is very well described. Further comparison for other parameter values (not shown) suggests

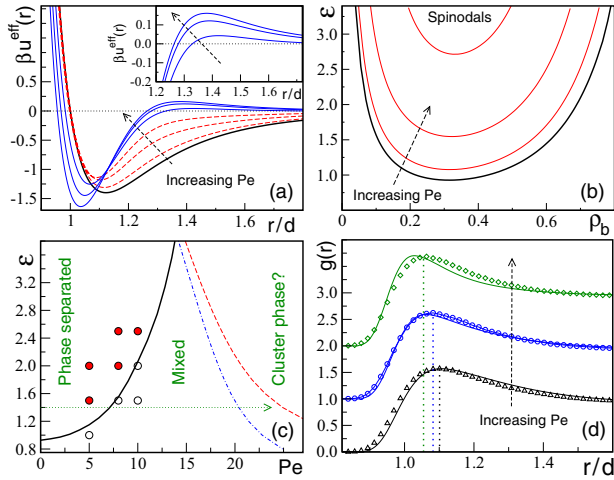


FIG. 2. (Color online) From active suppression of phase separation to a cluster phase. Passive potential $\beta u(r) = 4\epsilon(r^{-12} - r^{-6})$ with $\epsilon = 1.4$. (a) Effective potential (13) for $\tau = 0.025$ and $\text{Pe} = 0$ (black) 4, 8, 12 (red broken lines) and 20, 28, 36 (blue). Inset: Zoom of the repulsive peak for $\text{Pe} = 20, 28, 36$. (b) Spinodals for $\text{Pe} = 0, 4, 8, 12$. Increasing Pe increases ϵ_{crit} , the critical value of ϵ . (c) ϵ_{crit} as a function of Pe (black full line) and the locus of points for which the repulsive peak of βu^{eff} takes the value 0.1 (red dashed) and 0.05 (blue dot-dashed). Open (closed) circles indicate points where BD simulation find a mixed (phase-separated) state (see Fig. 3). Arrow indicates path taken in (a). (d) Theory (lines) and simulation (symbols) data (shifted for clarity) for $g(r)$ at $\epsilon = 0.5$, $\rho_b = 0.3$ for $\text{Pe} = 0$ (black), 12 (blue), and 20 (green). Dotted lines indicate peak positions.

that (13) combined with the SMSA theory provides an accurate account of the asymptotic decay of pair correlations.

In Fig. 1(d) we show the spinodal lines mapping the locus of points for which the static structure factor, $S(q) = [1 - \rho_b c(q)]^{-1}$, diverges at vanishing wave vector. Simulations have shown that MIPS is consistent with a spinodal instability [12]. As τ is decreased the critical point moves to higher values of Pe and to slightly higher densities. When compared with the spinodal of a standard Lennard-Jones system [e.g., the black curve in Fig. 2(b)] the critical points in Fig. 1(d) lie at rather higher values of ρ_b . This suggests that typical coexisting liquid densities for MIPS will be larger than those found in equilibrium phase separated systems, as has been observed in simulation [12, 14].

B. Suppression of phase separation

We next consider the influence of activity on a Lennard-Jones system, $\beta u(r) = 4\epsilon(r^{-12} - r^{-6})$. For a phase-separated passive system, recent experiments and simulations have demonstrated that increasing Pe first suppresses the phase separation [16] and then leads at higher Pe to a reentrant MIPS [14]. Schwarz-Linek *et al.* have argued that the suppression of phase separation at lower to intermediate Pe occurs in their system because particle pairs bound by the attractive (depletion) potential begin to actively escape the potential well, and that this can be mimicked using an effective potential less attractive and shorter ranged than the bare potential [16].

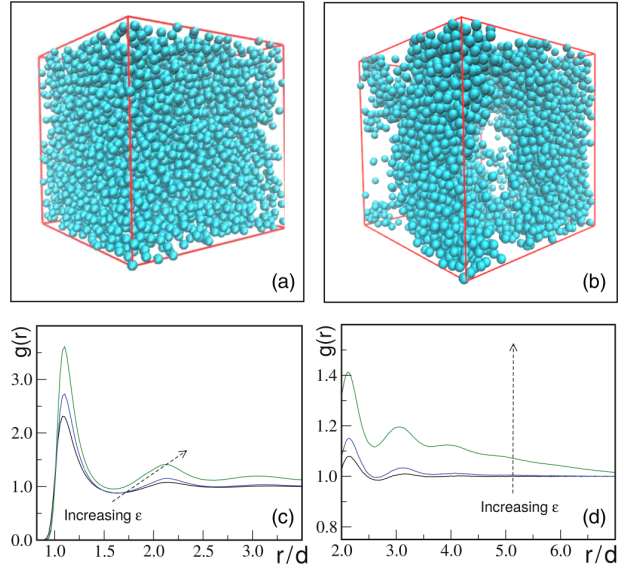


FIG. 3. (Color online) Simulated phase separation. (a) Snapshot of a mixed system at $t/\tau_B = 40$, $\text{Pe} = 8$, $\epsilon/(k_B T) = 1.5$. (b) Snapshot of a phase separating system at the same time and $\text{Pe} = 8$, $\epsilon = 2.5$. (c) The radial distribution function, $g(r)$, for $\epsilon = 1.5$ (black curve), 2 (blue curve), and 2.5 (green curve). (d) As in (c) but focusing on larger distances. From the snapshots together with the long-range behavior of the $g(r)$ we can distinguish between a mixed and a phase-separated system. The slow decay to the asymptotic value of unity, as shown in (d), indicates phase separation.

To investigate these phenomena we set $\epsilon = 1.4$, which ensures a phase-separated passive state [31], and consider the evolution of the effective potential as a function of Pe . In Fig. 2(a) we show that as Pe is increased from zero to the value 18 both the depth and range of the effective potential reduce significantly, consistent with the expectation of Schwarz-Linek *et al.* [16]. Spinodals within this range of Pe values, identifying where the static structure factor diverges at zero wave vector, are shown in Fig. 2(b). As Pe is increased the critical point moves to higher values of ϵ (cf. Figs. 1 and 3 in Ref. [16]). A passively phase-separated system will thus revert to a single phase upon increasing the activity. To examine this behavior in more detail we show in Fig. 2(c) the trajectory of the critical point in the (Pe, ϵ) plane. Above the line there exist bulk densities for which phase separation occurs.

In order to test the predicted trajectory of the critical point we have performed Brownian dynamics simulations at a bulk density $\rho_b = 0.4$, which lies close to the critical density [31], for various values of ϵ and the Pe values 5, 8, and 10. Visual inspection of the simulation snapshots reveals the existence of voids in the particle configurations corresponding to a phase-separated state [see Figs. 3(a) and 3(b) for snapshots]. This visual impression can be made more quantitative by calculating the radial distribution function. Phase-separating states generate a very characteristic slow decay of $g(r)$ [Figs. 3(c) and 3(d)], which provides a useful indicator. The open circles in Fig. 2(c) represent mixed states, whereas closed circles indicate phase separated state points. The phase

boundary predicted by the theory is highly consistent with the simulation data.

C. Cluster phase

Returning to Fig. 2(a), we find that for $Pe > 18$ the effective potential develops a repulsive barrier, which grows in height (see inset) with increasing Pe , while the potential minimum becomes deeper. It is well known that potentials with a short-ranged attraction and long-ranged repulsion (SALR potentials) exhibit unusual equilibrium phase behavior, including clustering and microphase separation [32,33]. Although the attractive component of the potential may favor phase separation, the long-range repulsion destabilizes distinct liquid and gas phases and causes them to break up into droplets or clusters. This represents a nonspinodal type of phase transition, characterized by a divergence in the structure factor at finite wave vector. The appearance of a repulsive barrier in the effective potential suggests that a similar mechanism may be at work in passively attractive systems subject to high Pe activity.

In Fig. 2(c) we show the locus of points where the effective potential peak height attains a given value (we choose 0.05 and 0.1 for illustration). When these “isorepulsion curves” are viewed together with the critical point trajectory the resulting phase diagram is very similar to that obtained by Redner *et al.* in their simulation study of two-dimensional active Lennard-Jones particles (cf. Fig. 1 in Ref. [14]). However, a detailed study of the connection between the potential barrier and high Pe clustering goes beyond the scope of the present work.

IV. DISCUSSION

In summary, we have shown that systems of active spherical Brownian particles can be mapped onto an equilibrium system interacting via an effective, activity-dependent many-body potential. The only required inputs are the bare potential, thermodynamic state point and the parameters specifying the state of activity. Our theory captures the phenomenon of MIPS in repulsive systems and provides first-principles predictions for the activity dependence of the pair correlations, in very good agreement with Brownian dynamics simulation. As far as we are aware no other approach is capable of predicting from the microscopic interactions the pair correlation functions of an active system. Further insight into the steady state particle distribution could in principle be obtained by investigating the three-body correlations. These could be obtained by employing the effective potential in a higher-order liquid state integral equation theory (see, e.g., Ref. [34] and references therein).

For passively attractive systems the theory rationalizes the experimental finding [16] that increasing activity can suppress passive phase separation. We find that as Pe is increased from zero to intermediate values the minimum of the effective potential becomes less deep, thus weakening the cohesion of the liquid phase. To the best of our knowledge no alternative theoretical explanation is currently available for phase-transition suppression in active suspensions. It is an appealing aspect of our theory that the suppression of passive phase separation follows naturally from the same approach which yields activity-induced attraction for repulsive potentials. For high values of Pe the appearance of a repulsive barrier in the

effective potential suggests that the reentrant phase separation observed in simulations [14] may be interpreted using concepts of equilibrium clustering in SALR potential systems. This will be a subject of future detailed investigations. It is known that care must be exercised when analyzing SALR potentials, as traditional liquid state theories can prove misleading [33].

A key step in our development is the Fox approximation [27], which yields an effective Markovian description of the coarse-grained equation (3). Making a Markovian approximation automatically imposes an effective equilibrium; however, we are aware that in certain situations this breaks down [10,19]. Establishing more clearly the range of validity of our approach, as well as its possible extensions, will be the subject of ongoing study. However, it is already clear that going beyond the Markovian approximation will be very challenging. Indeed, such a step may not even be desirable. Any kind of non-Markovian description would lead inevitably to a loss of the effective equilibrium picture and the physical intuition associated with it. It thus seems likely that practical improvements to the present approach will retain the Markovian description while seeking to optimize, or improve upon, the Fox approximation for certain classes of bare potential. Very recently, Maggi *et al.* have employed an alternative approach to treating stochastic processes driven by Ornstein-Uhlenbeck noise [35]. A comparison of their approach with the Fox method employed here would be very interesting.

With a view to further applications of our approach, we note that there has recently been considerable interest in active suspensions at very high densities [36–39]. In particular, it has been found using computer simulations that activity has a strong influence on the location of the hard-sphere glass transition, dynamic correlation functions, such as the intermediate scattering function, and static pair correlations [37]. Within our effective equilibrium framework, increasing the activity of a passively repulsive system generates an effective attraction. We can therefore anticipate that for volume fractions just above the glass transition it will be possible to observe a reentrant glass transition, namely, a melting of the glass followed by revitrification, as a function of increasing Pe . Moreover, the nontrivial evolution of the effective potential as a function of Pe for attractive bare potentials [cf. Fig. 2(a)] suggests these systems will present a rich variety of glassy states. Work along these lines is in progress.

Finally, we mention that a natural generalization of the present theory is to treat spatially inhomogeneous systems in external fields. Recent microscopic studies of active particles under confinement (e.g., in a harmonic trap [29]) have provided considerable insight; however, none of the existing approaches have considered effective *interparticle* interactions. Inhomogeneous generalization of the present theory enables the interaction between MIPS and external fields to be investigated on the microscopic level. Our preliminary investigations reveal, for example, activity-induced wetting at a planar substrate and capillary-condensation under confinement. This will be presented in a future publication.

ACKNOWLEDGMENTS

We thank Yaouen Fily, Ronald Fox, and Paolo Grigolini for helpful correspondence. We acknowledge funding provided

by the Swiss National Science Foundation. P.K. thanks the Elitenetzwerk Bayern (ENB) and Matthias Schmidt for financial support.

APPENDIX A: COARSE-GRAINED LANGEVIN EQUATION

Equation (2) describes the orientational diffusion of an active particle. The corresponding conditional probability distribution function $\Upsilon(\mathbf{p}, t | \mathbf{p}_0, t_0)$, where $t > t_0$, obeys a Fokker-Planck equation which can be obtained using usual techniques [40],

$$\frac{\partial}{\partial t} \Upsilon(\mathbf{p}, t | \mathbf{p}_0, t_0) = D_r \mathbf{R}^2 \Upsilon(\mathbf{p}, t | \mathbf{p}_0, t_0), \quad (\text{A1})$$

where $\mathbf{R} \equiv (\mathbf{p} \times \nabla_{\mathbf{p}})$ is the intrinsic angular momentum differential operator. Equation (A1) describes nothing but a diffusion process on the unit sphere. This problem is well known when studying, e.g., dielectric relaxation in polar liquids [41–44]. In spherical coordinates, (A1) becomes

$$\begin{aligned} & \frac{1}{D_r} \frac{\partial}{\partial t} \Upsilon(\Omega, t | \Omega_0, t_0) \\ &= \left[\frac{1}{\sin \vartheta} \frac{\partial}{\partial \vartheta} \left(\sin \vartheta \frac{\partial}{\partial \vartheta} \right) + \frac{1}{\sin^2 \vartheta} \frac{\partial^2}{\partial \varphi^2} \right] \Upsilon(\Omega, t | \Omega_0, t_0), \end{aligned} \quad (\text{A2})$$

where we have defined $\Omega \equiv (\vartheta, \varphi)$.

Assuming that Υ and its derivatives are continuous on the sphere [45], we expand the probability distribution function Υ in spherical harmonics

$$\Upsilon(\Omega, t | \Omega_0, t_0) = \sum_{l=0}^{\infty} \sum_{m=-l}^l A_{lm}(t | \Omega_0, t_0) Y_{lm}(\Omega), \quad (\text{A3})$$

where Y_{lm} are the spherical harmonics and A_{lm} are coefficients encoding the initial condition. We also recall that spherical harmonics are eigenvectors of the operator \mathbf{R}^2 (in spherical coordinates), namely, that

$$\mathbf{R}^2 Y_{lm} = -l(l+1) Y_{lm}. \quad (\text{A4})$$

Inserting (A3) in Eq. (A2) and using (A4) we obtain

$$\begin{aligned} & \sum_{l,m} \frac{\partial}{\partial t} A_{lm}(t | \Omega_0, t_0) Y_{lm}(\Omega) \\ &= -D_r \sum_{l,m} l(l+1) A_{lm}(t | \Omega_0, t_0) Y_{lm}(\Omega). \end{aligned} \quad (\text{A5})$$

Multiplying both sides of (A5) by $Y_{l'm'}^*(\Omega)$, integrating over solid angle and using the orthogonality property, $\int d\Omega Y_{l'm'}^*(\Omega) Y_{lm}(\Omega) = \delta_{m,m'} \delta_{l,l'}$, yields

$$\frac{\partial}{\partial t} A_{lm}(t | \Omega_0, t_0) = -D_r l(l+1) A_{lm}(t | \Omega_0, t_0), \quad (\text{A6})$$

which has the solution

$$A_{lm}(t | \Omega_0, t_0) = e^{-D_r l(l+1)(t-t_0)} a_{lm}(\Omega_0), \quad (\text{A7})$$

where the a_{lm} are a new set of coefficients. The probability distribution is thus given by

$$\Upsilon(\Omega, t | \Omega_0, t_0) = \sum_{l,m} e^{-D_r l(l+1)(t-t_0)} a_{lm}(\Omega_0) Y_{lm}(\Omega). \quad (\text{A8})$$

The initial condition,

$$\Upsilon(\Omega, t_0 | \Omega_0, t_0) = \delta(\Omega - \Omega_0), \quad (\text{A9})$$

together with the completeness relation of the spherical harmonics,

$$\delta(\Omega - \Omega_0) = \sum_{l=0}^{\infty} \sum_{m=-l}^l Y_{lm}(\Omega) Y_{lm}^*(\Omega_0), \quad (\text{A10})$$

allows the missing coefficients to be identified,

$$a_{lm}(\Omega_0) = Y_{lm}^*(\Omega_0). \quad (\text{A11})$$

The conditional probability distribution is now fully determined as

$$\Upsilon(\Omega, t | \Omega_0, t_0) = \sum_{l=0}^{\infty} \sum_{m=-l}^l e^{-D_r l(l+1)(t-t_0)} Y_{lm}^*(\Omega_0) Y_{lm}(\Omega). \quad (\text{A12})$$

As $t \rightarrow \infty$ only the terms with $l = 0$ survive. The steady-state distribution function is thus given by

$$\Upsilon_{\text{eq}}(\Omega) = \lim_{t \rightarrow \infty} \Upsilon(\Omega, t | \Omega_0, t_0) = (4\pi)^{-1}. \quad (\text{A13})$$

The conditional and equilibrium distributions, (A12) and (A13), respectively, can be used to coarse-grain the exact Langevin equations (1) and (2). The approach taken is to consider the orientation vector $\mathbf{p}_i(t)$ attached to particle i as a stochastic variable and to provide its full statistical characterization. In spherical coordinates the orientation vector is given explicitly by

$$\begin{aligned} \mathbf{p}(t) &= (p_x(t), p_y(t), p_z(t))^T \\ &= (\cos \varphi(t) \sin \vartheta(t), \sin \varphi(t) \sin \vartheta(t), \cos \vartheta(t))^T, \end{aligned} \quad (\text{A14})$$

where φ and ϑ are the azimuthal and polar angles, respectively. Using (A13) we have that

$$\langle p_z(t) \rangle = \int d\Omega \Upsilon_{\text{eq}}(\Omega) \cos \vartheta = 0, \quad (\text{A15})$$

together with analogous results for the x and y components:

$$\langle p_x(t) \rangle = 0 = \langle p_y(t) \rangle. \quad (\text{A16})$$

Defining the new stochastic variable by $\chi_i(t) \equiv v_0 \mathbf{p}_i(t)$, its first moment is thus given by

$$\langle \chi_i(t) \rangle = v_0 \langle \mathbf{p}_i(t) \rangle = \mathbf{0}. \quad (\text{A17})$$

Calculation of the equilibrium correlation matrix requires the conditional probability distribution function given by (A12). For example, for the zz component, we obtain

$$\begin{aligned} & \langle p_z(t) p_z(t_0) \rangle \\ &= \int d\Omega \int d\Omega_0 \cos \vartheta \cos \vartheta_0 \Upsilon(\Omega, t | \Omega_0, t_0) \Upsilon_{\text{eq}}(\Omega_0) \\ &= \frac{1}{3} \int d\Omega \int d\Omega_0 \sum_{l,m} e^{-D_r l(l+1)(t-t_0)} \\ & \quad \times Y_{10}^*(\Omega) Y_{lm}(\Omega) Y_{10}(\Omega_0) Y_{lm}^*(\Omega_0) \\ &= \frac{1}{3} e^{-2D_r |t-t_0|}, \end{aligned} \quad (\text{A18})$$

where we have expressed the cosine functions in terms of spherical harmonics, $Y_{10} = \sqrt{3/(4\pi)} \cos \vartheta = Y_{10}^*$, and used the orthogonality property. Calculations for the xx and yy components are performed in the same spirit. We thus obtain

$$\langle p_x(t)p_x(t_0) \rangle = \frac{1}{3}e^{-2D_r|t-t_0|} = \langle p_y(t)p_y(t_0) \rangle, \quad (\text{A19})$$

whereas off-diagonal components of the correlation matrix are all zero. We can thus conclude that

$$\langle \chi_i(t)\chi_j(t') \rangle = v_0^2 \langle \mathbf{p}_i(t)\mathbf{p}_j(t') \rangle = \frac{v_0^2}{3}e^{-2D_r|t-t'|} \mathbf{1}\delta_{ij}. \quad (\text{A20})$$

It has been shown [46] that the probability distribution function (A12) can be well approximated by an expression which generalizes the planar Gaussian function to the sphere. The new noise function $\chi_i(t)$ is thus approximately Gaussian distributed with zero mean and exponentially decaying correlations. The coarse-grained Langevin equation (3) thus describes a stochastic process with additive colored noise.

APPENDIX B: APPROXIMATE FOKKER-PLANCK EQUATION

To derive from (3) an approximate Fokker-Planck equation we apply the functional calculus methods of Fox [27]. We address the one-dimensional case before generalizing to higher dimension. Consider the stochastic differential equation

$$\dot{x}(t) = F(x) + g(x)\chi(t), \quad (\text{B1})$$

where $F(x)$ and $g(x)$ may be nonlinear functions in x . If $g(x) = 1$, the process is then called *additive*, otherwise it is called *multiplicative*. The noise function $\chi(t)$ is by definition Gaussian distributed with zero mean. Its second moment determines whether it is a *white* or *colored* noise. As we are interested here in the case of additive colored noise we set $g(x) = 1$.

In the framework of functional calculus, the Gaussian nature of $\chi(t)$ is expressed by the following probability distribution functional:

$$P[\chi] = N e^{-\frac{1}{2} \int ds \int ds' \chi(s)\chi(s')K(s-s')}, \quad (\text{B2})$$

where the function K is the inverse of the χ correlation function and the normalization constant is expressed by a path integral over χ :

$$N^{-1} = \int D[\chi] e^{-\frac{1}{2} \int ds \int ds' \chi(s)\chi(s')K(s-s')}. \quad (\text{B3})$$

The first and second moments of χ are given by

$$\langle \chi(t) \rangle = 0, \quad (\text{B4})$$

$$\langle \chi(t)\chi(s) \rangle = C(t-s). \quad (\text{B5})$$

Recalling that the functional derivative may be defined according to

$$\frac{\delta I[\phi]}{\delta \phi(t')} = \left. \frac{d}{d\lambda} I[\phi(t) + \lambda \delta(t-t')] \right|_{\lambda=0}, \quad (\text{B6})$$

we now derive two useful identities. The first concerns the functional derivative of the probability distribution

functional,

$$\begin{aligned} \frac{\delta P[\chi]}{\delta \chi(t)} &= \frac{\delta N}{\delta \chi(t)} e^{-\frac{1}{2} \int ds \int ds' \chi(s)\chi(s')K(s-s')} \\ &\quad + N \frac{\delta}{\delta \chi(t)} e^{-\frac{1}{2} \int ds \int ds' \chi(s)\chi(s')K(s-s')} \\ &= -P[\chi] \int ds K(t-s)\chi(s), \end{aligned} \quad (\text{B7})$$

where, using (B6) and (B4), it can be easily shown that $\delta N/\delta \chi(t) = 0$. The second identity demonstrates the inverse relation between the functions K and C . The second functional derivative of $P[\chi]$ yields

$$\begin{aligned} \frac{\delta^2 P[\chi]}{\delta \chi(t')\delta \chi(t)} &= P[\chi] \left\{ \int ds' \int ds K(t'-s')K(t-s)\chi(s')\chi(s) \right. \\ &\quad \left. - K(t-t') \right\}, \end{aligned} \quad (\text{B8})$$

where use of (B7) has been made. Using (B8) and (B5) together with the normalization $\int D[\chi]P[\chi] = 1$, leads to

$$\begin{aligned} 0 &= \int D[\chi] \frac{\delta^2 P[\chi]}{\delta \chi(t')\delta \chi(t)} \\ &= \int ds' K(t'-s') \int ds K(t-s)C(s-s') - K(t-t'), \end{aligned} \quad (\text{B9})$$

which implies that

$$\int ds K(t-s)C(s-s') = \delta(t-s'). \quad (\text{B10})$$

The solution to the stochastic process described by (B1), namely, the probability distribution functional for $x(t)$, is given by the formal expression

$$P(y,t) = \int D[\chi] P[\chi] \delta[y - x(t)]. \quad (\text{B11})$$

Taking the time derivative of (B11) yields

$$\begin{aligned} \frac{\partial}{\partial t} P(y,t) &= -\frac{\partial}{\partial y} [F(y)P(y,t)] \\ &\quad - \frac{\partial}{\partial y} \int D[\chi] \delta[y - x(t)] P[\chi] \chi(t). \end{aligned} \quad (\text{B12})$$

The product $P[\chi] \chi(t)$ appearing in the second term can be rewritten in the following way:

$$\begin{aligned} P[\chi] \chi(t) &= P[\chi] \int ds \delta(t-s)\chi(s) \\ &= - \int ds' C(t-s') \frac{\delta P[\chi]}{\delta \chi(s')}, \end{aligned} \quad (\text{B13})$$

where we have used (B10) and (B7). Inserting (B13) back into the second term of (B12) and integrating by parts gives us

$$\begin{aligned} &\int D[\chi] \delta[y - x(t)] P[\chi] \chi(t) \\ &= - \int ds' C(t-s') \int D[\chi] \left\{ \frac{\partial}{\partial y} \delta[y - x(t)] \right\} \frac{\delta x(t)}{\delta \chi(s')} P[\chi], \end{aligned} \quad (\text{B14})$$

which serves as the exact starting point for Fox's approximation scheme [27].

In order to progress further we need to calculate $\delta x(t)/\delta \chi(s')$. Applying the functional derivative with respect to $\chi(t')$ on (B1) yields a first-order differential equation,

$$\frac{d}{dt} \frac{\delta x(t)}{\delta \chi(t')} = \frac{\delta \dot{x}(t)}{\delta \chi(t')} = F'(x) \frac{\delta x(t)}{\delta \chi(t')} + \delta(t-t'), \quad (\text{B15})$$

the solution of which is

$$\begin{aligned} \frac{\delta x(t)}{\delta \chi(s')} &= \int_0^t ds e^{\int_s^t ds' F'[x(s)]} \delta(s-s') \\ &= e^{\int_{s'}^t ds F'[x(s)]} \Theta(t-s'), \end{aligned} \quad (\text{B16})$$

where Θ is the Heaviside step function, which we define here as follows:

$$\Theta(t-s') = \begin{cases} 1, & t > s' \\ \frac{1}{2}, & t = s' \\ 0, & t < s'. \end{cases}$$

Using (B16) in Eq. (B14) we can rewrite (B12) in an alternative form,

$$\begin{aligned} \frac{\partial}{\partial t} P(y,t) &= -\frac{\partial}{\partial y} [F(y)P(y,t)] + \frac{\partial^2}{\partial y^2} \left\{ \int_0^t ds' C(t-s') \right. \\ &\quad \left. \times \int D[\chi] P[\chi] e^{\int_{s'}^t ds F'[x(s)]} \delta[y-x(t)] \right\}, \end{aligned} \quad (\text{B17})$$

which already begins to resemble a Fokker-Planck-type equation. However, because of the non-Markovian nature of $\int_{s'}^t ds F'[x(s)]$ appearing in the exponential of (B17), it is apparent that a reduction of this term to an expression containing $P(y,t)$ is not possible. An approximation is required.

The colored noise of interest here is characterized by an exponentially decaying correlation function (A17). In the literature on non-Markovian processes the time-correlation functions are generally notated as follows:

$$C(t-s) = \frac{D}{\tau} e^{-\frac{|t-s|}{\tau}}, \quad (\text{B18})$$

with a diffusion coefficient D and a correlation time τ . In order to retain some coherence with the existing literature we will here employ the standard notation of (B18) and only use the relation of the parameters in Eq. (B18) to those of (A20) at the end of the calculation.

Returning to (B17), we first perform a change of variable, $t' \equiv t - s'$, in the time integral,

$$\int_0^t ds' C(t-s') e^{\int_{s'}^t ds F'[x(s)]} = \int_0^t dt' C(t') e^{\int_{t-t'}^t ds F'[x(s)]}, \quad (\text{B19})$$

and then expand the time integral over F' in terms of t' ,

$$\int_{t-t'}^t ds F'[x(s)] \approx F'[x(t)]t' - F''[x(t)]\dot{x}(t) \frac{t'^2}{2}. \quad (\text{B20})$$

Neglecting the t'^2 term in Eq. (B20) enables the integral in Eq. (B19) to be evaluated:

$$\begin{aligned} &\int_0^t ds' C(t-s') e^{\int_{s'}^t ds F'[x(s)]} \\ &\approx \int_0^t dt' C(t') e^{F'[x(t)]t'} \\ &= \frac{D}{\tau} \int_0^t dt' e^{-t'(-F'[x(t)] + \frac{1}{\tau})} \approx \frac{D}{1 - \tau F'[x(t)]}, \end{aligned} \quad (\text{B21})$$

where we used (B18), and the second approximation results from assuming a sufficiently large t . We can finally put (B21) back into (B17) to obtain an approximate Fokker-Planck equation:

$$\begin{aligned} \frac{\partial}{\partial t} P(y,t) &= -\frac{\partial}{\partial y} [F(y)P(y,t)] \\ &\quad + D \frac{\partial^2}{\partial y^2} \left[\frac{1}{1 - \tau F'(y)} P(y,t) \right]. \end{aligned} \quad (\text{B22})$$

This is Fox's result for the approximate Fokker-Planck equation corresponding to the non-Markovian process (B1). Equation (B22) implicitly defines a Markovian process, which approximates the non-Markovian process of physical interest. However, the question of whether this represents the best approximation remains a subject of debate. We note that equation (B22) has also been derived by Grigolini *et al.* [26] using alternative methods which do not make any assumptions of a short correlation time.

The one-dimensional Fokker-Planck equation (B22) can be generalized without much difficulty to describe a three-dimensional system of N particles. The dynamics of interest is described by the stochastic equation (3). We now adapt the standard notation used above to that employed in the main text, namely, $P(y,t) \rightarrow \Psi(\mathbf{r}^N, t)$, $\tau \rightarrow \tau_p = 1/(2D_r)$ and $D \rightarrow v_0^2/3$, and recall that $D_a = v_0^2/(6D_r)$ and $\zeta^{-1} = \beta D_i$ for the friction coefficient in Eq. (3). Making the appropriate replacements enables us to write the three-dimensional generalization of (B22),

$$\begin{aligned} &\frac{\partial}{\partial t} \Psi(\mathbf{r}^N, t) \\ &= -\sum_{i=1}^N \nabla_i \cdot D_i [\beta \mathbf{F}_i(\mathbf{r}^N) - \nabla_i] \Psi(\mathbf{r}^N, t) \\ &\quad - \sum_{i=1}^N \nabla_i \cdot \left\{ -D_a \nabla_i \left[\frac{1}{1 - \frac{D_0 \nabla_i \cdot \beta \mathbf{F}_i(\mathbf{r}^N)}{2D_r}} \Psi(\mathbf{r}^N, t) \right] \right\}. \end{aligned} \quad (\text{B23})$$

A simple rearrangement of terms in Eq. (B23) leads directly to Eqs. (5)–(8).

APPENDIX C: INTEGRAL EQUATION THEORY

To calculate the steady-state radial distribution function, $g(r)$, from the effective pair potential (13) we employ an equilibrium liquid state integral equation developed by Madden and Rice [30]. This soft mean-spherical approximation (SMSA) exploits the Weeks-Chandler-Anderson splitting of the pair

potential [47] into attractive and repulsive contributions, $u(r) = u_{\text{rep}}(r) + u_{\text{att}}(r)$, where the repulsive part is given by

$$u_{\text{rep}}(r) = \begin{cases} u(r) - u(r_{\min}) & r < r_{\min} \\ 0 & r > r_{\min} \end{cases}, \quad (\text{C1})$$

and the attractive part is given by

$$u_{\text{att}}(r) = \begin{cases} u(r) & r > r_{\min} \\ u(r_{\min}) & r < r_{\min} \end{cases}, \quad (\text{C2})$$

where r_{\min} is the position of the potential minimum. The total correlation function, $h(r) = g(r) - 1$, is related to the shorter range direct correlation function, $c(r)$, by the Ornstein-Zernike equation [48]:

$$h(r) = c(r) + \rho_b \int d\mathbf{r}' h(|\mathbf{r} - \mathbf{r}'|) c(r'). \quad (\text{C3})$$

The SMSA approximation is given by the closure relation:

$$c(r) = (1 - e^{\beta u_{\text{rep}}(r)})g(r) - \beta u_{\text{att}}(r). \quad (\text{C4})$$

For the Lennard-Jones potential the closure relation (C4) has been shown to provide results for $g(r)$ which are superior to both Percus-Yevick (PY) and Hypernetted Chain (HNC) theories [30]. Moreover, the SMSA theory predicts a true spinodal line in the parameter space, namely, a locus of points for which the static structure factor, $S(k) = (1 - \rho_b \tilde{c}(k))^{-1}$, diverges at vanishing wave vector. This behavior is a consequence of the assumed asymptotic form of the direct correlation function, $c(r) \sim -\beta u_{\text{att}}(r)$. Other standard integral equation theories,

such as PY and HNC, do not exhibit a complete spinodal line, but rather a region within which the theory breaks down (“no solutions region”) [49].

APPENDIX D: BROWNIAN DYNAMICS SIMULATIONS

To benchmark our theoretical predictions we perform Brownian dynamics simulations of N particles, randomly initialized without overlap. The system is confined to a periodic cubic box, the size of which is determined by the number density according to $L^3 = N/\rho_b$, where L is the side length. The Langevin equations of motion (1) and (2) are integrated via a standard Brownian dynamics scheme [50] with a constant time step of $\delta t/\tau_B = 10^{-5}$. Both the translational and rotational noise are Gaussian random variables with a standard deviation of $\sigma_t = (2D_0T)^{\frac{1}{2}}$ and $\sigma_r = (2D_rT)^{\frac{1}{2}}$, respectively.

For the soft repulsive potential to be considered in this work, $\beta u(r) = r^{-12}$, we employ $N = 2000$ particles. The potential is truncated and shifted at $r_{\text{cut}}/d = 2$. To provide good statistics for the static quantities the simulations are carried out for 10^6 time steps, sampling every 1000 steps, which is equivalent to a total run time of $t_{\text{tot}}/\tau_B = 10$ and a sampling rate of $\tau_B/t_{\text{sample}} = 100$. For the second system we will consider, the Lennard-Jones system, $\beta u(r) = 4\epsilon(r^{-12} - r^{-6})$, we simulate a larger system of 5000 particles. The integration time of the equations of motion is the same as in the repulsive system, as is the cutoff radius. In this case, the runtime is 10^7 and the particle positions are sampled every 10^4 steps.

-
- [1] J. Palacci, C. Cottin-Bizonne, C. Ybert, and L. Bocquet, *Phys. Rev. Lett.* **105**, 088304 (2010).
- [2] A. Erbe, M. Zientara, L. Baraban, C. Kreidler, and P. Leiderer, *J. Phys. Condens. Matter* **20**, 404215 (2008).
- [3] J. R. Howse, R. A. L. Jones, A. J. Ryan, T. Gough, R. Vafabakhsh, and R. Golestanian, *Phys. Rev. Lett.* **99**, 048102 (2007).
- [4] R. Dreyfus, J. Baudry, M. L. Roper, M. Fermigier, H. A. Stone, and J. Bibette, *Nature (London)* **437**, 862 (2005).
- [5] J. Palacci, S. Sacannal, A. P. Steinberg, D. J. Pine, and P. M. Chaikin, *Science* **339**, 936 (2013).
- [6] T. Vicsek and A. Zafiris, *Phys. Rep.* **517**, 71 (2012).
- [7] S. Ramaswamy, *Annu. Rev. Condens. Matter Phys.* **1**, 323 (2010).
- [8] P. Romanczuk, M. Bär, W. Ebeling, B. Lindner, and L. Schimansky-Geier, *Eur. Phys. J. Special Topics* **202**, 1 (2012).
- [9] M. E. Cates, *Rep. Prog. Phys.* **75**, 042601 (2012).
- [10] M. E. Cates and J. Tailleur, *Annu. Rev. Condens. Matter Phys.* **6**, 219 (2015).
- [11] J. Tailleur and M. E. Cates, *Phys. Rev. Lett.* **100**, 218103 (2008).
- [12] Y. Fily and M. C. Marchetti, *Phys. Rev. Lett.* **108**, 235702 (2012).
- [13] J. Stenhammar, A. Tiribocchi, R. J. Allen, D. Marenduzzo, and M. E. Cates, *Phys. Rev. Lett.* **111**, 145702 (2013).
- [14] G. S. Redner, A. Baskaran, and M. F. Hagan, *Phys. Rev. E* **88**, 012305 (2013).
- [15] D. Levis and L. Berthier, *Phys. Rev. E* **89**, 062301 (2014).
- [16] J. Schwarz-Linek *et al.*, *Proc. Natl. Acad. Sci. USA* **109**, 4052 (2012).
- [17] F. Ginot, I. Theurkauff, D. Levis, C. Ybert, L. Bocquet, L. Berthier, and C. Cottin-Bizonne, *Phys. Rev. X* **5**, 011004 (2015).
- [18] A. Wysocki, R. G. Winkler, and G. Gompper, *Europhys. Lett.* **105**, 48004 (2014).
- [19] M. E. Cates and J. Tailleur, *Europhys. Lett.* **101**, 20010 (2013).
- [20] J. Bialké, H. Löwen, and T. Speck, *Europhys. Lett.* **103**, 30008 (2013).
- [21] A. P. Solon, Y. Fily, A. Baskaran, M. E. Cates, Y. Kafri, M. Kardar, and J. Tailleur, [arXiv:1412.3952](https://arxiv.org/abs/1412.3952).
- [22] S. C. Takatori, W. Yan, and J. F. Brady, *Phys. Rev. Lett.* **113**, 028103 (2014).
- [23] J. Stenhammar, D. Marenduzzo, R. J. Allen, and M. E. Cates, *Soft Matter* **10**, 1489 (2014).
- [24] N. G. van Kampen, *Phys. Rep.* **24**, 171 (1976).
- [25] N. G. van Kampen, *Braz. J. Phys.* **28**, 90 (1998).
- [26] S. Faetti, L. Fronzoni, P. Grigolini, and R. Mannella, *J. Stat. Phys.* **52**, 951 (1988).
- [27] R. F. Fox, *Phys. Rev. A* **33**, 467 (1986).
- [28] R. F. Fox, *Phys. Rev. A* **34**, 4525(R) (1986).
- [29] A. Pototsky and H. Stark, *Europhys. Lett.* **98**, 50004 (2012).
- [30] W. Madden and S. Rice, *J. Chem. Phys.* **72**, 4208 (1980).
- [31] Useful tables of simulation data are to be found in J. Barker and D. H. Henderson, *Rev. Mod. Phys.* **48**, 587 (1976).
- [32] R. Sear and W. Gelbart, *J. Chem. Phys.* **110**, 4582 (1997).
- [33] A. J. Archer and N. B. Wilding, *Phys. Rev. E* **76**, 031501 (2007).
- [34] J. M. Brader, *J. Chem. Phys.* **128**, 104503 (2008).
- [35] C. Maggi, U. M. B. Marconi, N. Gnan, and R. Di Leonardo, [arXiv:1503.03123v2](https://arxiv.org/abs/1503.03123v2).

- [36] T. F. F. Farage and J. M. Brader, [arXiv:1403.0928](#).
- [37] R. Ni, M. A. Cohen Stuart, and M. Dijkstra, *Nat. Commun.* **4**, 2704 (2013).
- [38] L. Berthier and J. Kurchan, *Nature Phys.* **9**, 310 (2013).
- [39] G. Szamel, E. Flenner, and L. Berthier, [arXiv:1501.01333](#).
- [40] C. Gardiner, *Handbook of Stochastic Methods* (Springer, Berlin, 1985).
- [41] P. Debye, *Polar Molecules* (Chemical Catalog Company, New York, 1929).
- [42] E. Fatuzzo and P. R. Mason, *Proc. Phys. Soc.* **90**, 741 (1967).
- [43] T.-W. Nee and R. Zwanzig, *J. Chem. Phys.* **52**, 6353 (1970).
- [44] B. J. Berne, *J. Chem. Phys.* **62**, 1154 (1975).
- [45] G. B. Arfken, H. J. Weber, and F. A. Harris, *Mathematical Methods for Physicists* (Elsevier, Amsterdam, 2013).
- [46] A. Ghosh, J. Samuel, and S. Sinha, *Europhys. Lett.* **98**, 30003 (2012).
- [47] J. Weeks, D. Chandler, and H. Anderson, *J. Chem. Phys.* **54**, 5237 (1971).
- [48] J.-P. Hansen and I. R. McDonald, *Theory of Simple Liquids* (Academic Press, London, 1986).
- [49] J. M. Brader, *Int. J. Thermophys.* **27**, 394 (2006).
- [50] M. P. Allen and D. J. Tildesley, *Computer Simulation of Liquids* (Oxford University Press, Oxford, 1991).

Nonequilibrium Phase Behavior from Minimization of Free Power Dissipation

Philip Krinninger,¹ Matthias Schmidt,^{1,*} and Joseph M. Brader²

¹*Theoretische Physik II, Physikalisches Institut, Universität Bayreuth, D-95440 Bayreuth, Germany*

²*Soft Matter Theory, University of Fribourg, CH-1700 Fribourg, Switzerland*

(Received 23 May 2016; revised manuscript received 16 August 2016; published 11 November 2016)

We develop a general theory for describing phase coexistence between nonequilibrium steady states in Brownian systems, based on power functional theory [M. Schmidt and J. M. Brader, *J. Chem. Phys.* **138**, 214101 (2013)]. We apply the framework to the special case of fluid-fluid phase separation of active soft sphere swimmers. The central object of the theory, the dissipated free power, is calculated via computer simulations and compared to a simple analytical approximation. The theory describes well the simulation data and predicts motility-induced phase separation due to avoidance of dissipative clusters.

DOI: 10.1103/PhysRevLett.117.208003

Phase transitions in soft matter occur both in equilibrium and in nonequilibrium situations. Examples of the latter type include the glass transition [1], various types of shear-banding instabilities observed in colloidal suspensions [2,3], shear-induced demixing in semidilute polymeric solutions [4], and motility-induced phase separation in assemblies of active particles [5,6]. In contrast to phase transitions in equilibrium, which obey the statistical mechanics of Boltzmann and Gibbs, very little is known about general properties of transitions between out-of-equilibrium states. A corresponding universal framework for describing nonequilibrium soft matter is lacking at present.

Theoretical progress has recently been made for the case of many-body systems governed by overdamped Brownian dynamics, encompassing a broad spectrum of physical systems [7]. It has been demonstrated that the dynamics of such systems can be described by a unique time-dependent power functional $R_t[\rho, \mathbf{J}]$, where the arguments are the space- and time-dependent one-body density distribution, $\rho(\mathbf{r}, t)$, and the one-body current distribution, $\mathbf{J}(\mathbf{r}, t)$, in the case of a simple substance [8,9]. Both these fields are microscopically sharp and act as trial variables in a variational theory. The power functional theory is regarded to be “important, [as it] provides (i) a rigorous framework for formulating dynamical treatments within the [density functional theory] formalism and (ii) a systematic means of deriving new approximations” [10].

The physical time evolution is that which minimizes $R_t[\rho, \mathbf{J}]$ at time t with respect to $\mathbf{J}(\mathbf{r}, t)$, while keeping $\rho(\mathbf{r}, t)$ fixed. Hence,

$$\frac{\delta R_t[\rho, \mathbf{J}]}{\delta \mathbf{J}(\mathbf{r}, t)} = 0 \quad (1)$$

at the minimum of the functional. Here the variation is performed at fixed time t with respect to the position-dependent current. The density distribution is then obtained from integrating the continuity equation, $\partial \rho(\mathbf{r}, t) / \partial t = -\nabla \cdot \mathbf{J}(\mathbf{r}, t)$, in time. The power functional

possesses units of energy per time and can be split according to

$$R_t[\rho, \mathbf{J}] = P_t[\rho, \mathbf{J}] + \dot{F}[\rho] - X_t[\rho, \mathbf{J}], \quad (2)$$

where $P_t[\rho, \mathbf{J}]$ accounts for the irreversible energy loss due to dissipation, $\dot{F}[\rho]$ is the total time derivative of the intrinsic (Helmholtz) free energy density functional [7,11], and $X_t[\rho, \mathbf{J}]$ is the external power, given by

$$X_t[\rho, \mathbf{J}] = \int d\mathbf{r} \mathbf{J}(\mathbf{r}, t) \cdot \mathbf{F}_{\text{ext}}(\mathbf{r}, t) - \rho(\mathbf{r}, t) \dot{V}_{\text{ext}}(\mathbf{r}, t), \quad (3)$$

where $\dot{V}_{\text{ext}}(\mathbf{r}, t)$ is the partial time derivative of the external potential $V_{\text{ext}}(\mathbf{r}, t)$, and $\mathbf{F}_{\text{ext}}(\mathbf{r}, t)$ is the external one-body force field, which in general consists of a sum of a conservative contribution, $-\nabla V_{\text{ext}}(\mathbf{r}, t)$, and a further nonconservative term. The power dissipation is conveniently split into ideal and excess (above ideal) contributions: $P_t[\rho, \mathbf{J}] = P_t^{\text{id}}[\rho, \mathbf{J}] + P_t^{\text{exc}}[\rho, \mathbf{J}]$, where $P_t^{\text{exc}}[\rho, \mathbf{J}]$ is nontrivial and arises from the internal interactions between the particles. The exact free power dissipation of the ideal gas is local in time and space and given by

$$P_t^{\text{id}}[\rho, \mathbf{J}] = \frac{\gamma}{2} \int d\mathbf{r} \frac{\mathbf{J}(\mathbf{r}, t)^2}{\rho(\mathbf{r}, t)}, \quad (4)$$

where γ is the friction constant of the Brownian particles against the (implicit) solvent. This framework is formally exact and goes beyond dynamical density functional theory [11–13]; the latter follows from neglecting the excess dissipation, $P_t^{\text{exc}}[\rho, \mathbf{J}] = 0$.

In this Letter, we apply the general framework of power functional theory to treat phase coexistence of nonequilibrium steady states. Such a state of N particles in a volume V at temperature T is characterized by a value of the total power functional taken at the (local) minimum, $R_t^0(N, V, T) \equiv R_t[\rho^0, \mathbf{J}^0]$, where the superscript 0 indicates a quantity at the minimum. We define the chemical power

derivative ν and the (negative) volumetric power derivative π via partial differentiation,

$$\nu = \left. \frac{\partial R_t^0}{\partial N} \right|_{V,T}, \quad \pi = - \left. \frac{\partial R_t^0}{\partial V} \right|_{N,T}, \quad (5)$$

where ν and π possess units of energy per time and pressure per time, respectively. In the limit of large N and large V , the specific free power per volume, $r_t(\rho_b) = R_t^0/V$, will depend only on the (bulk) number density $\rho_b = N/V$; this implies the identity $R_t^0 = -\pi V + \nu N$, which neglects possible surface contributions. The simple relations $\nu = \partial r_t / \partial \rho_b$ and $\pi = -r_t + \rho_b \nu$ follow straightforwardly. We shall demonstrate below that the free power density $r_t(\rho_b)$ is the relevant physical quantity for analyzing phase behavior out of equilibrium.

We assume that two coexisting nonequilibrium steady states, A and B , are characterized by particle number N_A and N_B and by volume V_A and V_B , respectively. The density in phase A (B) is $\rho_A = N_A/V_A$ ($\rho_B = N_B/V_B$). Hence, in a phase-separated state, the total power is a weighted sum,

$$R_t^0 = r_t(\rho_A)V_A + r_t(\rho_B)V_B, \quad (6)$$

where the partial volumes of the two phases are $V_A/V = (\rho_B - \rho_b)/(\rho_B - \rho_A)$ and $V_B/V = (\rho_b - \rho_A)/(\rho_B - \rho_A)$, with $\rho_A \leq \rho_b \leq \rho_B$.

The task of finding a global minimum of $R_t[\rho, \mathbf{J}]$ can now be facilitated by a Maxwell common tangent construction on $r_t(\rho_b)$, which implies the identities

$$r_t'(\rho_A) = r_t'(\rho_B) = \frac{r_t(\rho_B) - r_t(\rho_A)}{\rho_B - \rho_A}, \quad (7)$$

where $r_t'(\rho_b) = \partial r_t(\rho_b) / \partial \rho_b$. As a consequence, both the chemical and the volumetric derivatives have the same value in the coexisting phases:

$$\nu_A = \nu_B, \quad \pi_A = \pi_B, \quad (8)$$

and equality of temperature is trivial by construction.

In order to illustrate this framework, we apply it to treat active Brownian particles, which form a class of systems attracting much current interest [5,14–16]. We consider spherical particles in d -dimensional space, with position coordinates $\mathbf{r}^N \equiv \{\mathbf{r}_1 \dots \mathbf{r}_N\}$ and (unit vector) orientations $\boldsymbol{\omega}^N \equiv \{\boldsymbol{\omega}_1 \dots \boldsymbol{\omega}_N\}$; here the orientational motion of each $\boldsymbol{\omega}_i$, where $i = 1 \dots N$, is freely diffusive with orientational diffusion constant D_{rot} . The swimming is due to an orientation-dependent external force field $\mathbf{F}_{\text{ext}}(\boldsymbol{\omega}_i) = \gamma s \boldsymbol{\omega}_i$, which is nonconservative and does not depend explicitly on \mathbf{r} and t ; here s is the speed for free swimming. We follow Refs. [14,15] and use the Weeks-Chandler-Andersen model, i.e., a Lennard-Jones pair potential, which is cut and shifted at its minimum, such that the resulting short-ranged pair force is continuous and purely repulsive.

For numerical convenience, our Brownian dynamics (BD) simulations will be performed in $d = 2$.

Power functional theory provides a microscopic many-body expression for R_t^0 [8]. Omitting an irrelevant rotational contribution, this is given (up to a constant C) by

$$R_t^0 = -\frac{\gamma}{2} \left\langle \sum_i \mathbf{v}_i(t)^2 \right\rangle + C, \quad (9)$$

where the sum is over all particles and the angles denote a steady state average. To directly simulate the dissipated free power, we use a discretized version of the instantaneous velocity [17]: $\mathbf{v}_i(t) = [\mathbf{r}_i(t + \Delta t) - \mathbf{r}_i(t - \Delta t)] / (2\Delta t)$, where Δt is the time step of the standard (Euler) computer simulation algorithm, where $\mathbf{r}_i(t + \Delta t) = \mathbf{r}_i(t) + \gamma^{-1} \Delta t [-\nabla_i U(\mathbf{r}^N) + \boldsymbol{\xi}_i(t) + \mathbf{F}_{\text{ext}}(\boldsymbol{\omega}_i(t))]$, with $\boldsymbol{\xi}_i(t)$ being a Gaussian-distributed delta-correlated noise term, with finite-difference, equal-time strength $\langle \boldsymbol{\xi}_i(t) \cdot \boldsymbol{\xi}_j(t) \rangle = \delta_{ij} k_B T d / (\gamma \Delta t)$; $C = N k_B T d / (2\Delta t)$ is an irrelevant constant, and k_B is the Boltzmann constant. The external power is given by

$$X_t = \left\langle \sum_i \mathbf{v}_i(t) \cdot \mathbf{F}_{\text{ext}}(\boldsymbol{\omega}_i(t)) \right\rangle, \quad (10)$$

and we define the corresponding internal power, due to interparticle interactions and Brownian forces, as

$$I_t = \left\langle \sum_i \mathbf{v}_i(t) \cdot [-\nabla_i U(\mathbf{r}^N) + \boldsymbol{\xi}_i(t)] \right\rangle. \quad (11)$$

This allows us to split (9) into a sum of external and internal contributions,

$$R_t^0 = -I_t/2 - X_t/2. \quad (12)$$

By inserting (2) into (1) and observing the structure of (4), it is straightforward to show that

$$I_t = -\dot{F} - 2P_t^{\text{exc}} + \int d\mathbf{r} d\boldsymbol{\omega} \mathbf{J}(\mathbf{r}, \boldsymbol{\omega}, t) \cdot \left. \frac{\delta P_t^{\text{exc}}[\rho, \mathbf{J}]}{\delta \mathbf{J}(\mathbf{r}, \boldsymbol{\omega}, t)} \right|_0, \quad (13)$$

where the integrand is evaluated at the minimum and we included the argument $\boldsymbol{\omega}$, treating the system effectively as a mixture of different components [18].

To sample (9) efficiently in simulation, we decompose the velocity as $\mathbf{v}_i(t) = [\Delta \mathbf{r}_i(t - \Delta t) + \Delta \mathbf{r}_i(t)] / (2\Delta t)$, where $\Delta \mathbf{r}_i(t) = \mathbf{r}_i(t + \Delta t) - \mathbf{r}_i(t)$, given via the Euler algorithm as a sum of three contributions, i.e., intrinsic, $\Delta \mathbf{r}_i^{\text{int}}(t) = -\Delta t \nabla_i U(\mathbf{r}^N(t))$; random, $\Delta \mathbf{r}_i^{\text{ran}}(t) = \Delta t \boldsymbol{\xi}_i(t)$; and external, $\Delta \mathbf{r}_i^{\text{ext}}(t) = \Delta t \mathbf{F}_{\text{ext}}(\boldsymbol{\omega}_i(t))$. Multiplying out (9) yields 36 contributions, of which we sample only the three nontrivial types: $\langle \Delta \mathbf{r}_i^{\text{int}}(t) \cdot \Delta \mathbf{r}_i^{\text{int}}(t) \rangle$ and $\langle \Delta \mathbf{r}_i^{\text{int}}(t) \cdot \Delta \mathbf{r}_i^{\text{ext}}(t) \rangle$ (where also similar contributions arise with one or both displaced time arguments), as well as $\langle \Delta \mathbf{r}_i^{\text{ran}}(t - \Delta t) \cdot \Delta \mathbf{r}_i^{\text{int}}(t) \rangle$. We use $N = 1000$ and adjust V in

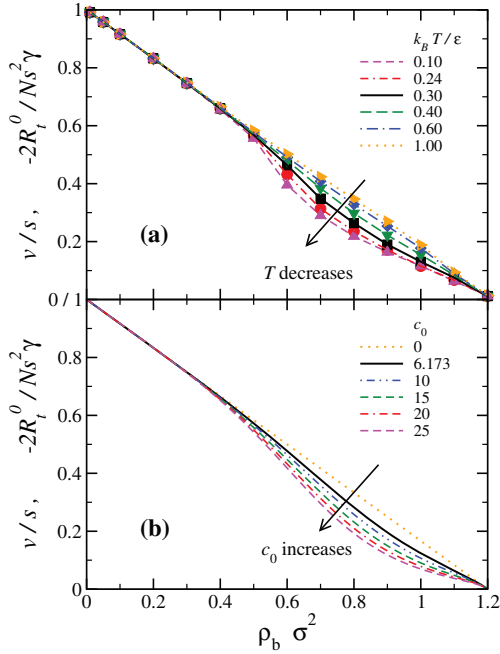


FIG. 1. (a) Scaled average forward swimming speed v/s (symbols) and scaled free power $-2R_t^0/(Ns^2\gamma)$ per particle (lines), as obtained from BD computer simulations via Eqs. (9) and (10), respectively, for temperatures $k_B T/\epsilon = 0.1-1$ (as indicated). (b) Theoretical results corresponding to (a), as given by Eqs. (17) and (19), where $m = 5$, $\rho_0\sigma^2 = 1.2$, and for values of $c_0 = 0-25$ as indicated.

order to control the density in the square simulation box with periodic boundaries. The time step is chosen as $\Delta t/\tau_0 = 10^{-5}$, where the time scale is $\tau_0 = \gamma\sigma^2/\epsilon$, with Lennard-Jones diameter σ and energy scale ϵ . We allow the system to reach a steady state in 10^7 steps and collect data for a further 10^8 steps. The rotational diffusion constant is set to $D_{\text{rot}} = 3k_B T/(\gamma\sigma^2)$, and the external field strength is chosen as $s = 24\sigma/\tau_0$. The Peclet number [14,15] is $\text{Pe} \equiv 3s/(D_{\text{rot}}\sigma) = \gamma s\sigma/(k_B T)$.

Figure 1(a) shows simulation results for R_t^0 and X_t , as respectively given by (9) and (10), as a function of density. Due to the simple form of the external force, the external power (10) is trivially related to the (well-studied [14–16]) average forward swimming speed v via $X_t = \gamma s v N$, where $v = \langle \sum_i \mathbf{v}_i(t) \cdot \boldsymbol{\omega}_i(t) \rangle / N$. Remarkably, we find that R_t^0 coincides with $-X_t/2$ within our numerical precision. This implies that (i) the internal dissipation is negligible, $I_t \approx 0$ [cf. (12)] and (ii) that the value of the power functional for active particles is a known quantity. We have systematically studied the variation with temperature (as is analogous to varying Pe [14,15]). While hardly any effect for low densities is observed, a dip develops for $\rho\sigma^2 \gtrsim 0.5$; cf. Fig. 1(a) [19].

We next seek to develop a simple theoretical model to capture the key features of the simulation data; the

corresponding results shown in Fig. 1(b) will be discussed below. We assume $P_t^{\text{exc}}[\rho, \mathbf{J}]$ to possess a simple Markovian, spatially nonlocal form:

$$P_t^{\text{exc}}[\rho, \mathbf{J}] = \frac{\gamma}{2} \int d1 \int d2 \rho(1)\rho(2) \left(\frac{\mathbf{J}(1)}{\rho(1)} - \frac{\mathbf{J}(2)}{\rho(2)} \right)^2 M(1,2), \quad (14)$$

where $1 \equiv \mathbf{r}, \boldsymbol{\omega}$ and $2 \equiv \mathbf{r}', \boldsymbol{\omega}'$. Here $M(1,2)$ is a (dimensionless) correlation kernel that couples the particles at points 1 and 2, similar to the mean-field form of the excess free energy functional in equilibrium density functional theory [7,11]. Note that the term in brackets in (14) is the (squared) velocity difference between the two points. We parameterize the current, which in general depends on particle position \mathbf{r} and orientation $\boldsymbol{\omega}$, as $\mathbf{J}(\mathbf{r}, \boldsymbol{\omega}, t) = J_b \boldsymbol{\omega}$, where J_b is a variational parameter that determines the (homogeneous) bulk current in direction $\boldsymbol{\omega}$. This implies $v = J_b/\rho_b$. Inserting into (14) and observing the general structure (2), we obtain

$$\frac{R_t}{\gamma V} = \frac{J_b^2}{2\rho_b} + \frac{M_0}{2} J_b^2 - s J_b, \quad (15)$$

where the right-hand side consists of a sum of contributions due to ideal dissipation (P_{id}), excess contribution to dissipation (P_{exc}), and external power (X_t). The coefficient M_0 is density dependent and can be expressed as a moment of the correlation kernel [9] $M(1,2)$, as $M_0 = \int d\mathbf{r} d\boldsymbol{\omega} d\boldsymbol{\omega}' (\boldsymbol{\omega} - \boldsymbol{\omega}')^2 M(1,2)$, where due to symmetries $M(1,2)$ depends only on the differences $\mathbf{r} - \mathbf{r}'$ and $\boldsymbol{\omega} - \boldsymbol{\omega}'$, and M_0 is hence independent of \mathbf{r}' . Clearly, in steady states $\dot{F}[\rho] = 0$.

The minimization principle (1) implies $\partial R_t/\partial J_b = 0$ for (15), which yields

$$J_b = s\rho_b/(1 + M_0\rho_b). \quad (16)$$

Using (16) in order to eliminate M_0 from (15) gives the value at the minimum

$$R_t^0 = -\gamma s J_b V/2, \quad (17)$$

which implies that $R_t^0 = -X_t/2$, where here the external power is $X_t = \gamma s J_b V$. A detailed derivation will be given elsewhere. The internal contribution $I_t = 0$, as $\dot{F} = 0$ in steady state, and the additional contributions in (13) vanish for the present form (14) of $P_{\text{exc}}[\rho, \mathbf{J}]$, which is quadratic in $\mathbf{J}(\mathbf{r}, \boldsymbol{\omega}, t)$.

We assume a simple analytical expression,

$$M_0 = (\rho_0 - \rho_b)^{-1} + c_0 \rho_b^m / \rho_0^{m+1}, \quad (18)$$

where ρ_0 is the jamming density at which the dynamics arrests, $c_0 \geq 0$ is a temperature-dependent dimensionless constant, and the exponent $m > 0$ is a measure for the number of particles that cause the additional dissipation due to local cluster formation [second term in (18)]. We expect the exponent m to grow with d , as clusters consist of an increasing number of particles upon increasing d . Furthermore, we expect c_0 to decrease to zero with increasing temperature, as clusters are broken up by thermal motion. We leave a microscopic derivation of M_0 , e.g. starting from the correlation kernel $M(1, 2)$ (which is, in principle, accessible via simulations [20]) to future work. Equation (18) can be interpreted as describing an overall increase, and eventual divergence, of dissipation with density plus a specific dissipation channel due to small groups of the order of m particles that block each other. Blocking is relevant only at intermediate densities, high enough so that the m th density order contributes, but low enough in order to be not overwhelmed by the singularity.

Inserting (18) into (16) yields

$$\frac{J_b}{s\rho_b} = \frac{1-x}{1+c_0x^{m+1}(1-x)}, \quad (19)$$

where we have defined the scaled density $x = \rho_b/\rho_0$. In case of high temperature, where $c_0 \rightarrow 0$, this reduces to the simple and well-known (see, e.g., [14–16]) linear (velocity) relationship $v/s \equiv J_b/(s\rho_b) = 1-x$. In Fig. 1(b), we show the theoretical results for the (scaled) external and total free power per particle corresponding to the simulation results in Fig. 1(a). Clearly, despite the simplicity of (18), the theory reproduces the simulation data very well.

As outlined above, in order to assess phase behavior, the relevant quantity is the free power per volume r_t (rather than per particle), which we show in Fig. 2, obtained from simulations [Fig. 2(a)] and theory [Fig. 2(b)]. For low temperatures $k_B T/\epsilon = 0.1, 0.24$, the simulation data clearly show a change in curvature, which we attribute to a first-order phase transition in the finite system [21]. (In an infinite system, we expect no negative curvature to occur and the coexistence region to be characterized by a strictly linear variation of r_t with ρ_b .) For $k_B T/\epsilon = 0.3$, a quasilinear part can be observed, which we interpret as being very close to a nonequilibrium critical point. The theoretical curve displays the same type of behavior, which we attribute to the mean-field character of the approximation (14). We can now apply the general phase coexisting conditions (7) and (8) to the active system. A representative double tangent is shown in Fig. 2(b). The low-density (high-density) coexisting phase is characterized by a high (low) value of X_t .

The phase diagram (cf. Fig. 3) displays two-phase coexistence between a high-density and a low-density active fluid. We find the simulation results [Fig. 3(a)] for the binodal obtained from double tangent construction [on the results shown above in Fig. 2(a)] as a function of

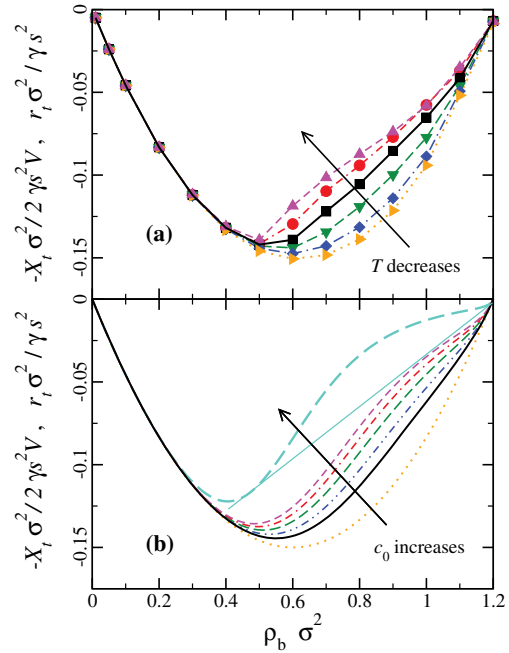


FIG. 2. The same as Fig. 1, but scaled per volume V rather than per particle N ; the conversion factor is $-2V/\sigma^2$, such that $r_t\sigma^2/(\gamma s^2)$ and $-X_t\sigma^2/(2\gamma s^2V)$ are shown as a function of $\rho_b\sigma^2$. The straight line in (b) indicates the double tangent for the case $c_0 = 100$; the black solid line indicates the result at the critical value of c_0 .

$k_B T/\epsilon$ to be consistent with the behavior of the tail ($5 < r/\sigma < 10$) of the radial pair distribution function $g(r)$. A characteristic slow decay indicates the occurrence of phase separation (see, e.g., [22]). The corresponding theoretical phase diagram is shown in Fig. 3(b), where we also display the spinodal, defined as the point(s) of inflection of $r_t(\rho_b)$. The phase separation vanishes upon increasing $1/c_0$ at an upper nonequilibrium critical point. Although we have not attempted to model the dependence of $1/c_0$ on T systematically, the agreement between simulation and theoretical results is striking. Our simulation results for the phase behavior underestimate the boundaries given by Stenhammar *et al.* [14,15]; this is not surprising given that these authors investigated significantly larger systems. In simulations, we have found only a slight decrease of the slope of $v(\rho_b)$ for increasing s , and a corresponding increase in the jamming density, but with little effect on the phase separation itself. This is consistent with the fact that $P_{\text{exc}}[\rho, \mathbf{J}]$, and hence c_0 , is an intrinsic quantity. The conditions for spinodal and binodal both differ from the density “where macroscopic MIPS [motility-induced phase separation] is initiated by spinodal decomposition” [6], $v'/v = -1/\rho_b$, where $v' = dv(\rho_b)/d\rho_b$; this can be rephrased as $d(\rho_b v)/d\rho_b = 0$, implying, within $I_t = 0$, that $r'_t(\rho_b) = 0$. This condition is quite different from the spinodal within power functional

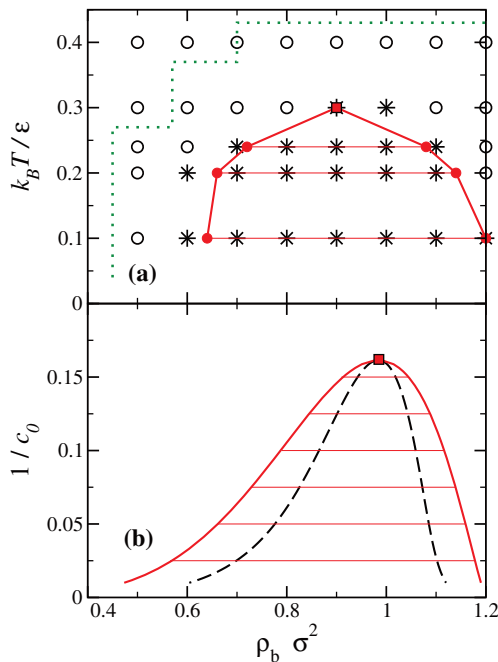


FIG. 3. (a) Phase diagram for active particles, obtained from simulations, as a function of scaled density $\rho_b \sigma^2$ and scaled temperature $k_B T / \epsilon$. Shown are the binodal (red solid line) obtained from double tangent construction (red solid symbols), horizontal tie lines (thin red lines), and estimate for the critical point (red square). Also shown are single-phase (open symbols) and phase-separated (stars) states based on the analysis of the decay of $g(r)$. The phase boundary of Refs. [14,15] is also shown (green dotted line). (b) The same as (a), but obtained from power functional theory and shown as a function $1/c_0$ instead of scaled temperature. The dashed line indicates the spinodal.

theory, $r'_t(\rho_b) = 0$, or equivalently $v''/v' = -2/\rho_b$. Furthermore, for linear variation of v with ρ_b , i.e., $c_0 = 0$, we find phase separation to be absent, in contrast to Ref. [6]; cf. Eqs. (35)–(37) and Fig. 5 therein.

We have developed a general approach, based on power functional theory [8], to treat coexistence between non-equilibrium steady states in Brownian systems. Our theory is fundamentally different from other approaches to active systems (e.g., [5,22,23]) which were developed specifically for phase separation. We rather identify a generating functional providing a unified, internally self-consistent description of out-of-equilibrium states. The free power density plays a role in nonequilibrium systems analogous to that of the free energy density in equilibrium, although it is an entirely distinct physical quantity.

*Matthias.Schmidt@uni-bayreuth.de

[1] G. L. Hunter and E. Weeks, *Rep. Prog. Phys.* **75**, 066501 (2012).

- [2] V. Chikkadi, D. M. Miedema, M. T. Dang, B. Nienhuis, and P. Schall, *Phys. Rev. Lett.* **113**, 208301 (2014).
- [3] J. K. G. Dhont, M. P. Lettinga, Z. Dogic, T. A. J. Lenstra, H. Wang, S. Rathgeber, P. Carletto, L. Willner, H. Frielinghaus, P. Lindner, *Faraday Discuss.* **123**, 157 (2003).
- [4] A. Onuki, *Phase Transition Dynamics* (Cambridge University Press, Cambridge, UK, 2002).
- [5] Y. Fily, S. Henkes, and M. C. Marchetti, *Soft Matter* **10**, 2132 (2014); J. Bialké, H. Löwen, and T. Speck, *Europhys. Lett.* **103**, 30008 (2013).
- [6] M. E. Cates and J. Tailleur, *Annu. Rev. Condens. Matter Phys.* **6**, 219 (2015).
- [7] J. P. Hansen and I. R. McDonald, *Theory of Simple Liquids*, 4th ed. (Academic, Amsterdam, 2013).
- [8] M. Schmidt and J. M. Brader, *J. Chem. Phys.* **138**, 214101 (2013).
- [9] J. M. Brader and M. Schmidt, *J. Chem. Phys.* **139**, 104108 (2013).
- [10] R. Evans, M. Oettel, R. Roth, and G. Kahl, *J. Phys. Condens. Matter* **28**, 240401 (2016).
- [11] R. Evans, *Adv. Phys.* **28**, 143 (1979).
- [12] U. M. B. Marconi and P. Tarazona, *J. Chem. Phys.* **110**, 8032 (1999).
- [13] A. J. Archer and R. Evans, *J. Chem. Phys.* **121**, 4246 (2004).
- [14] J. Stenhammar, A. Tiribocchi, R. J. Allen, D. Marenduzzo, and M. E. Cates, *Phys. Rev. Lett.* **111**, 145702 (2013).
- [15] J. Stenhammar, D. Marenduzzo, R. J. Allen, and M. E. Cates, *Soft Matter* **10**, 1489 (2014).
- [16] A. P. Solon, J. Stenhammar, R. Wittkowski, M. Kardar, Y. Kafri, M. E. Cates, and J. Tailleur, *Phys. Rev. Lett.* **114**, 198301 (2015); A. P. Solon, Y. Fily, A. Baskaran, M. E. Cates, Y. Kafri, M. Kardar, and J. Tailleur, *Nat. Phys.* **11**, 673 (2015).
- [17] A. Fortini, D. de las Heras, J. M. Brader, and M. Schmidt, *Phys. Rev. Lett.* **113**, 167801 (2014). The trajectory-based velocity is analogous to the operator description of Refs. [8,9].
- [18] J. M. Brader and M. Schmidt, *J. Phys. Condens. Matter* **27**, 194106 (2015).
- [19] Nonlinear behavior of simulation results for $v(\rho)$ has been reported before; see Fig. S3 in the Supplemental Material of Ref. [14].
- [20] T. Schindler and M. Schmidt, *J. Chem. Phys.* **145**, 064506 (2016).
- [21] We expect the precise form of $r_t(\rho)$ and, hence, the value of the phase coexistence densities to be affected by finite size effects.
- [22] T. F. F. Farage, P. Krinninger, and J. M. Brader, *Phys. Rev. E* **91**, 042310 (2015).
- [23] I. Theurkauff, C. Cottin-Bizonne, J. Palacci, C. Ybert, and L. Bocquet, *Phys. Rev. Lett.* **108**, 268303 (2012); G. S. Redner, M. F. Hagan, and A. Baskaran, *Phys. Rev. Lett.* **110**, 055701 (2013); I. Buttinoni, J. Bialké, F. Kümmel, H. Löwen, C. Bechinger, and T. Speck, *Phys. Rev. Lett.* **110**, 238301 (2013); G. S. Redner, C. G. Wagner, A. Baskaran, M. F. Hagan, *Phys. Rev. Lett.* **117**, 148002 (2016); D. Richard, H. Löwen, and T. Speck, *Soft Matter* **12**, 5257 (2016).

Erratum: Nonequilibrium Phase Behavior from Minimization of Free Power Dissipation [Phys. Rev. Lett. 117, 208003 (2016)]

Philip Krinninger, Matthias Schmidt, and Joseph M. Brader

(Received 5 June 2017; published 13 July 2017)

DOI: [10.1103/PhysRevLett.119.029902](https://doi.org/10.1103/PhysRevLett.119.029902)

In deriving the nonequilibrium phase coexistence conditions (8) via the double tangent construction (7), as exemplified in Fig. 2(b) and leading to the results in Fig. 3, we assumed the concept of minimization of free power dissipation, $R_t[\rho, \mathbf{J}]$. However, while minimization of $R_t[\rho, \mathbf{J}]$ with respect to the current distribution $\mathbf{J}(\mathbf{r}, \boldsymbol{\omega}, t)$ generates a one-body force balance equation of motion (1), we had implicitly assumed [1] that the functional is also minimal with respect to the density distribution $\rho(\mathbf{r}, \boldsymbol{\omega}, t)$. This additional minimization is not present in power functional theory [8], which rather states that

$$\frac{\delta R_t[\rho, \mathbf{J}]}{\delta \rho(\mathbf{r}, \boldsymbol{\omega}, t)} = \alpha(\mathbf{r}, \boldsymbol{\omega}, t), \quad (20)$$

where $\alpha(\mathbf{r}, \boldsymbol{\omega}, t)$ is a Lagrange multiplier corresponding to the constraint between $\rho(\mathbf{r}, \boldsymbol{\omega}, t)$ and $\mathbf{J}(\mathbf{r}, \boldsymbol{\omega}, t)$ that is imposed by the continuity equation.

For our test case of motility-induced phase separation in active Brownian particles, recent simulation data [2,3] very clearly points to the fact that both π and ν possess different values in the coexisting phases. Hence the conclusion that (8) offers a shortcut to phase coexistence, bypassing the need to solve the force balance equation (1) across the interface, is not valid. This does not affect the validity of the excess dissipation functional (14), as demonstrated in Figs. 1 and 2, which hence offers a practical way to theoretically address the interfacial problem.

We thank D. de las Heras, T. Speck, J. Rodenburg, R. van Roij, S. Paliwal, and M. Dijkstra for useful discussions.

[1] J. Rodenburg and R. van Roij (private communication).

[2] S. Paliwal and M. Dijkstra (private communication).

[3] T. Speck (private communication).

Power functional theory for active Brownian particles: general formulation and power sum rules

Philip Krinninger^{1,*} and Matthias Schmidt¹

¹*Theoretische Physik II, Physikalisches Institut, Universität Bayreuth, D-95440 Bayreuth, Germany*
(Dated: September 21, 2018)

We generalize power functional theory [M. Schmidt and J. M. Brader, *J. Chem. Phys.* **138**, 214101 (2013)] to Brownian many-body systems with orientational degrees of freedom. The framework allows to study active particles in general inhomogeneous and time-dependent nonequilibrium. Swimming is induced by an external force field. We prove for steady states that the free power equals half the negative dissipated external work per time, and is hence trivially related to the average forward swim speed of the particles. The variational theory expresses the free power as a functional microscopic one-body density and current distribution. Both fields are time-, position- and orientation-dependent, and the total current consists of translational and rotational parts. Minimization of the free power functional with respect to the current(s) yields the physical dynamics of the system. We give a simple approximation for the superadiabatic (above free energy) contribution which describes excess dissipation in homogeneous bulk fluids due drag. In steady states, we evaluate the free power using Brownian dynamics simulations for short-ranged soft repulsive spheres. We describe the necessary sampling strategies and show that the theory provides good account of the simulation data.

I. INTRODUCTION

The class of active systems covers a wide variety of biological and physical systems. Activity refers to an intrinsic motility of the individual units, such as cells, bacteria or particular colloids. The growing interest in active systems over the last decade is poignantly illustrated by the large number of review articles that address the topic [1–18]. A variety of collective phenomena has been addressed in e.g. systems of microorganisms [2, 19], cells [20], and bacteria [6, 8, 21–30]. Further examples include the collective motion of flocks [1, 31–33], school of fish [34], and opinion formation in social science [35].

One of the most successful model to describe collective behavior is the Viscek model [36], and its variations [37–45]. The Viscek model has been used for example to study lane formation [39, 43, 46], soft deformable particles [47], order-disorder transition [37], and swarming turbulence [41]. A popular application is the description of active nematics. For active rods the collective properties [48, 49] and swarming behavior [50] were studied. In active nematics velocity correlations [51], orientational order and fluctuations have been investigated [52–54].

There exists a variety of experiments and applications, such as active glasses and gels [55–60] and the collective motion of vibrated polar disks and granular materials [61–64]. Experiments dealing with active colloidal particles use e.g. Janus particles [65, 66] or other colloids whose surface suitably is manipulated. Janus particles are built by e.g. by coating on hemisphere of SiO₂ beads with a thin layer of graphite onto one hemisphere [65]. When illuminated with a widened laser, the light is absorbed by the graphite hemisphere. This locally heats up

the solvent above the critical temperature, causing a local demixing, which generates a phoretic force that propels the Janus particle. In Ref. [67] a polymer sphere encapsulated most of an anti-ferromagnetic cube, which was then only partially exposed to the solvent. Illuminated with blue light, the colloids were able to self-propel and form clusters. Unlike other propulsion mechanisms, e.g., driven by chemical gradients, such light-induced motion does not need fuel [66, 68, 69].

A body of work has been based on hydrodynamic frameworks [7], addressing the behaviour of flocks [70], phase coexistence [71], pattern formation [72], confined collective motion [73], and microorganisms [2]. Furthermore hydrodynamic approaches give the opportunity to study e.g. self-propulsion mechanisms [74, 75], synchronization of anisotropic particles [76–78], and dynamics near a wall [79].

Active Brownian particles (ABP) form a simple microscopic model for active matter. This type of particles undergo Brownian motion with a built-in orientation degree of freedom, which itself diffuses freely, and gives the direction of the self-propulsion. In particular spherical particles serve as a minimal model for active colloids. The ABP model is very popular for studying phase separation of active particles, which is based on the particles' motility. This motility-induced phase separation (MIPS) occurs between non-equilibrium steady states in systems with purely repulsive interparticle interactions. The simplicity of the ABP model has lead to a thriving number of publications based on computer simulations and theoretical approaches to describe MIPS [80–103]. Recent theoretical developments include a mode coupling theory for ABP [104–106], a field theory for phase separation [107], and how swimmer-swimmer correlations affect the collective behavior of active suspensions [108].

Approaches for describing MIPS were based on continuum theory [95, 96] and a hydrodynamic, coarse-graining

*Electronic address: Philip.Krinninger@uni-bayreuth.de

theory [82, 94]. In both approaches the average propulsion speed as a function of bulk density, $v(\rho_b)$, plays an important role. Using continuum theory [95, 96] $v(\rho_b)$ is obtained by microscopic estimations of a random walk hindered by collisions. The authors of Refs. [95, 96] argue that using $v(\rho_b)$ it is possible to construct an effective free energy, which predicts the existence of phase separation. Furthermore they present a formalism which allows the detailed study of phase separation dynamics. The approach introduced in Refs. [82] and [94] is based on the microscopic many-body Smoluchowski equation. The authors derive coarse-grained equations for one tagged particle, in which again an effective (density-dependent) swimming speed $v(\rho_b)$ enters. From the effective hydrodynamics the authors identify an instability region of the homogeneous system, causing a dynamic instability. The fact that this indeed leads to phase separation can be demonstrated by comparison to computer simulations. Recent work showed [109] that $v(\rho_b)$ can also be obtained by Green-Kubo relations, which might in a next step be used as an input for coarse-grained frameworks. Summarizing, both theoretical approaches are able to predict the onset and existence of MIPS (with reasonable approximations), but a detailed description of stable phase coexistence is still missing.

Closely related to MIPS is the clustering of self-propelled particles and active clusters [28, 39, 65, 66, 81, 110–118]. The kinetics of the formation of the dense phase can be modeled analogously to classical nucleation theory [119]. Supported by simulations, it has been shown that, within this modeling, some properties, such as the location of the binodal and nucleation rates, can be obtained. Another approach is the active phase-field crystal model [120, 121].

Given the number of applications and phenomenological observations, the attempt at unification via formulating thermodynamics and statistical mechanics for active matter seems well justified [29, 84, 101, 122–132]. Under special investigation is the possibility to find an equation of state and a closed form for the pressure in active systems [89, 126, 133–139]. Especially in the context of MIPS the surface tension of the gas-liquid interface in systems with phase coexistence has been of significant interest [140–142]. Recent results suggest that the interfacial tension is negative [140], which violates the physical intuition earned from equilibrium statistical mechanics.

A fundamentally different approach is the effective equilibrium description of ABPs. The basic idea behind this framework is to eliminate the orientational degrees of freedom by integrating them out, resulting in a Langevin equation for a non-Markovian dynamics for the translational coordinates [143]. The underlying stochastic process is an Ornstein-Uhlenbeck process. There are two concepts which allow to represent this process using effective Markovian dynamics: The unified colored noise approximation (UCNA) introduced by Hänggi and Jung [144, 145], and the Fox approximation [146, 147]. Applying the former to ABPs allows to study a vari-

ety of problems, e.g. statistical properties such as the velocity distribution of ABPs [148]. Furthermore the UCNA is also used as a first step to formulate a statistical mechanics theory [124] and describe critical phenomena [149]. The Fox approximation is used to study the physics of ABPs [139, 143, 150, 151]. Within this approach an approximated Fokker-Plank equation is derived, whereby one can define an effective interaction between the particles, due to activity [143]. The existence of such an effective interaction has been proposed earlier, because of the similarities of MIPS and equilibrium phase transitions [152]. The application of Fox's approximation [143, 150] and the UCNA [153] gave an explicit formulation. Interfacial properties, pressure and tension have been studied as well in both approximations [139, 141, 154]. Very recent work by Wittmann *et al.* [155, 156] shows nicely the equivalence of both approaches and gives insight into previous results. The authors present new findings regarding interaction forces, phase equilibria, structure, and mechanical properties.

In this work we present a theory for active Brownian particles with orientational degrees of freedom. Our approach is based on the recently developed power functional theory (PFT) [157]. This framework allows the description of many-body systems that follow over-damped Brownian dynamics. These are described by a unique power functional $R_t[\rho, \mathbf{J}]$ of the one-body density distribution ρ and the one-body current distribution \mathbf{J} , which both depend on position \mathbf{r} and time t [157]. Minimizing the power functional with respect to the current gives the physical time evolution of the system. Therefore R_t can be regarded as an analogue to the free energy functional in equilibrium statistical physics. One central significance of the power functional is that its derivative determines the forces acting in overdamped systems. Therein lies the second analogy to equilibrium systems, where the thermodynamic potentials appear also as abstract quantities that are only detectable through their derivatives. The theory is generally formulated in the Smoluchowski picture, starting from the many-body probability distribution Φ .

Dynamical density functional theory (DDFT) is a widely used approach, e.g. for studying sheared systems [158, 159], spinodal decomposition [160], and systems with orientational degrees of freedom [161]. DDFT can be viewed as an extension to density functional theory (DFT) to nonequilibrium systems [162, 163]. However, in contrast to DDFT, PFT is formally exact in the sense that no adiabatic assumption is involved in order to describe the time evolution of the density profile. Hence PFT goes beyond the DDFT description and allows the study of additional forces in the system that are not contained in the adiabatic construction. These forces are called superadiabatic forces and are accessible via computer simulations [164–166]. Superadiabatic forces, and hence PFT, may serve therefore as a tool to describe nonequilibrium phenomena which are not fully understood, such as the laning transition

in colloidal systems [167, 168], where DDFT only fits when adding phenomenological terms [169, 170]. Moreover PFT potentially gives opportunities to describe a whole class of nonequilibrium system from first principles in a general and unified way. Furthermore PFT was also formulated for quantum [171] and classical Hamiltonian [172] many-body systems. For overdamped Brownian system, nonequilibrium Ornstein-Zernike equations were formulated for two-body dynamic correlation functions [173, 174]. Much recent progress has been made in the development of PFT approximations for simple fluids [175, 176] and for corresponding computer simulation techniques [177, 178].

Recently PFT has been used for the description of ABPs [179] by taking the orientational degree of freedom of the particles into account, which can be viewed as a generalization of the PFT for mixtures [180]. Here we give a complete account of the theory and present further comparisons to computer simulation results. We also derive several exact sum rules for nonequilibrium steady states, Eqs. (43), (44) and (49) below.

The paper is organized as follows. In Sec. II we formulate power functional theory for active particles. We start from the microscopic (Smoluchowski) many-body description of the active system and show the representation of PFT on the one-body level in Sec. II A. We then focus on steady states and derive an exact non-equilibrium sum rule for the splitting into internal and external contributions to the free power in Sec. II B. We give an approximation for the excess dissipation in Sec. II C and formulate the Langevin dynamics of the ABP model in Sec. III. Furthermore we give details about the Brownian dynamics computer simulations and the external power in the Langevin description is presented. In the Sec. IV we present our results obtained by simulations and theory. We conclude in Sec. V.

II. POWER FUNCTIONAL THEORY

A. General framework

We consider N active particles with position coordinates $\{\mathbf{r}_1, \dots, \mathbf{r}_N\} \equiv \mathbf{r}^N$ in d -dimensional space, and orientations $\{\boldsymbol{\omega}_1, \dots, \boldsymbol{\omega}_N\} \equiv \boldsymbol{\omega}^N$, where particle i at position \mathbf{r}_i swims with speed s in direction $\boldsymbol{\omega}_i$, with $|\boldsymbol{\omega}_i| = 1$. We consider possibly anisotropic inter-particle interaction potentials $u(\mathbf{r}^N, \boldsymbol{\omega}^N)$. The Smoluchowski equation for the time-dependent probability distribution $\Phi(\mathbf{r}^N, \boldsymbol{\omega}^N, t)$ of an ensemble of such systems is

$$\frac{\partial}{\partial t} \Phi(\mathbf{r}^N, \boldsymbol{\omega}^N, t) = - \sum_i (\nabla_i \cdot \hat{\mathbf{v}}_i + \nabla_i^\omega \cdot \hat{\mathbf{v}}_i^\omega) \Phi(\mathbf{r}^N, \boldsymbol{\omega}^N, t), \quad (1)$$

where ∇_i is the derivative with respect to \mathbf{r}_i , and ∇_i^ω is the derivative with respect to $\boldsymbol{\omega}_i$ (acting on the unit sphere); $\hat{\mathbf{v}}_i$ and $\hat{\mathbf{v}}_i^\omega$ are the translational velocity and ro-

tational velocity operators, respectively. The former is given by

$$\gamma \hat{\mathbf{v}}_i = -(\nabla_i u) - (\nabla_i v_i^{\text{ext}}) + \mathbf{X}_i + \gamma s \boldsymbol{\omega}_i - k_B T \nabla_i, \quad (2)$$

where $u(\mathbf{r}^N, \boldsymbol{\omega}^N)$ is the interparticle interaction potential, $v_i^{\text{ext}}(\mathbf{r}, \boldsymbol{\omega}, t)$ is a position-, orientation, and time-dependent external potential, $\mathbf{X}(\mathbf{r}, \boldsymbol{\omega}, t)$ is an external non-conservative force; we use $v_i^{\text{ext}} = v_i^{\text{ext}}(\mathbf{r}_i, \boldsymbol{\omega}_i, t)$ and $\mathbf{X}_i = \mathbf{X}(\mathbf{r}_i, \boldsymbol{\omega}_i, t)$ as short-hand notation; γ is the friction coefficient for translational motion, $s = \text{const}$ is the swimming speed of an isolated particle, k_B is the Boltzmann constant and T is absolute temperature. The vector fields $\nabla_i u$ and $\nabla_i v_i^{\text{ext}}$ act via multiplication in (1); only the thermal diffusive term (last contribution in (2)) acts via differentiation.

The rotational velocity operator is given by

$$\gamma^\omega \hat{\mathbf{v}}_i^\omega = -(\nabla_i^\omega u) - (\nabla_i^\omega v_i^{\text{ext}}) + \mathbf{X}_i^\omega - k_B T \nabla_i^\omega, \quad (3)$$

where γ^ω is the rotational friction coefficient, and $\mathbf{X}_i^\omega \equiv \mathbf{X}^\omega(\mathbf{r}_i, \boldsymbol{\omega}_i, t)$, where $\mathbf{X}^\omega(\mathbf{r}, \boldsymbol{\omega}, t)$ is a non-conservative external torque field.

Following the procedure of Ref. [157], we introduce variational fields $\tilde{\mathbf{v}}^N \equiv \{\tilde{\mathbf{v}}_1, \dots, \tilde{\mathbf{v}}_N\}$ and $\tilde{\mathbf{v}}^{\omega N} \equiv \{\tilde{\mathbf{v}}_1^\omega, \dots, \tilde{\mathbf{v}}_N^\omega\}$ for the translational and rotational velocity, respectively. Each variational field is a configuration space function, i.e. $\tilde{\mathbf{v}}_i \equiv \tilde{\mathbf{v}}_i(\mathbf{r}^N, \boldsymbol{\omega}^N, t)$ and $\tilde{\mathbf{v}}_i^\omega \equiv \tilde{\mathbf{v}}_i^\omega(\mathbf{r}^N, \boldsymbol{\omega}^N, t)$ for all $i = 1, \dots, N$.

We define a generator that depends on the trial fields via

$$\begin{aligned} \mathcal{R}_t = \int d\mathbf{r}^N d\boldsymbol{\omega}^N \sum_i & \left[\gamma \left(\frac{\tilde{\mathbf{v}}_i^2}{2} - \tilde{\mathbf{v}}_i \cdot \hat{\mathbf{v}}_i \right) \right. \\ & \left. + \gamma^\omega \left(\frac{(\tilde{\mathbf{v}}_i^\omega)^2}{2} - \tilde{\mathbf{v}}_i^\omega \cdot \hat{\mathbf{v}}_i^\omega \right) \right] \Phi(\mathbf{r}^N, \boldsymbol{\omega}^N, t). \end{aligned} \quad (4)$$

Due to its quadratic structure, the generator is instantaneously (i.e. at fixed time t and fixed distribution Φ) minimized by the true value of each of the trial fields, and hence when evaluated at the minimum

$$\frac{\delta \mathcal{R}_t}{\delta \tilde{\mathbf{v}}_i} = 0, \quad (5)$$

$$\frac{\delta \mathcal{R}_t}{\delta \tilde{\mathbf{v}}_i^\omega} = 0, \quad (6)$$

which implies that

$$\tilde{\mathbf{v}}_i \Phi = \hat{\mathbf{v}}_i \Phi, \quad (7)$$

$$\tilde{\mathbf{v}}_i^\omega \Phi = \hat{\mathbf{v}}_i^\omega \Phi \quad (8)$$

at the given time t . Hence the trial fields at the minimum of the functional can “stand in” for the action of the corresponding operators. Clearly the minimum corresponds to the physical dynamics, as the trial fields possess the “correct” values that determine the actual time evolution. Here the translational contribution to the power functional takes on the value

$$\mathcal{R}_t^{0, \text{trans}} = -\frac{\gamma}{2} \int d\mathbf{r}^N d\boldsymbol{\omega}^N \sum_i \tilde{\mathbf{v}}_i^2 \Phi(\mathbf{r}^N, \boldsymbol{\omega}^N, t), \quad (9)$$

where the superscript 0 indicates the value at the minimum. The total value of \mathcal{R}_t at the minimum consists of translational and rotational contributions:

$$\mathcal{R}_t^0 = -\frac{1}{2} \int d\mathbf{r}^N d\boldsymbol{\omega}^N \sum_i \left(\gamma \tilde{\mathbf{v}}_i^2 + \gamma^\omega (\tilde{\mathbf{v}}_i^\omega)^2 \right) \Phi(\mathbf{r}^N, \boldsymbol{\omega}^N, t), \quad (10)$$

Furthermore, we can use \mathcal{R}_t as a generator for the one-body fields of interest, via functional differentiation [157],

$$\frac{\delta \mathcal{R}_t}{\delta \mathbf{X}(\mathbf{r}, \boldsymbol{\omega}, t)} = \mathbf{J}(\mathbf{r}, \boldsymbol{\omega}, t), \quad (11)$$

$$\frac{\delta \mathcal{R}_t}{\delta \mathbf{X}^\omega(\mathbf{r}, \boldsymbol{\omega}, t)} = \mathbf{J}^\omega(\mathbf{r}, \boldsymbol{\omega}, t), \quad (12)$$

where the translational and rotational one-body currents are defined, respectively, via

$$\mathbf{J}(\mathbf{r}, \boldsymbol{\omega}, t) = \quad (13)$$

$$\int d\mathbf{r}^N d\boldsymbol{\omega}^N \sum_i \delta(\mathbf{r} - \mathbf{r}_i) \delta^\omega(\boldsymbol{\omega} - \boldsymbol{\omega}_i) \hat{\mathbf{v}}_i \Phi(\mathbf{r}^N, \boldsymbol{\omega}^N, t),$$

$$\mathbf{J}^\omega(\mathbf{r}, \boldsymbol{\omega}, t) = \quad (14)$$

$$\int d\mathbf{r}^N d\boldsymbol{\omega}^N \sum_i \delta(\mathbf{r} - \mathbf{r}_i) \delta^\omega(\boldsymbol{\omega} - \boldsymbol{\omega}_i) \hat{\mathbf{v}}_i^\omega \Phi(\mathbf{r}^N, \boldsymbol{\omega}^N, t),$$

where $\delta(\cdot)$ indicates the three-dimensional Dirac distribution and $\delta^\omega(\cdot)$ is the Dirac distribution on the unit sphere.

The one-body currents are related to the temporal change of the one-body density via the continuity equation

$$\frac{\partial \rho(\mathbf{r}, \boldsymbol{\omega}, t)}{\partial t} = -\nabla \cdot \mathbf{J}(\mathbf{r}, \boldsymbol{\omega}, t) - \nabla^\omega \cdot \mathbf{J}^\omega(\mathbf{r}, \boldsymbol{\omega}, t), \quad (15)$$

as can be shown from integrating (1) over the degrees of freedom of $N - 1$ swimmers. Here the one-body density distribution is defined via

$$\rho(\mathbf{r}, \boldsymbol{\omega}, t) = \quad (16)$$

$$\int d\mathbf{r}^N d\boldsymbol{\omega}^N \sum_i \delta(\mathbf{r} - \mathbf{r}_i) \delta^\omega(\boldsymbol{\omega} - \boldsymbol{\omega}_i) \Phi(\mathbf{r}^N, \boldsymbol{\omega}^N, t).$$

In order to connect the many-body theory with the one-body level, we perform a constrained Levy search [181, 182] as

$$R_t[\rho, \mathbf{J}, \mathbf{J}^\omega] = \min_{\tilde{\mathbf{v}}^N, \tilde{\mathbf{v}}^{\omega, N} \rightarrow \rho, \mathbf{J}, \mathbf{J}^\omega} \mathcal{R}_t, \quad (17)$$

where the constraints are obtained by replacing the operators on the right hand sides of Eqs. (13) and (14) by

their respective trial fields, i.e.

$$\mathbf{J}(\mathbf{r}, \boldsymbol{\omega}, t) = \quad (18)$$

$$\int d\mathbf{r}^N d\boldsymbol{\omega}^N \sum_i \delta(\mathbf{r} - \mathbf{r}_i) \delta^\omega(\boldsymbol{\omega} - \boldsymbol{\omega}_i) \tilde{\mathbf{v}}_i \Phi(\mathbf{r}^N, \boldsymbol{\omega}^N, t),$$

$$\mathbf{J}^\omega(\mathbf{r}, \boldsymbol{\omega}, t) = \quad (19)$$

$$\int d\mathbf{r}^N d\boldsymbol{\omega}^N \sum_i \delta(\mathbf{r} - \mathbf{r}_i) \delta^\omega(\boldsymbol{\omega} - \boldsymbol{\omega}_i) \tilde{\mathbf{v}}_i^\omega \Phi(\mathbf{r}^N, \boldsymbol{\omega}^N, t).$$

In equilibrium systems, the method of constrained search provides an alternative to the more familiar Mermin-Evans foundation of density functional theory [162, 183]. The advantages of the Levy method are that no Legendre transform is required and that the intrinsic free energy functional is given as an explicit (many-body) expression.

As a consequence of the constrained search (17), the variational principle is now elevated to the one-body level, such that both

$$\frac{\delta R_t[\rho, \mathbf{J}, \mathbf{J}^\omega]}{\delta \mathbf{J}(\mathbf{r}, \boldsymbol{\omega}, t)} = 0, \quad (20)$$

$$\frac{\delta R_t[\rho, \mathbf{J}, \mathbf{J}^\omega]}{\delta \mathbf{J}^\omega(\mathbf{r}, \boldsymbol{\omega}, t)} = 0, \quad (21)$$

hold at the minimum of the functional. Here the (partial) functional derivatives are performed at fixed $\rho(\mathbf{r}, \boldsymbol{\omega}, t)$. As we will show below, (20) and (21) constitute a force balance and a torque balance equation, which together with the continuity equation (15) completely determine the dynamics. One advantage of this setup is that the different contributions to the total force and total torque can be systematically formulated. In particular, one can identify the genuine nonequilibrium contributions as being superadiabatic, i.e. above free energy contributions, as we will show in the following.

The structure laid out so far implies that the internal and external contributions to the total power functional can be separated according to

$$R_t[\rho, \mathbf{J}, \mathbf{J}^\omega] = W_t[\rho, \mathbf{J}, \mathbf{J}^\omega] - X_t[\rho, \mathbf{J}, \mathbf{J}^\omega] \quad (22)$$

where $W_t[\rho, \mathbf{J}, \mathbf{J}^\omega]$ is an intrinsic contribution, solely dependent on the interparticle interactions $u(\mathbf{r}^N, \boldsymbol{\omega}^N)$. The external power is generated from the external forces and torques (both of which act local in time and space) according to

$$X_t[\rho, \mathbf{J}, \mathbf{J}^\omega] = \int d\mathbf{r} d\boldsymbol{\omega} [\mathbf{J} \cdot (-\nabla v^{\text{ext}} + \mathbf{X} + \gamma s \boldsymbol{\omega}) + \mathbf{J}^\omega \cdot (-\nabla^\omega v^{\text{ext}} + \mathbf{X}^\omega)]. \quad (23)$$

We next split the internal contribution in (22) into ideal and excess (over ideal) parts

$$W_t = W_t^{\text{id}} + W_t^{\text{exc}}, \quad (24)$$

where the intrinsic ideal (i.e. in a system with no internal interactions) power functional is given by

$$W_t^{\text{id}}[\rho, \mathbf{J}, \mathbf{J}^\omega] = \int d\mathbf{r}d\boldsymbol{\omega} \left[\frac{\gamma \mathbf{J}^2 + \gamma^\omega (\mathbf{J}^\omega)^2}{2\rho} + k_B T (\mathbf{J} \cdot \nabla + \mathbf{J}^\omega \cdot \nabla^\omega) \ln \rho \right]. \quad (25)$$

Here the right hand side can be split into a sum

$$W_t^{\text{id}}[\rho, \mathbf{J}, \mathbf{J}^\omega] = P_t^{\text{id}}[\rho, \mathbf{J}, \mathbf{J}^\omega] + \dot{F}_{\text{id}}[\rho], \quad (26)$$

with contributions due to dissipation, P_t^{id} , and adiabatic (reversible) ideal free energy changes, $\dot{F}_{\text{id}}[\rho]$. Here

$$F_{\text{id}}[\rho] = k_B T \int d\mathbf{r}d\boldsymbol{\omega} \rho(\mathbf{r}, \boldsymbol{\omega}) (\ln(\rho(\mathbf{r}, \boldsymbol{\omega}) \Lambda^d) - 1) \quad (27)$$

is the intrinsic Helmholtz free energy functional of an ideal gas of uniaxial rotators in d spatial dimensions; Λ is the (irrelevant) thermal de Broglie wavelength, and the overdot in (26) indicates a derivative with respect to time. Explicitly, the dissipative and reversible ideal intrinsic contributions are given by

$$P_t^{\text{id}}[\rho, \mathbf{J}, \mathbf{J}^\omega] = \int d\mathbf{r}d\boldsymbol{\omega} \frac{\gamma \mathbf{J}^2 + \gamma^\omega (\mathbf{J}^\omega)^2}{2\rho}, \quad (28)$$

$$\dot{F}_{\text{id}}[\rho]/(k_B T) = \int d\mathbf{r}d\boldsymbol{\omega} (\mathbf{J} \cdot \nabla + \mathbf{J}^\omega \cdot \nabla^\omega) \ln(\rho \Lambda^d), \quad (29)$$

where (29) is obtained from (27) via the chain rule, replacing the partial time derivative of the density distribution $\dot{\rho}$ via the continuity equation (15), and integration by parts in both position and orientation.

The functional derivatives of the ideal intrinsic contribution (25) are then obtained as

$$\begin{aligned} \frac{\delta W_t^{\text{id}}}{\delta \mathbf{J}(\mathbf{r}, \boldsymbol{\omega}, t)} &= \frac{\gamma \mathbf{J}(\mathbf{r}, \boldsymbol{\omega}, t)}{\rho(\mathbf{r}, \boldsymbol{\omega}, t)} + k_B T \nabla \ln \rho(\mathbf{r}, \boldsymbol{\omega}, t), \quad (30) \\ \frac{\delta W_t^{\text{id}}}{\delta \mathbf{J}^\omega(\mathbf{r}, \boldsymbol{\omega}, t)} &= \frac{\gamma^\omega \mathbf{J}^\omega(\mathbf{r}, \boldsymbol{\omega}, t)}{\rho(\mathbf{r}, \boldsymbol{\omega}, t)} + k_B T \nabla^\omega \ln \rho(\mathbf{r}, \boldsymbol{\omega}, t), \end{aligned} \quad (31)$$

where the arguments of $W_t^{\text{id}}[\rho, \mathbf{J}, \mathbf{J}^\omega]$ have been omitted for clarity. The variational principle (20) and (21) can be then cast into the form of a force balance and a torque balance equation, which are given, respectively, by

$$\begin{aligned} \frac{\gamma \mathbf{J}(\mathbf{r}, \boldsymbol{\omega}, t)}{\rho(\mathbf{r}, \boldsymbol{\omega}, t)} &= \gamma s \boldsymbol{\omega} - k_B T \nabla \ln \rho(\mathbf{r}, \boldsymbol{\omega}, t) - \frac{\delta W_t^{\text{exc}}}{\delta \mathbf{J}(\mathbf{r}, \boldsymbol{\omega}, t)} \\ &\quad - \nabla v^{\text{ext}}(\mathbf{r}, \boldsymbol{\omega}, t) + \mathbf{X}(\mathbf{r}, \boldsymbol{\omega}, t), \quad (32) \\ \frac{\gamma^\omega \mathbf{J}^\omega(\mathbf{r}, \boldsymbol{\omega}, t)}{\rho(\mathbf{r}, \boldsymbol{\omega}, t)} &= -k_B T \nabla^\omega \ln \rho(\mathbf{r}, \boldsymbol{\omega}, t) - \frac{\delta W_t^{\text{exc}}}{\delta \mathbf{J}^\omega(\mathbf{r}, \boldsymbol{\omega}, t)} \\ &\quad - \nabla^\omega v^{\text{ext}}(\mathbf{r}, \boldsymbol{\omega}, t) + \mathbf{X}^\omega(\mathbf{r}, \boldsymbol{\omega}, t). \quad (33) \end{aligned}$$

In order to describe the contribution due to internal interactions, we assume a splitting of the intrinsic excess functional into adiabatic and superadiabatic (above

“adiabatic”, i.e. equilibrium) contributions,

$$W_t^{\text{exc}}[\rho, \mathbf{J}, \mathbf{J}^\omega] = \dot{F}^{\text{exc}}[\rho] + P_t^{\text{exc}}[\rho, \mathbf{J}, \mathbf{J}^\omega], \quad (34)$$

where the total time derivative of the intrinsic excess (over ideal gas) Helmholtz free energy functional $F^{\text{exc}}[\rho]$, which is due to the intrinsic interaction potential $u(\mathbf{r}^N, \boldsymbol{\omega}^N)$, is

$$\begin{aligned} \dot{F}^{\text{exc}}[\rho] &= \\ &\int d\mathbf{r}d\boldsymbol{\omega} \left(\mathbf{J}(\mathbf{r}, \boldsymbol{\omega}, t) \cdot \nabla + \mathbf{J}^\omega(\mathbf{r}, \boldsymbol{\omega}, t) \cdot \nabla^\omega \right) \frac{\delta F^{\text{exc}}[\rho]}{\delta \rho(\mathbf{r}, \boldsymbol{\omega}, t)}, \end{aligned} \quad (35)$$

and $P_t^{\text{exc}}[\rho, \mathbf{J}, \mathbf{J}^\omega]$ is the superadiabatic contribution, which also originates from the internal interactions, and describes the difference to the equilibrium physics. $P_t^{\text{exc}}[\rho, \mathbf{J}, \mathbf{J}^\omega]$ depends in general non-locally in time and in space on its (functional) arguments. The functional derivative in (35) is taken with respect to an equilibrium density distribution $\rho_{\text{eq}}(\mathbf{r}, \boldsymbol{\omega})$ (which is independent of time), as is appropriate for the equilibrium excess free energy functional $F[\rho_{\text{eq}}]$. This functional derivative is then evaluated at the time-dependent density, i.e. at $\rho_{\text{eq}}(\mathbf{r}, \boldsymbol{\omega}) = \rho(\mathbf{r}, \boldsymbol{\omega}, t)$. Note that this identity defines the adiabatic state [164]. Similar to the derivation of (29), one obtains (35) from applying the chain rule, replacing $\dot{\rho}$ via (15) and then “reversing” the action of the nabla operators by partial integration, i.e. building the adjoint operators.

Inserting the splitting (24), (25), (29), (28), and (34) into (22) yields a decomposition which is identical to the case of systems with only translational degrees of freedom [157]:

$$R_t = P_t^{\text{id}} + P_t^{\text{exc}} + \dot{F}_{\text{id}} + \dot{F}^{\text{exc}} - X_t. \quad (36)$$

Evaluating the functional at the physical time evolution yields

$$\mathcal{R}_t^0 = R_t^0 \equiv R_t[\rho, \mathbf{J}, \mathbf{J}^\omega], \quad (37)$$

where \mathcal{R}_t^0 is defined via (10).

B. Steady state sum rules

The formulation in Sec. II A is general and applies to arbitrary time-dependent situations. We will henceforth consider steady states, i.e. where the one-body distributions carry no time dependence. This still includes cases with flow, $\mathbf{J}, \mathbf{J}^\omega \neq 0$, as long as the currents are time-independent and divergence-free, such that $\dot{\rho} = 0$ follows from (15). We split the value of the free power (37) into a contribution from internal forces, I_t , and an external contribution, X_t , according to

$$R_t^0 = -I_t/2 - X_t/2. \quad (38)$$

Here the external part of the free power is determined by (23) at the physical dynamics. On the many-body level, this is given by

$$X_t = \int d\mathbf{r}^N d\boldsymbol{\omega}^N \sum_i (\mathbf{f}_i^{\text{ext}} \cdot \hat{\mathbf{v}}_i + \mathbf{f}_i^{\boldsymbol{\omega}, \text{ext}} \cdot \hat{\mathbf{v}}_i^{\boldsymbol{\omega}}) \Phi(\mathbf{r}^N, \boldsymbol{\omega}^N, t), \quad (39)$$

where $\mathbf{f}_i^{\text{ext}} = -(\nabla_i v_i^{\text{ext}}) + \mathbf{X}_i + \gamma s \boldsymbol{\omega}$ is the external force and $\mathbf{f}_i^{\boldsymbol{\omega}, \text{ext}} = -(\nabla_i^{\boldsymbol{\omega}} v_i^{\text{ext}}) + \mathbf{X}_i^{\boldsymbol{\omega}}$ is the external torque. The internal part in (38) is given by

$$I_t = \int d\mathbf{r}^N d\boldsymbol{\omega}^N \sum_i \left\{ [-\nabla_i u(\mathbf{r}^N, \boldsymbol{\omega}^N) - k_B T \nabla_i \ln \Phi] \cdot \hat{\mathbf{v}}_i + [-\nabla_i^{\boldsymbol{\omega}} u(\mathbf{r}^N, \boldsymbol{\omega}^N) - k_B T \nabla_i^{\boldsymbol{\omega}} \ln \Phi] \cdot \hat{\mathbf{v}}_i^{\boldsymbol{\omega}} \right\} \Phi, \quad (40)$$

where the arguments of $\Phi(\mathbf{r}^N, \boldsymbol{\omega}^N, t)$ have been left away for clarity. Here the operators ∇_i and $\nabla_i^{\boldsymbol{\omega}}$ only act inside of the brackets. Integration by parts and rearranging gives

$$I_t = \int d\mathbf{r}^N d\boldsymbol{\omega}^N [u(\mathbf{r}^N, \boldsymbol{\omega}^N) + k_B T \ln \Phi(\mathbf{r}^N, \boldsymbol{\omega}^N, t)] \times \sum_i (\nabla_i \cdot \hat{\mathbf{v}}_i + \nabla_i^{\boldsymbol{\omega}} \cdot \hat{\mathbf{v}}_i^{\boldsymbol{\omega}}) \Phi(\mathbf{r}^N, \boldsymbol{\omega}^N, t). \quad (41)$$

Using the Smoluchowski equation (1) in order to replace the sum allows to obtain

$$I_t = - \int d\mathbf{r}^N d\boldsymbol{\omega}^N [u(\mathbf{r}^N, \boldsymbol{\omega}^N) + k_B T \ln \Phi(\mathbf{r}^N, \boldsymbol{\omega}^N, t)] \times \frac{\partial}{\partial t} \Phi(\mathbf{r}^N, \boldsymbol{\omega}^N, t). \quad (42)$$

In steady state the partial time derivative of Φ vanishes and hence we can conclude that

$$I_t = 0. \quad (43)$$

Using the splitting (38) the free power in steady state is thus trivially related to the external contribution,

$$R_t^0 = -X_t/2. \quad (44)$$

We next seek to exploit the availability of the two splittings of R_t , given by (36) and (38), in steady state. We start by rewriting (28) as

$$P_t^{\text{id}} = \frac{1}{2} \int d\mathbf{r} d\boldsymbol{\omega} \left(\mathbf{J} \cdot \frac{\gamma \mathbf{J}}{\rho} + \mathbf{J}^{\boldsymbol{\omega}} \cdot \frac{\gamma \mathbf{J}^{\boldsymbol{\omega}}}{\rho} \right). \quad (45)$$

Inserting the force balance equations (32) and (33) and rearranging yields

$$P_t^{\text{id}} = \frac{1}{2} \int d\mathbf{r} d\boldsymbol{\omega} \left[\mathbf{J} \cdot (\gamma s \boldsymbol{\omega} - \nabla v^{\text{ext}} + \mathbf{X} - k_B T \nabla \ln \rho) + \mathbf{J}^{\boldsymbol{\omega}} \cdot (-\nabla^{\boldsymbol{\omega}} v^{\text{ext}} + \mathbf{X}^{\boldsymbol{\omega}} - k_B T \nabla^{\boldsymbol{\omega}} \ln \rho) \right] - \frac{1}{2} \int d\mathbf{r} d\boldsymbol{\omega} \left(\mathbf{J} \cdot \frac{\delta W_t^{\text{exc}}}{\delta \mathbf{J}} + \mathbf{J}^{\boldsymbol{\omega}} \cdot \frac{\delta W_t^{\text{exc}}}{\delta \mathbf{J}^{\boldsymbol{\omega}}} \right). \quad (46)$$

Integration by parts of the terms $\mathbf{J} \cdot k_B T \nabla \ln \rho$ and $\mathbf{J}^{\boldsymbol{\omega}} \cdot k_B T \nabla^{\boldsymbol{\omega}} \ln \rho$ and using the continuity equation (15), gives the time derivative of the density. As $\dot{\rho} = 0$ in steady state, the first integral in (46) reduces to the external power X_t , cf. (23). The second integral in (46) is determined by the superadiabatic contribution P_t^{exc} , as (34) reduces to $W_t^{\text{exc}} = P_t^{\text{exc}}$ in steady state, because then $\dot{F}_{\text{exc}} = 0$. Thus the free power in steady state is given by inserting (46) into (36), which yields upon observing that $\dot{F}_{\text{id}} = 0$ the result

$$R_t^0 = P_t^{\text{exc}} - \frac{X_t}{2} - \frac{1}{2} \int d\mathbf{r} d\boldsymbol{\omega} \left(\mathbf{J} \cdot \frac{\delta P_t^{\text{exc}}}{\delta \mathbf{J}} + \mathbf{J}^{\boldsymbol{\omega}} \cdot \frac{\delta P_t^{\text{exc}}}{\delta \mathbf{J}^{\boldsymbol{\omega}}} \right). \quad (47)$$

Comparing to (38) yields

$$I_t = -2P_t^{\text{exc}} + \int d\mathbf{r} d\boldsymbol{\omega} \left(\mathbf{J} \cdot \frac{\delta P_t^{\text{exc}}}{\delta \mathbf{J}} + \mathbf{J}^{\boldsymbol{\omega}} \cdot \frac{\delta P_t^{\text{exc}}}{\delta \mathbf{J}^{\boldsymbol{\omega}}} \right). \quad (48)$$

Using (43) the value of the superadiabatic functional in steady state is determined by the superadiabatic force, $\delta P_t^{\text{exc}} / \delta \mathbf{J}(\mathbf{r}, \boldsymbol{\omega}, t)$, and by the superadiabatic torque, $\delta P_t^{\text{exc}} / \delta \mathbf{J}^{\boldsymbol{\omega}}(\mathbf{r}, \boldsymbol{\omega}, t)$, via

$$P_t^{\text{exc}} = \frac{1}{2} \int d\mathbf{r} d\boldsymbol{\omega} \left(\mathbf{J} \cdot \frac{\delta P_t^{\text{exc}}}{\delta \mathbf{J}} + \mathbf{J}^{\boldsymbol{\omega}} \cdot \frac{\delta P_t^{\text{exc}}}{\delta \mathbf{J}^{\boldsymbol{\omega}}} \right), \quad (49)$$

where all quantities are evaluated at the physical dynamics.

C. Excess dissipation functional

We next assume a model form for the excess dissipation functional which is instantaneous in time (i.e. Markovian) and given by

$$P_t^{\text{exc}} = \frac{\gamma}{2} \int d1 d2 \rho(1) \rho(2) \left(\frac{\mathbf{J}(1)}{\rho(1)} - \frac{\mathbf{J}(2)}{\rho(2)} \right)^2 M(1, 2), \quad (50)$$

where the roman numerals refer to one position and one orientation, i.e. $1 \equiv \mathbf{r}, \boldsymbol{\omega}$ and $2 \equiv \mathbf{r}', \boldsymbol{\omega}'$, and $M(1, 2)$ is a convolution kernel, which depends on the differences $\mathbf{r} - \mathbf{r}'$ and $\boldsymbol{\omega} - \boldsymbol{\omega}'$.

For a bulk steady state the number density becomes a constant, $\rho(\mathbf{r}, \boldsymbol{\omega}, t) = \rho_b$, and the current reduces to $\mathbf{J}(\mathbf{r}, \boldsymbol{\omega}, t) = J_b \boldsymbol{\omega}$, where $J_b = \text{const}$. Furthermore $\mathbf{J}^{\boldsymbol{\omega}}(\mathbf{r}, \boldsymbol{\omega}, t) = 0$ and $\dot{F} = 0$, due to the steady state condition. The power functional, (36), then reduces to

$$R_t = P_t^{\text{id}} - \gamma s \int d1 \mathbf{J}(1) \cdot \boldsymbol{\omega} + P_t^{\text{exc}} \quad (51)$$

$$= \frac{\gamma}{2} \int d1 \frac{\mathbf{J}(1)^2}{\rho(1)} - \gamma s \int d1 \mathbf{J}(1) \cdot \boldsymbol{\omega} \quad (52)$$

$$+ \frac{\gamma}{2} \int d1 d2 \rho(1) \rho(2) \left(\frac{\mathbf{J}(1)}{\rho(1)} - \frac{\mathbf{J}(2)}{\rho(2)} \right)^2 M(1, 2)$$

which can be simplified to

$$\frac{R_t(J_b)}{4\pi V} = \frac{\gamma J_b^2}{2\rho_b} + \frac{\gamma M_0}{2} J_b^2 - \gamma s J_b, \quad (53)$$

where

$$M_0 = \int d2(\boldsymbol{\omega} - \boldsymbol{\omega}')^2 M(1, 2) \quad (54)$$

is a density-dependent parameter, which is independent of J_b . In (53) J_b acts as a variational parameter. In order to apply the fundamental variational principle (20), we thus minimize (53) with respect to J_b ,

$$\frac{\partial R_t}{\partial J_b} = \gamma \frac{J_b}{\rho_b} + \gamma M_0 J_b - \gamma s = 0. \quad (55)$$

As a result we obtain the relationship $J_b - s\rho_b = -M_0 J \rho_b$, from which the bulk current can be obtained as

$$J_b = \frac{s\rho_b}{1 + M_0\rho_b}. \quad (56)$$

Rearranging yields $M_0 = (s\rho_b - J_b)/\rho_b J_b$. Inserting this result in (53) leads to

$$\frac{R_t^0}{4\pi V} = -\frac{\gamma s}{2} J_b. \quad (57)$$

where R_t^0 denotes (as before) the value of the power functional at the minimum.

The ansatz for the currents, $\mathbf{J} = J_b \boldsymbol{\omega}$, $\mathbf{J}^\omega = 0$, allows the calculation of the external power X_t , and the internal power I_t . The external power (23) reduces to $X_t = \gamma s \int d1 \mathbf{J}(1) \cdot \boldsymbol{\omega}$, in the absence of further external forces (besides swimming) and torques. As $\boldsymbol{\omega}$ is a unit vector one obtains

$$\frac{X_t}{4\pi V} = \gamma s J_b. \quad (58)$$

Hence from comparing (57) and (58) we explicitly verify that $R_t^0 = -X_t/2$ holds, i.e. the present approximation for the excess dissipation functional respects the sum rule (44).

Evaluating the internal power (48) yields

$$\frac{I_t}{4\pi V} = -\gamma M_0 J_b^2 + \gamma M_0 \mathbf{J}_b^2 = 0, \quad (59)$$

and therefore the exact sum rule (43), $I_t = 0$, is also satisfied within the current approximation.

By inserting (56) in (57) we obtain

$$\frac{R_t^0}{4\pi V} = -\frac{\gamma s^2 \rho_b}{2(1 + M_0\rho_b)}. \quad (60)$$

It remains to specify the kernel, $M(1, 2)$, in order to arrive at a closed theory. We assume that the kernel $M(1, 2)$ and hence its moment M_0 , (54), increase with density. We choose the simple functional form [179]

$$M_0 = \frac{1}{\rho_0 - \rho_b} + \frac{c_0 \rho_b^m}{\rho_0^{m+1}}, \quad (61)$$

where m is a positive integer and ρ_0 , and c_0 are constants. For $\rho_b \rightarrow \rho_0$ jamming occurs (such that the bulk density is restricted to the interval $0 \leq \rho_b \leq \rho_0$) and hence $M_0 \rightarrow \infty$. Insertion into Eq. (56) yields

$$\frac{J_b}{s\rho_b} = \frac{1 - x}{1 + c_0 x^{m+1}(1 - x)}, \quad (62)$$

where $x = \rho_b/\rho_0$ is a scaled density.

Within the approximation (50) the free power per volume becomes

$$\frac{R_t^0}{4\pi V} = \frac{\gamma s^2 \rho_b}{2} \frac{x - 1}{1 + c_0 x^{m+1}(1 - x)}, \quad (63)$$

which yields the free power per particle via division by $\rho_b = N/V$ as

$$\frac{R_t^0}{4\pi N} = \frac{\gamma s^2}{2} \frac{x - 1}{1 + c_0 x^{m+1}(1 - x)}. \quad (64)$$

We will show below that this simple functional form can provide a reliable account of the Brownian dynamics simulation data.

III. BROWNIAN DYNAMICS SIMULATIONS

The simulated system consists of $N = 5000$ spherical Brownian particles in two dimensions. The dynamics of the particles are represented by the over-damped Langevin equations

$$\dot{\mathbf{r}}_i(t) = s\boldsymbol{\omega}_i(t) + \gamma^{-1} \mathbf{f}_i^{\text{int}}(\mathbf{r}^N) + \boldsymbol{\xi}_i(t), \quad (65)$$

$$\dot{\varphi}_i(t) = \eta_i, \quad (66)$$

where, as before, $i = 1 \dots N$ labels the particles. The self propulsion of each particle is along its unit orientation vector $\boldsymbol{\omega}_i(t) = (\sin \varphi_i(t), \cos \varphi_i(t))$ with the (free) swim speed s . The angle $\varphi_i(t)$ then describes the orientation of particle i at time t . The stochastic vector $\boldsymbol{\xi}_i$ and the stochastic scalar η_i are Gaussian distributed with zero mean and auto-correlations

$$\langle \boldsymbol{\xi}_i(t) \boldsymbol{\xi}_j(t') \rangle = 2D_{\text{trans}} \mathbf{1} \delta_{ij} \delta(t - t'), \quad (67)$$

$$\langle \eta_i(t) \eta_j(t') \rangle = 2D_{\text{rot}} \delta_{ij} \delta(t - t'), \quad (68)$$

where $D_{\text{trans}} = k_B T/\gamma$ and $D_{\text{rot}} = k_B T/\gamma^\omega$ are the translational and the rotational diffusion coefficient, respectively, and $\mathbf{1}$ is the 2×2 unit matrix. The inter-particle interaction force $\mathbf{f}_i^{\text{int}}(\mathbf{r}^N)$ is generated from the potential $u(\mathbf{r}^N)$ by $\mathbf{f}_i^{\text{int}}(\mathbf{r}^N) = -\nabla_i u(\mathbf{r}^N)$. Here we restrict ourselves to spherically symmetric pair interactions $u(\mathbf{r}^N) = \sum_{i,j,i < j} \phi(r_{ij})$, leading to forces of the form

$$\mathbf{f}_i^{\text{int}}(\mathbf{r}^N) = -\nabla_i \sum_{j,j \neq i} \phi(r_{ij}), \quad (69)$$

where $r_{ij} = |\mathbf{r}_i(t) - \mathbf{r}_j(t)|$. We use the Weeks-Chandler-Anderson (WCA) [95, 184] pair potential, which is a

Lennard-Jones potential that is cut at its minimum and shifted so it remains continuous:

$$\phi(r_{ij}) = 4\epsilon \left[(\sigma/r_{ij})^{12} - (\sigma/r_{ij})^6 \right] + \epsilon, \text{ for } r_{ij} < 2^{1/6}\sigma. \quad (70)$$

Then (69) creates a purely repulsive interparticle interaction force and avoids artifacts at the cut-off.

A common measure for the activity of the particles is the Peclet number, which is defined as (see e.g. [179])

$$\text{Pe} = \frac{3s}{D_{\text{rot}}\sigma}. \quad (71)$$

This dimensionless number relates the two quantities that characterize the activity of the particles, namely s and D_{rot} .

The descretized dynamics proceed according to the Euler algorithm

$$\mathbf{r}_i(t + \Delta t) = \mathbf{r}_i(t) + \dot{\mathbf{r}}_i(t)\Delta t, \quad (72)$$

$$\boldsymbol{\omega}_i(t + \Delta t) = \boldsymbol{\omega}_i(t) + \dot{\boldsymbol{\omega}}_i(t)\Delta t, \quad (73)$$

where $\dot{\mathbf{r}}_i(t)$ and $\dot{\boldsymbol{\omega}}_i(t)$ are given by Eqs. (65) and (66), respectively. Additionally the orientation vector $\boldsymbol{\omega}_i(t)$ is normalized to unit length at each time step to avoid effects on the propulsion speed.

We carry out Brownian dynamics (BD) simulations in 2D with a fixed time step of $\Delta t/\tau_0 = 10^{-5}$, with the natural time unit $\tau_0 = \sigma^2\gamma/\epsilon$. The fundamental units of the system are σ , γ and ϵ , where σ represents the size of the repulsive (LJ) core and ϵ its energy scale. All simulations are performed at fixed ratio between the rotational diffusion constant and the translation diffusion constant, $D_{\text{rot}}/D_{\text{trans}} = 3\sigma^{-2}$, and a fixed propulsion speed of $s\tau_0/\sigma = 24$. The particles are placed in a square, periodic box with side length $L = (N/\rho_b)^{1/2}$, where $\rho_b = N/V$, with V being the (two-dimensional) volume of the simulation box. We investigate the properties of the system as a function of the bulk density ρ_b , and of the temperature T . We carried out simulations with bulk densities in the range of $\rho_b\sigma^2 = 0.1$ to 1.2 in steps of 0.1. In addition we performed simulations with $\rho_b\sigma^2 = 0.01$ and $\rho_b\sigma^2 = 0.05$. For each density we consider the temperatures of $k_B T/\epsilon = 0.1, 0.2, 0.3, 0.4, 0.6$. We let the system reach the steady state for $n_{\text{equi}} = 10^7$ integration steps, followed by $n_{\text{sample}} = 10^8$ steps in which the sampled data is collected.

With these choices of parameters the Peclet number (71) can be re-expressed as

$$\text{Pe} = \frac{s\gamma\sigma}{k_B T}. \quad (74)$$

All results presented below are averages over time and over particles and are calculated according to $\langle \mathcal{A}_i(j) \rangle = \frac{1}{N} \sum_{i=1}^N \frac{1}{n_{\text{sample}}} \sum_{j=1}^{n_{\text{sample}}} \mathcal{A}_i(j)$, where $\mathcal{A}_i(j)$ stands for an arbitrary (sampled) quantity for particle i at each discrete time point j . Hence this corresponds to the configuration space average.

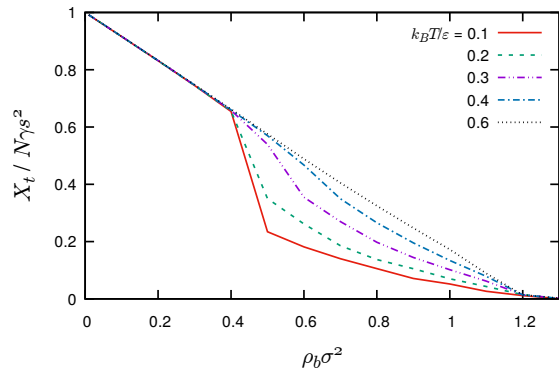


FIG. 1: Scaled external power X_t as a function of density. Temperatures are shown from $k_B T/\epsilon = 0$ to 1 as indicated by colors and line styles.

An important example is the external power, given by

$$X_t = \left\langle \sum_i \mathbf{f}_i^{\text{ext}}(t) \cdot \mathbf{v}_i(t) \right\rangle, \quad (75)$$

where the external force is $\mathbf{f}_i^{\text{ext}} = \gamma s \boldsymbol{\omega}_i$ and the velocity \mathbf{v}_i is the velocity of the particles.

IV. RESULTS

Figure 1 shows the external power X_t as a function of density for different temperatures. For temperatures $k_B T/\epsilon > 0.4$ the external power is linear in ρ_b , where the value for $\rho_b \rightarrow 0$ is purely determined by the external forces, i.e. collision between the particles occur very unlikely. When decreasing the temperature, $k_B T/\epsilon \leq 0.4$, the external power develops a dip, i.e., a deviation from the linear shape. This region, where the external power is smaller than expected from a linear dependence on the bulk density, covers the range of $0.4 \lesssim \rho_b\sigma^2 \lesssim 1.2$. Hence for those set of parameters less external power needs to be provided for the dynamics of the system. As $R_t = -X_t/2$ in steady state this dip will develop also in the free power.

Figure 2(a) shows simulation results for the scaled free power per particle obtained from the external power. The free power is the central object in PFT and occurs in the theory as a consequence of general considerations for nonequilibrium systems. It is thus quite surprising that for the present case of active Brownian particles the free power is directly related to the average propulsion speed per particle $v(\rho_b)$, which appears as an important quantity in existing hydrodynamic theories [9, 94–96]. The average self-propulsion speed is defined as the part of velocity of a particle in the direction of its orientation, averaged over the whole system [9, 82, 93, 95],

$$v = \frac{1}{N} \left\langle \sum_i \mathbf{v}_i(t) \cdot \boldsymbol{\omega}_i(t) \right\rangle, \quad (76)$$

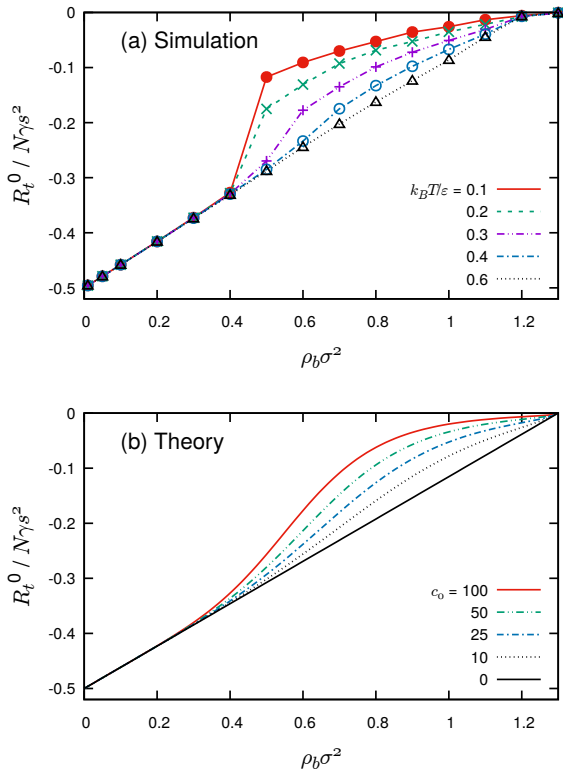


FIG. 2: (a) Scaled free power $R_t^0 / (N\gamma s^2)$ obtained from BD simulations via sampling X_t as a function of density. Temperatures are shown from $k_B T / \epsilon = 0$ to 1 as indicated by colors and line styles. (b) Theoretical results corresponding to (a), as given by (64). The jamming density is fixed to $\rho_0 \sigma^2 = 1.3$, $m = 5$ and values of c_0 are 0 – 100 as indicated.

where $\mathbf{v}_i(t)$ is velocity of the position of the particles, which we implement as a central derivative of the position of the particles, $\mathbf{v}_i(t) = (\mathbf{r}_i(t + \Delta t) - \mathbf{r}_i(t - \Delta t)) / (2\Delta t)$ [164, 179]. Therefore interparticle interactions change the velocity of the particles depending of the value of the bulk density. Thus v is density-dependent, $v(\rho_b)$. In the low-density limit, $\rho_b \rightarrow 0$, interparticle forces play no role. Hence $v(\rho_b \rightarrow 0) = \langle \sum_i (s\boldsymbol{\omega}_i(t) + \boldsymbol{\xi}_i(t)) \cdot \boldsymbol{\omega}_i(t) \rangle / N = s$.

Multiplying both sides of (76) by γs yields

$$\gamma s v(\rho_b) = \frac{1}{N} \left\langle \sum_i \mathbf{v}_i(t) \cdot (\gamma s \boldsymbol{\omega}_i(t)) \right\rangle. \quad (77)$$

The term between the angle brackets in (77) is X_t . Thus $v(\rho_b)$ is proportional to X_t as

$$X_t = N\gamma s v(\rho_b). \quad (78)$$

We have studied systematically the dependence of the external, and hence the free, power on temperature. Note that according to (74) this is analogous to varying Pe [95].

Similar to the external power, the free power decrease linearly with increasing density for $k_B T / \epsilon > 0.4$, because with increasing density the dissipation per particle decreases due to collisions. This leads to a linear decrease in the free power until the dynamics arrest and jamming occurs at ρ_0 (see also Sec. II C).

For temperatures $k_B T / \epsilon \leq 0.4$ the decrease of R_t^0 is nonlinear. While hardly any effect for low densities is observed, a significant dip develops for $\rho_b \sigma^2 \gtrsim 0.4$. The physical reason for this dip is an additional dissipation process, which decreases the free power per particle even more than the excluded volume of the surrounding particles. We interpret this as a local clustering of the particles, as clustered particles dissipate less power to the solvent, compared to free particles. Whether the presence of a dip is related to the onset of phase separation is an open question [179]. A detailed discussion of motility induced phase separation is beyond the scope of this work. However, a body of work on this topic exists [80–102, 179]. Comparing phase diagrams of different authors, see e.g. Fig. 6 in Ref. [94], and Ref. [96], shows that the onset of phase separation occurs in the same range as the dip in R_t^0 develops.

In Sec. II we defined an excess dissipation functional (50) and we showed that with a simple approximation an analytic expression for R_t^0 can be obtained, cf. (64). Numerical results for the scaled free power per particle, obtained using this expression, are shown in Fig. 2(b) as a function of ρ_b for different values of the parameter c_0 . In order to fit the simulation results, we fixed the exponent in (64) to $m = 5$, the jamming density to $\rho_0 \sigma^2 = 1.3$, and increased c_0 from zero to 100. This corresponds to decreasing the temperature in simulations, as a comparison with Fig. 2(a) reveals. Investigating in more detail the exact functional dependence of c_0 on temperature remains a task for future studies. This could involve a microscopic derivation of the moment, M_0 , of the correlation kernel, $M(1, 2)$. Nevertheless, we expect c_0 to decrease to zero with increasing temperature, because thermal motion tends to break up clusters and thus works against phase separation [179]. Comparing Fig. 2(a) and Fig 2(b) it is evident that our approximate form for the excess dissipation functional, (50), can reproduce the simulation results quite well, although the approximation for P_t^{exc} describes single-phase fluids, while the simulation results show MIPS. Hence PFT potentially serves as a theoretical tool to describe MIPS. This is an open problem for future work.

V. CONCLUSIONS

In this work we have investigated the steady state properties of active Brownian particles by applying PFT [157], suitably generalized to deal with orientational degrees of freedom. We have obtained the value of the power functional, via sampling of the external power, directly from active Brownian dynamics simulations. A

possibility to sample the free power directly is proposed elsewhere [179]. We leave a detailed formulation of the free power sampling for future work.

For the system under consideration the free power is straightforwardly related to the average forward swim speed of the particles. We have shown that the free power, and hence the average forward swim speed, exhibit a departure from linearity (‘dip’) when dissipative clusters form in the system. However, the focus here is on clarifying details of the power functional approach for active particles and simulation method, rather than the analysis of cluster formation [119–121] and nonequilibrium steady states [82, 93, 95]. Using the constrained search method, we generate from the many-body starting point of PFT a one-body variational theory, for which the trial fields are the density, translational current and rotational current, respectively. A simple approximation to the dissipation functional generates an analytic variational theory. From the data shown in Fig. 2, one can conclude that the behavior of the full many-body system can be captured by the one-body theory. This one-body theory enables an intuitive physical interpretation of the simulation data, although some model input,

most notable $c_0(T)$, still remained to be elucidated on the microscopic level. A possible way to achieve this is via studying dynamical two-body (van Hove) correlation functions, either via the nonequilibrium Ornstein-Zernike route [173, 174], or via the dynamical test particle limit [185, 187] for which PFT provides an in principle exact implementation [186]. Note that even within the dynamical density functional approximation, the dynamical test particle limit constitutes a valuable computational tool [188, 189]. Furthermore the occurrence of phase separation is not yet included in the approximation presented here, and requires further work [190]. Obtaining microscopically based approximations to the dissipation functional and applying those to relevant situations, as e.g. the influence of gravity [191], are useful future steps. Furthermore we showed that the internal power vanishes in steady state. The free power is thus purely determined by the external power, i.e., the self-propulsion of the particles.

Acknowledgements. We thank Joseph M. Brader, Daniel de las Heras, Sophie Hermann, Martin Oettel and Johannes Bleibel for useful discussions.

-
- [1] J. Toner, Y. Tu, and S. Ramaswamy, *Ann. Phys.* **318**, 170 (2005).
 - [2] E. Lauga and T. R. Powers, *Rep. Prog. Phys.* **72**, 096601 (2009).
 - [3] S. Ramaswamy, *Annu. Rev. Cond. Matter Phys.* **1**, 323 (2010).
 - [4] P. Romanczuk, M. Bär, W. Ebeling, B. Lindner, and L. Schimansky-Geier, *Eur. Phys. J. Special Topics* **202**, 1 (2012).
 - [5] T. Vicsek and A. Zafeiris, *Phys. Rep.* **517**, 71 (2012).
 - [6] M. E. Cates, *Rep. Prog. Phys.* **75**, 042601 (2012).
 - [7] M. C. Marchetti, J. F. Joanny, S. Ramaswamy, T. B. Liverpool, J. Prost, M. Rao, and R. A. Simha, *Rev. Mod. Phys.* **85**, 1143 (2013).
 - [8] A. P. Solon, M. E. Cates, and J. Tailleur, *Eur. Phys. J. Special Topics* **224**, 1231 (2015).
 - [9] M. E. Cates and J. Tailleur, *Ann. Rev. Cond. Matter Phys.* **6**, 219 (2015).
 - [10] J. Elgeti, R. G. Winkler, and G. Gompper, *Rep. Prog. Phys.* **78**, 056601 (2015).
 - [11] A. M. Menzel, *Phys. Rep.* **554**, 1 (2015).
 - [12] C. Bechinger, R. Di Leonardo, H. Löwen, C. Reichhardt, G. Volpe, and G. Volpe, *Rev. Mod. Phys.* **88**, 045006 (2016).
 - [13] S. J. Ebbens, *Cur. Op. Coll. Interf. Sci.* **21**, 14 (2016).
 - [14] S. H. L. Klapp, *Cur. Op. Coll. Interf. Sci.* **21**, 76 (2016).
 - [15] M. C. Marchetti, Y. Fily, S. Henkes, A. Patch, and D. Yllanes, *Cur. Op. Coll. Interf. Sci.* **21**, 34 (2016).
 - [16] A. M. Menzel, *New J. Phys.* **18**, 071001 (2016).
 - [17] A. E. Patteson, A. Gopinath, and P. E. Arratia, *Cur. Op. Coll. Interf. Sci.* **21**, 86 (2016).
 - [18] A. Zöttl and H. Stark, *J. Phys.: Cond. Mat.* **28**, 253001 (2016).
 - [19] I. S. Aranson, A. Sokolov, J. O. Kessler, and R. E. Goldstein, *Phys. Rev. E* **75**, 040901 (R) (2007).
 - [20] B. Szabó, G. J. Szöllösi, B. Gönci, Z. Jurányi, D. Selmeczi, and T. Vicsek, *Phys. Rev. E* **74**, 061908 (2006).
 - [21] A. Czirók, E. Ben-Jacob, I. Cohen, and T. Vicsek, *Phys. Rev. E* **54**, 1791 (1996).
 - [22] J. Dunkel, S. Heidenreich, K. Drescher, H. H. Wensink, M. Bär, and R. E. Goldstein, *Phys. Rev. Lett.* **110**, 228102 (2013).
 - [23] A. Jepsen, V. A. Martinez, J. Schwarz-Linek, A. Morozov, and W. C. K. Poon, *Phys. Rev. E* **88**, 041002 (R) (2013).
 - [24] T. V. Kasyap, D. L. Koch, and M. Wu, *Phys. Fluids* **26**, 081901 (2014).
 - [25] M. J. Kim and K. S. Breuer, *Phys. Fluids* **16**, L78 (2004).
 - [26] K. C. Leptos, J. S. Guasto, J. P. Gollub, A. I. Pesci, and R. E. Goldstein, *Phys. Rev. Lett.* **103**, 198103 (2009).
 - [27] E. Lushi, H. Wioland, and R. E. Goldstein, *Proc. Nat. Acad. Sci.* **111**, 9733 (2014).
 - [28] A. P. Petroff, X. L. Wu, and A. Libchaber, *Phys. Rev. Lett.* **114**, 158102 (2015).
 - [29] J. Tailleur and M. E. Cates, *Phys. Rev. Lett.* **100**, 218103 (2008).
 - [30] X. L. Wu and A. Libchaber, *Phys. Rev. Lett.* **84**, 3017 (2000).
 - [31] G. Grégoire, H. Chaté, and Y. Tu, *Physica D* **181**, 157 (2003).
 - [32] J. Toner and Y. Tu, *Phys. Rev. Lett.* **75**, 4326 (1995).
 - [33] J. Toner and Y. Tu, *Phys. Rev. E* **58**, 4828 (1998).
 - [34] D. S. Cambuí and A. Rosas, *Physica A* **391**, 3908 (2012).
 - [35] F. Schweitzer and J. A. Holyst, *Eur. Phys. J. B* **15**, 723 (2000).
-

- [36] T. Vicsek, A. Czirok, E. Ben-Jacob, I. Cohen, and O. Shochet, *Phys. Rev. Lett.* **75**, 1226 (1995).
- [37] M. Romenskyy and V. Lobaskin, *Eur. Phys. J. B* **86**, 91 (2013).
- [38] H. Chaté, F. Ginelli, G. Grégoire, and F. Raynaud, *Phys. Rev. E* **77**, 046113 (2008).
- [39] A. M. Menzel, *J. Phys.: Cond. Mat.* **25**, 505103 (2013).
- [40] M. Romensky, V. Lobaskin, and T. Ihle, *Phys. Rev. E* **90**, 063315 (2014).
- [41] R. Großmann, P. Romanczuk, M. Bär, and L. Schimansky-Geier, *Phys. Rev. Lett.* **113**, 258104 (2014).
- [42] E. Ferrante, A. E. Turgut, M. Dorigo, and C. Huepe, *Phys. Rev. Lett.* **111**, 268302 (2013).
- [43] M. Meschede and O. Hallatschek, *New J. Phys.* **15**, 045027 (2013).
- [44] H. Chaté, F. Ginelli, G. Grégoire, F. Peruani, and F. Raynaud, *Eur. Phys. J. B* **64**, 451 (2008).
- [45] K. H. Nagai, Y. Sumino, R. Montagne, I. S. Aranson, and H. Chaté, *Phys. Rev. Lett.* **114**, 168001 (2015).
- [46] F. Kogler and S. H. L. Klapp, *Eur. Phys. Lett.* **110**, 10004 (2015).
- [47] A. M. Menzel and T. Ohta, *Eur. Phys. Lett.* **99**, 58001 (2012).
- [48] M. Abkenar, K. Marx, T. Auth, and G. Gompper, *Phys. Rev. E* **88**, 062314 (2013).
- [49] F. Ginelli, F. Peruani, M. Bär, and H. Chaté, *Phys. Rev. Lett.* **104**, 184502 (2010).
- [50] H. H. Wensink and H. Löwen, *J. Phys.: Cond. Mat.* **24**, 464130 (2012).
- [51] S. P. Thampi, R. Golestanian, and J. M. Yeomans, *Phys. Rev. Lett.* **111**, 118101 (2013).
- [52] S. J. Decamp, G. S. Redner, A. Baskaran, M. F. Hagan, and Z. Dogic, *Nat. Mater.* **14**, 1110 (2015).
- [53] E. Bertin, H. Chaté, F. Ginelli, S. Mishra, A. Peshkov, and S. Ramaswamy, *New J. Phys.* **15**, 085032 (2013).
- [54] H. Chaté, F. Ginelli, and R. Montagne, *Phys. Rev. Lett.* **96**, 180602 (2006).
- [55] L. Berthier and J. Kurchan, *Nat. Phys.* **9**, 310 (2013).
- [56] R. Ni, M. a. C. Stuart, and M. Dijkstra, *Nat. Comm.* **4**, 2704 (2013).
- [57] L. Berthier, *Phys. Rev. Lett.* **112**, 220602 (2014).
- [58] R. Ni, M. a. C. Stuart, M. Dijkstra, and P. G. Bolhuis, *Soft Matter* **10**, 6609 (2014).
- [59] T. F. F. Farage and J. M. Brader, arXiv 1403.0928 (2014).
- [60] J. Prost, F. Jülicher, and J.-F. Joanny, *Nat. Phys.* **11**, 111 (2015).
- [61] J. Deseigne, O. Dauchot, and H. Chaté, *Phys. Rev. Lett.* **105**, 098001 (2010).
- [62] J. Deseigne, S. Léonard, O. Dauchot, and H. Chaté, *Soft Matter* **8**, 5629 (2012).
- [63] C. A. Weber, T. Hanke, J. Deseigne, S. Léonard, O. Dauchot, E. Frey, and H. Chaté, *Phys. Rev. Lett.* **110**, 208001 (2013).
- [64] L. Walsh, C. G. Wagner, S. Schlossberg, C. Olson, A. Baskaran, and N. Menon, *Soft Matter* **13**, 8964 (2017).
- [65] I. Buttinoni, J. Bialké, F. Kümmel, H. Löwen, C. Bechinger, and T. Speck, *Phys. Rev. Lett.* **110**, 238301 (2013).
- [66] I. Theurkauff, C. Cottin-Bizonne, J. Palacci, C. Ybert, and L. Bocquet, *Phys. Rev. Lett.* **108**, 268303 (2012).
- [67] J. Palacci, S. Sacanna, A. P. Steinberg, D. J. Pine, and P. M. Chaikin, *Science* **239**, 936 (2013).
- [68] R. Golestanian, T. B. Liverpool, and A. Ajdari, *Phys. Rev. Lett.* **94**, 220801 (2005).
- [69] Y. Hong, N. M. K. Blackman, N. D. Kopp, A. Sen, and D. Velegol, *Phys. Rev. Lett.* **99**, 178103 (2007).
- [70] J. Toner, *Phys. Rev. E* **86**, 031918 (2012).
- [71] J. Blaschke, M. Mauerer, K. Menon, A. Zöttl, and H. Stark, *Soft Matter* **12**, 9821 (2016).
- [72] S. Mishra, A. Baskaran, and M. C. Marchetti, *Phys. Rev. E* **81**, 061916 (2010).
- [73] A. Zöttl and H. Stark, *Phys. Rev. Lett.* **112**, 118101 (2014).
- [74] M. Leoni and T. B. Liverpool, *Eur. Phys. J. E* **65**, 126 (2012).
- [75] B. Bet, G. Boosten, M. Dijkstra, and R. van Roij, *J. Chem. Phys.* **146**, 084904 (2017).
- [76] M. Leoni and T. B. Liverpool, *Phys. Rev. Lett.* **112**, 148104 (2014).
- [77] M. Leoni and T. B. Liverpool, *Phys. Rev. E* **85**, 040901(R) (2012).
- [78] S. FÜRTHAUER and S. Ramaswamy, *Phys. Rev. Lett.* **111**, 238102 (2013).
- [79] Y. Ibrahim and T. B. Liverpool, *Europhys. Lett.* **111**, 48008 (2015).
- [80] J. Barré, R. Chétrite, M. Muratori, and F. Peruani, *J. Stat. Phys.* **158**, 589 (2014).
- [81] J. Bialké, T. Speck, and H. Löwen, *J. Non-Cryst. Solids* **407**, 367 (2015).
- [82] J. Bialké, H. Löwen, and T. Speck, *Europhys. Lett.* **103**, 30008 (2013).
- [83] M. E. Cates and J. Tailleur, *Europhys. Lett.* **101**, 20010 (2013).
- [84] S. Paliwal, J. Rodenburg, R. Van Roij, and M. Dijkstra, *New J. Phys.* **20**, 015003 (2018).
- [85] Y. Fily, A. Baskaran, and M. F. Hagan, *Soft Matter* **10**, 5609 (2014).
- [86] Y. Fily and M. C. Marchetti, *Phys. Rev. Lett.* **108**, 235702 (2012).
- [87] G. Gonnella, D. Marenduzzo, A. Suma, and A. Tiribocchi, *Comptes Rend. Phys.* **16**, 316 (2015).
- [88] D. Levis, J. Codina, and I. Pagonabarraga, *Soft Matter* **13**, 8113 (2017).
- [89] V. Prymidis, S. Paliwal, M. Dijkstra, and L. Filion, *J. Chem. Phys.* **145**, 124904 (2016).
- [90] G. S. Redner, A. Baskaran, and M. F. Hagan, *Phys. Rev. E* **88**, 012305 (2013).
- [91] J. T. Siebert, J. Letz, T. Speck, and P. Virnau, *Soft Matter* **13**, 1020 (2017).
- [92] T. Speck, *Eur. Phys. J. ST* **225**, 2287 (2016).
- [93] T. Speck, J. Bialké, A. M. Menzel, and H. Löwen, *Phys. Rev. Lett.* **112**, 218304 (2014).
- [94] T. Speck, A. M. Menzel, J. Bialké, and H. Löwen, *J. Chem. Phys.* **142**, 224109 (2015).
- [95] J. Stenhammar, A. Tiribocchi, R. J. Allen, D. Marenduzzo, and M. E. Cates, *Phys. Rev. Lett.* **111**, 145702 (2013).
- [96] J. Stenhammar, D. Marenduzzo, R. J. Allen, and M. E. Cates, *Soft Matter* **10**, 1489 (2014).
- [97] J. Stenhammar, R. Wittkowski, D. Marenduzzo, and M. E. Cates, *Phys. Rev. Lett.* **114**, 018301 (2015).
- [98] A. Suma, G. Gonnella, D. Marenduzzo, and E. Orlandini, *Europhys. Lett.* **108**, 56004 (2014).
- [99] B. Trefz, S. K. Das, S. A. Egorov, P. Virnau, and K. Binder, *J. Chem. Phys.* **144**, 144902 (2016).
- [100] C. Tung, J. Harder, C. Valeriani, and A. Cacciuto, *Soft Matter* **12**, 555 (2015).

- [101] B. van der Meer, V. Prymidis, M. Dijkstra, and L. Filion, arXiv 1609.03867 (2016).
- [102] A. Wysocki, R. G. Winkler, and G. Gompper, *Europhys. Lett.* **105**, 48004 (2014).
- [103] G. S. Redner, M. F. Hagan, and A. Baskaran, *Phys. Rev. Lett.* **110**, 055701 (2013).
- [104] A. Liluashvili, K. Onoby, and T. Voigtmann, *Phys. Rev. E* **96**, 062608 (2017).
- [105] M. Feng, Z. Hou, *Soft Matter* **13**, 4464 (2017).
- [106] S. K. Nandi and N. S. Gov, *Soft Matter* **13**, 7609 (2017).
- [107] R. Wittkowski, A. Tiribocchi, J. Stenhammar, R. J. Allen, D. Marenduzzo, and M. E. Cates, *Nat. Comm.* **5**, 4351 (2014).
- [108] J. Stenhammar, C. Nardini, R. W. Nash, D. Marenduzzo, and A. Morozov, *Phys. Rev. Lett.* **119**, 028005 (2017).
- [109] A. Sharma and J. M. Brader, *J. Chem. Phys.* **145**, 161101 (2016).
- [110] J. Bialké, T. Speck, and H. Löwen, *Phys. Rev. Lett.* **108**, 168301 (2012).
- [111] E. Ferrante, A. E. Turgut, M. Dorigo, and C. Huepe, *New J. Phys.* **15**, 095011 (2013).
- [112] D. Levis and L. Berthier, *Phys. Rev. E* **89**, 062301 (2014).
- [113] E. Mani and H. Löwen, *Phys. Rev. E* **92**, 032301 (2015).
- [114] O. Pohl and H. Stark, *Phys. Rev. Lett.* **112**, 238303 (2014).
- [115] O. Pohl and H. Stark, *Eur. Phys. J. E* **38**, 93 (2015).
- [116] C. A. Weber, C. Bock, and E. Frey, *Phys. Rev. Lett.* **112**, 168301 (2014).
- [117] D. Richard, H. Löwen, and T. Speck, *Soft Matter* **12**, 1 (2016).
- [118] V. Prymidis, H. Sielcken, and L. Filion, *Soft Matter* **11**, 4158 (2015).
- [119] G. S. Redner, C. G. Wagner, A. Baskaran, and M. F. Hagan, *Phys. Rev. Lett.* **117**, 148002 (2016).
- [120] A. M. Menzel and H. Löwen, *Phys. Rev. Lett.* **110**, 055702 (2013).
- [121] A. M. Menzel, T. Ohta, and H. Löwen, *Phys. Rev. E* **89**, 022301 (2014).
- [122] É. Fodor, C. Nardini, M. E. Cates, J. Tailleur, P. Visco, and F. van Wijland, *Phys. Rev. Lett.* **117**, 038103 (2016).
- [123] R. Großmann, F. Peruani, and M. Bär, *New J. Phys.* **18**, 043009 (2015).
- [124] U. M. B. Marconi and C. Maggi, *Soft Matter* **11**, 8768 (2015).
- [125] Z. K. Preisler and M. Dijkstra, *Soft Matter* **12**, 6043 (2016).
- [126] J. Rodenburg, M. Dijkstra, and R. van Roij, *Soft Matter* **13**, 8957 (2017).
- [127] T. Speck, *Europhys. Lett.* **144**, 30006 (2016).
- [128] S. C. Takatori and J. F. Brady, *Phys. Rev. E* **91**, 032117 (2015).
- [129] S. C. Takatori and J. F. Brady, *Soft Matter* **11**, 7920 (2015).
- [130] S. C. Takatori and J. F. Brady, *Curr. Op. Coll. Interf. Sci.* **21**, 24 (2015).
- [131] A. Tiribocchi, R. Wittkowski, D. Marenduzzo, and M. E. Cates, *Phys. Rev. Lett.* **115**, 188302 (2015).
- [132] W. Yan and J. F. Brady, *J. Fluid Mech.* **785**, R1 (2015).
- [133] A. Patch, D. Yllanes, and M. C. Marchetti, *Phys. Rev. E* **95**, 012601 (2016).
- [134] S. A. Mallory, A. Šarić, C. Valeriani, and A. Cacciuto, *Phys. Rev. E* **89**, 052303 (2014).
- [135] F. Smallenburg and H. Löwen, *Phys. Rev. E* **92**, 032304 (2015).
- [136] A. P. Solon, J. Stenhammar, R. Wittkowski, M. Kardar, Y. Kafri, M. E. Cates, and J. Tailleur, *Phys. Rev. Lett.* **114**, 198301 (2015).
- [137] T. Speck and R. L. Jack, *Phys. Rev. E* **93**, 062605 (2016).
- [138] R. G. Winkler, A. Wysocki, and G. Gompper, *Soft Matter* **11**, 6680 (2015).
- [139] R. Wittmann and J. M. Brader, *Europhys. Lett.* **114**, 68004 (2016).
- [140] J. Bialké, J. T. Siebert, H. Löwen, and T. Speck, *Phys. Rev. Lett.* **115**, 098301 (2015).
- [141] U. M. B. Marconi, C. Maggi, and S. Melchionna, *Soft Matter* **12**, 5727 (2016).
- [142] S. Paliwal, V. Prymidis, L. Filion, and M. Dijkstra, *J. Chem. Phys.* **147**, 084902 (2017).
- [143] T. F. F. Farage, P. Krinninger, and J. M. Brader, *Phys. Rev. E* **91**, 042310 (2015).
- [144] P. Jung and P. Hänggi, *Phys. Rev. A* **35**, 4464 (1987).
- [145] P. Jung and P. Hänggi, *Adv. Chem. Phys.* **89**, 239 (1995).
- [146] R. F. Fox, *Phys. Rev. A* **33**, 467 (1986).
- [147] R. F. Fox, *Phys. Rev. A* **34**, 4525 (1986).
- [148] U. M. B. Marconi, N. Gnan, C. Maggi, and R. Di Leonardo, *Sci. Rep.* **6**, 23297 (2016).
- [149] M. Paoluzzi, C. Maggi, U. M. B. Marconi, and N. Gnan, *Phys. Rev. E* **94**, 052602 (2016).
- [150] M. Rein and T. Speck, *Eur. Phys. J. E* **39**, 84 (2016).
- [151] A. Sharma, R. Wittmann, and J. M. Brader, *Phys. Rev. E* **95**, 012115 (2017).
- [152] J. Schwarz-Linek, C. Valeriani, A. Cacciuto, M. E. Cates, D. Marenduzzo, A. N. Morozov, and W. C. K. Poon, *Proc. Nat. Aca. Sci.* **109**, 4052 (2012).
- [153] U. M. B. Marconi, M. Paoluzzi, and C. Maggi, *Mol. Phys.* **114**, 2400 (2016).
- [154] C. Maggi, U. M. B. Marconi, N. Gnan, and R. Di Leonardo, *Sci. Rep.* **5**, 10742 (2015).
- [155] R. Wittmann, C. Maggi, A. Sharma, A. Scacchi, J. M. Brader, and U. M. B. Marconi, *J. Stat. Mech.*, 113207 (2017).
- [156] R. Wittmann, U. M. B. Marconi, C. Maggi, and J. M. Brader, *J. Stat. Mech.*, 113208 (2017).
- [157] M. Schmidt and J. M. Brader, *J. Chem. Phys.* **138**, 214101 (2013).
- [158] A. Scacchi, M. Krüger, and J. M. Brader, *J. Phys.: Cond. Matt.* **28**, 244023 (2016).
- [159] J. Reinhardt, F. Weysser, and J. M. Brader, *Europhys. Lett.* **102**, 28011 (2013).
- [160] A. J. Archer and R. Evans, *J. Chem. Phys.* **121**, 4246 (2004).
- [161] M. Rex, H. H. Wensink, and H. Löwen, *Phys. Rev. E* **76**, 021403 (2007).
- [162] R. Evans, *Adv. Phys.* **28**, 143 (1979).
- [163] U. M. B. Marconi and P. Tarazona, *J. Phys.: Cond. Matt.* **110**, 8032 (1999).
- [164] A. Fortini, D. de las Heras, J. M. Brader, and M. Schmidt, *Phys. Rev. Lett.* **113**, 167801 (2014).
- [165] T. Schindler and M. Schmidt, *J. Chem. Phys.* **145**, 064506 (2016).
- [166] E. Bernreuther and M. Schmidt, *Phys. Rev. E* **94**, 022105 (2016).

- [167] T. Glanz and H. Löwen, *J. Phys.: Cond. Matt.* **24**, 464114 (2012).
- [168] T. Geigenfeind, D. de las Heras, and M. Schmidt, to be published (2018).
- [169] J. Chakrabarti, J. Dzubiella, and H. Löwen, *Europhys. Lett.* **61**, 415 (2003).
- [170] J. Chakrabarti, J. Dzubiella, and H. Löwen, *Phys. Rev. E* **70**, 012401 (2004).
- [171] M. Schmidt, *J. Chem. Phys.* **143**, 174108 (2015).
- [172] M. Schmidt, *J. Chem. Phys.* **148**, 044502 (2018).
- [173] J. M. Brader and M. Schmidt, *J. Chem. Phys.* **139**, 104108 (2013).
- [174] J. M. Brader and M. Schmidt, *J. Chem. Phys.* **140**, 034104 (2014).
- [175] D. de las Heras and Matthias Schmidt, *Phys. Rev. Lett.* **120**, 028001 (2018).
- [176] N. C. X. Stuhlmüller, T. Eckert, D. de las Heras and M. Schmidt, *Phys. Rev. Lett.* **121**, 098002 (2018).
- [177] D. Borgis, R. Assaraf, B. Rotenberg, and R. Vuilleumier, *Mol. Phys.* **111**, 3486 (2013).
- [178] D. de las Heras and M. Schmidt, *Phys. Rev. Lett.* **120**, 218001 (2018).
- [179] P. Krinninger, M. Schmidt, and J. M. Brader, *Phys. Rev. Lett.* **117**, 208003 (2016); Erratum: **119**, 029902 (2017).
- [180] J. M. Brader, M. Schmidt, *J. Phys.: Condens. Matter* **27**, 194106 (2015).
- [181] M. Levy, *Proc. Nat. Acad. Sci.* **76**, 6062 (1979).
- [182] W. S. B. Dwandaru and M. Schmidt, *Phys. Rev. E* **83**, 061133 (2011).
- [183] N. D. Mermin, *Phys. Rev.* **137**, A1441 (1965).
- [184] J. D. Weeks, D. Chandler, and H. C. Andersen, *J. Chem. Phys.* **54**, 5237 (1971).
- [185] A. J. Archer, P. Hopkins, and M. Schmidt, *Phys. Rev. E* **75**, 040501(R) (2007).
- [186] J. M. Brader, M. Schmidt, *J. Phys.: Condens. Matter* **27**, 194106 (2015).
- [187] P. Hopkins, A. Fortini, A.J. Archer, and M. Schmidt, *J. Chem. Phys.* **133**, 224505 (2010).
- [188] D. Stopper, R. Roth, H. Hansen-Goos, *J. Chem. Phys.* **143**, 181105 (2015).
- [189] D. Stopper, A. L. Thorneywork, R. P. A. Dullens, R. Roth, *J. Chem. Phys.* **148**, 104501 (2018).
- [190] P. Krinninger, S. Hermann, D. de las Heras and M. Schmidt (to be published).
- [191] S. Hermann and M. Schmidt, *Soft Matter* **14**, 1614 (2018).

The abstract of the future publication on interfaces in phase-separated active Brownian particles is reproduced in the following. The simulation data that are part of this paper is described and presented in Sec. 4.

Interfaces in phase-separated active Brownian particles

Philip Krinninger,¹ Sophie Hermann,¹ Daniel de las Heras,¹ and Matthias Schmidt¹

¹*Theoretische Physik II, Physikalisches Institut, Universität Bayreuth, D-95440 Bayreuth, Germany*

We investigate motility-induced phase separation that occurs in active Brownian particles, modelled as repulsive spheres that are driven out of equilibrium by a swimming force of constant magnitude and freely diffusing orientation. We compare Brownian dynamics computer simulation data for the structure of the free interface between the two bulk phases against the predictions of an analytical interfacial model. The physical effects that occur both at the interface and in bulk are rationalized, and results for the inhomogeneous density, current and polarization profile are presented.

Acknowledgements

First of all, I like to thank Matthias Schmidt. It was a real pleasure to work with you. Thank you for your continuous support, encouragement, and your infectious enthusiasm for teaching and research. Especially thank you for organizing great BBQs I enjoyed a lot. Thank you for giving me the opportunity to write my own Power Functional story.

I want to thank all my colleagues at TP2 who joined, left, and are part of the group. I had a lot of fun working with you. Thank you for the great time in the last six years. Thank you Dani and Andrea for all the things I learned from you. Thank you Thomas, Lucas and Sophie for our stimulating discussions. Special thanks go to Dani, Thomas, and Sophie for proof-reading the manuscript.

I want to thank Joe Brader, Thomas Farage, and all members of the Soft Matter Theory group in Fribourg for the great time I had during my visits in Switzerland and our fruitful discussions and collaboration.

I want to thank my friends Adal, Armin, Daniel, Tino, Basti, and many more that I cannot name individually. Thank you all for the great time during all these years in Bayreuth. I also like to thank the Fachschaft MPI and the "Dunstkreis". Especially your never ending supply with coffee is gratefully acknowledged.

I want to thank my whole family, especially my parents Karin and Franz. Your never ending support during these long years of studying, but also before and afterwards, gave me the opportunity to come to this point.

And very special thanks go to Daniela. I thank you for your patience with me and especially thank you for being at my side on all the ways we are going.